Theses and Dissertations--Mechanical Engineering

Mechanical Engineering

2020

ELECTROPHORESIS IN HETEROGENEOUS HYDROGELS AND APPLICATIONS IN SURFACE PATTERNING

Ning Ge
University of Kentucky, michaelgening@gmail.com
Author ORCID Identifier:
ⓘ https://orcid.org/0000-0003-3702-9838
Digital Object Identifier: https://doi.org/10.13023/etd.2020.169

Right click to open a feedback form in a new tab to let us know how this document benefits you.

STUDENT AGREEMENT:

I represent that my thesis or dissertation and abstract are my original work. Proper attribution has been given to all outside sources. I understand that I am solely responsible for obtaining any needed copyright permissions. I have obtained needed written permission statement(s) from the owner(s) of each third-party copyrighted matter to be included in my work, allowing electronic distribution (if such use is not permitted by the fair use doctrine) which will be submitted to UKnowledge as Additional File.

I hereby grant to The University of Kentucky and its agents the irrevocable, non-exclusive, and royalty-free license to archive and make accessible my work in whole or in part in all forms of media, now or hereafter known. I agree that the document mentioned above may be made available immediately for worldwide access unless an embargo applies.

I retain all other ownership rights to the copyright of my work. I also retain the right to use in future works (such as articles or books) all or part of my work. I understand that I am free to register the copyright to my work.

REVIEW, APPROVAL AND ACCEPTANCE

The document mentioned above has been reviewed and accepted by the student's advisor, on behalf of the advisory committee, and by the Director of Graduate Studies (DGS), on behalf of the program; we verify that this is the final, approved version of the student's thesis including all changes required by the advisory committee. The undersigned agree to abide by the statements above.

<div align="right">

Ning Ge, Student

Dr. Christine A. Trinkle, Major Professor

Dr. Alexandre Martin, Director of Graduate Studies

</div>

ELECTROPHORESIS IN HETEROGENEOUS HYDROGELS AND APPLICATIONS
IN SURFACE PATTERNING

_____

DISSERTATION
_____

A dissertation submitted in partial fulfillment of the
requirements for the degree of Doctor of Philosophy in the
College of Engineering
at the University of Kentucky

By
Ning Ge
Lexington, Kentucky

Director: Dr. Christine Ann Trinkle, Professor of Mechanical Engineering
Lexington, Kentucky

ABSTRACT

ELECTROPHORESIS IN HETEROGENEOUS HYDROGELS AND APPLICATIONS
IN SURFACE PATTERNING

The creation of chemical micropatterns on surfaces makes it possible to add unique chemical functionality to surfaces, modifying properties such as wettability, or even adding the ability to selectively bind other molecules. The creation of biochemical surface patterning in particular is useful in a variety of fields including tissue engineering and high-throughput drug screening. There are many existing surface patterning techniques which focus on precise control over the patterned geometry, even down to submicron scale features, but they do not allow local control over chemical concentration. So the results are high resolution patterns with binary concentration. There are also existing methods to generate surface gradients of chemicals, but the focus there is to produce unidirectional concentration variation over a large surface. Normally these two methods—surface patterning and surface gradient generation—are incompatible with each other. So despite the large number of applications where simultaneous control over chemical placement and concentration would be useful, there is a dearth of options for doing so. In addition, it would be valuable to make micro patterned surfaces in a simple and approachable way, because fields where it could be most beneficial (such as tissue culture) are populated by individuals who are typically not microfabrication experts.

The goal of this research is to develop an easy and low cost method for creating biochemical surface patterns with microscale feature resolution and local control over chemical concentration. The method described here leverages the force on charged protein molecules in an electric field to drive the molecules in a given direction. The speed with which these molecules move depends on the properties of the molecules themselves and the medium through which they travel. By creating a material with heterogeneous regions—in this work, a hydrogel with different mesh densities—it is possible to have local spatial control over the speed of protein movement. In this work, this concept was used to drive biomolecules (proteins) onto a target paper surface, and then local protein concentration was measured using fluorescence or intensity of a protein stain. In addition, these patterns were achieved using materials and methods that are easily accessible to individuals in most biochemical or tissue culture laboratories.

KEYWORDS: Surface Patterning, Electrophoresis, Hydrogel, Gradient Generation, Grayscale

Ning Ge
(Name of Student)

April 13, 2020
Date

ELECTROPHORESIS IN HETEROGENEOUS HYDROGELS AND APPLICATIONS
IN SURFACE PATTERNING

By
Ning Ge

Christine Ann Trinkle
Director of Dissertation

Alexandre Martin
Director of Graduate Studies

April 27, 2020
Date

To *my family.*

ACKNOWLEDGEMENTS

TABLE OF CONTENTS

LIST OF TABLES

LIST OF FIGURES

LIST OF SYMBOLS

Symbols	Representations
A_s	Local surface area
c	Surface concentration of particles
D^{gel}	Molecular diffusion coefficient in a hydrogel
D^{soln}	Molecular diffusion coefficient in free solution
$\boldsymbol{E}$	Electric field
E_x	Young's modulus in x-direction
F	Compressive force
$\boldsymbol{F_d}$	Drag force
$\boldsymbol{F_e}$	Electrophoretic driving force
h	Hydrogel thickness/height
J	Flux (molecules passing through unit surface area per unit time)
k	Stiffness coefficient
k_B	Boltzmann constant
n	Volumetric concentration of particles
N'	Number of particles passing through arbitrary surface between two time points
Q	Charge on a particle
r	Effective molecular radius
S	Arbitrary surface orthogonal to the particles moving trajectory
t	time
u	Molecular mobility of particles within a given medium
$\boldsymbol{v}$	Molecular velocity
$\boldsymbol{v_s}$	Molecular velocity at steady state
η	Dynamic viscosity of surrounding media
κ^{-2}	Darcy permeability
%C	Crosslinking ratio (g bisacrylamide per 100 g total acrylamide polymer)
%T	Concentration of monomer (grams per 100 ml solution)

CHAPTER 1. INTRODUCTION

1.1   Background and Motivation

The creation of protein micropatterns on surfaces is useful in a variety of fields including tissue engineering and high-throughput drug screening. However, the equipment required to create functional surface patterns—especially "grayscale" patterns where independent control over species placement and density are needed—is often expensive and not widely available. And because fields where these kinds of patterns could be most beneficial are populated by individuals who are typically not microfabrication experts, it is important to have methods that are accessible by these populations.

The goal of this research is to develop an easy and low-cost method for creating biochemical surface patterns with microscale feature resolution and local control over chemical concentration. The method described here leverages the force on charged protein molecules in an electric field to drive the molecules in a given direction. The speed with which these molecules move depends on the molecules themselves and the medium through which they travel. By creating a material with heterogeneous regions—in this work, a hydrogel with different mesh densities—it is possible to have local spatial control over the speed of protein movement. This dissertation describes using this concept to drive biomolecules (proteins) onto a target paper surface, and then measuring local protein concentration using fluorescence or intensity of a protein stain.

1.2   Organization of Chapters

In this dissertation, a novel surface patterning method has been proposed, analyzed theoretically, and verified experimentally. In chapter 2, current surface patterning

techniques and methods, especially those focusing on biochemical surface patterning, are introduced and discussed. Chapter 3 contains the fundamental theoretical analysis for the electrophoretic patterning method presented in this dissertation, including theoretical predictions of a variety of patterning scenarios. In chapter 4, the complete empirical work is presented and discussed, including the development of the patterning method over time, as well as the drawbacks of early designs and experimental limitations of the current system. In chapter 5, the conclusion of the work is addressed, including some recommendations for future work.

CHAPTER 2. LITERATURE REVIEW

2.1   UV-/Photo-lithography

UV-lithography (photolithography) is well known for its general applications. It has also been an important pre-requisite procedure for soft-lithography methods. UV-lithography is a process by using light sensitive materials to transfer the geometric features from photomasks to surfaces. Areas that have been exposed to UV lights would cure and solidify. The unexposed areas will be washed away to leave the patterns on surfaces. Typical UV-lithography methods include photomasks, which are usually expensive and not modifiable, so total cost would be high if several iterations of designs are required. The UV-lithography process is shown in Figure 2.1 from A to D, including surface substrate preparation, photoresist chemicals spin coating, pre-baking, exposure through photomasks, post-baking, and unexposed areas removal by using the developer. There are two lithographic types, positive and negative. Showing in the figure is negative type, that photoresist chemicals exposing to UV light cure and the rest unexposed chemicals would be washed away by the developer. The undeveloped photoresist usually works as a mask to protect the lower layer material from being etched. This is a popular subsequent process to transfer photoresist pattern to lower layer materials.
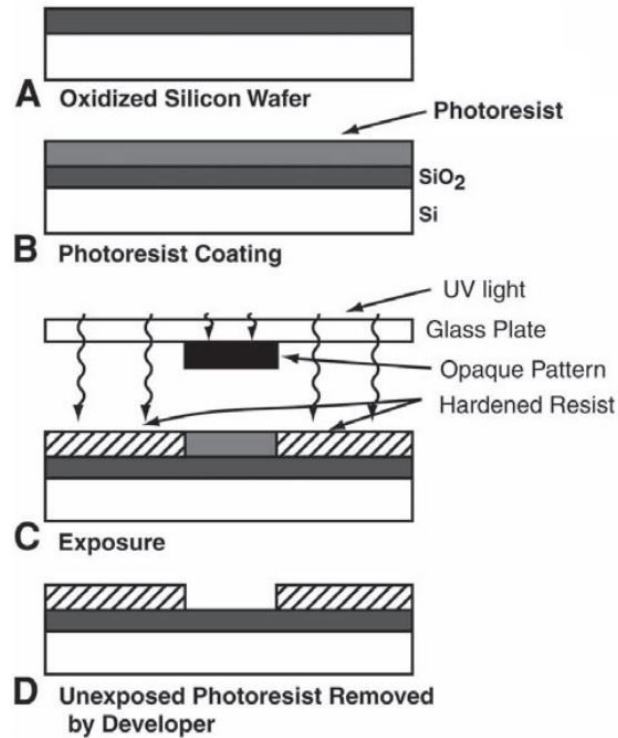
Figure 2.1 Process flow of typical photolithography. Example is (A) Si wafer. The process steps are (B) photoresist coating and soft baking, (C) UV exposure followed with hard baking, (D) development. Reprinted with permission from [1]. Copyright (2006) Humana Press Inc.

Chemical surface patterning is very similar to traditional photolithography procedures. Photosensitive chemicals would be spin coated, then exposed to UV light through patterned photomasks. Triggered by UV light, this coated layer of chemicals would form the demanded pattern. Unlike traditional photolithography which mostly utilized this pattern layer as etching mask, this pattern would be further treated such as silanization for biomolecules to attach to. Goudar et al. have successfully patterned proteins arrays by using this method. [2] They chose a positive photoresist to form the initial patterns. It was followed with silanising 3-aminopropyltriethoxysilane (APTES) for further protein attachment.

4

Similarly, Kurland et al. have patterned proteins with photolithography. Differently, they directly employed another photoresist, the "silk protein photoresist". [3] This silk fibroin from Bombyx mori silkworm cocoons has been modified via reagent 2-isocyanatoethyl methacrylate (IEM), so it yields a photocrosslinkable fibroin photoresist. It was used as negative photoresist that is crosslinked under UV exposure to generate 2D patterns on silicon and glass substrates, as shown in Figure 2.3.
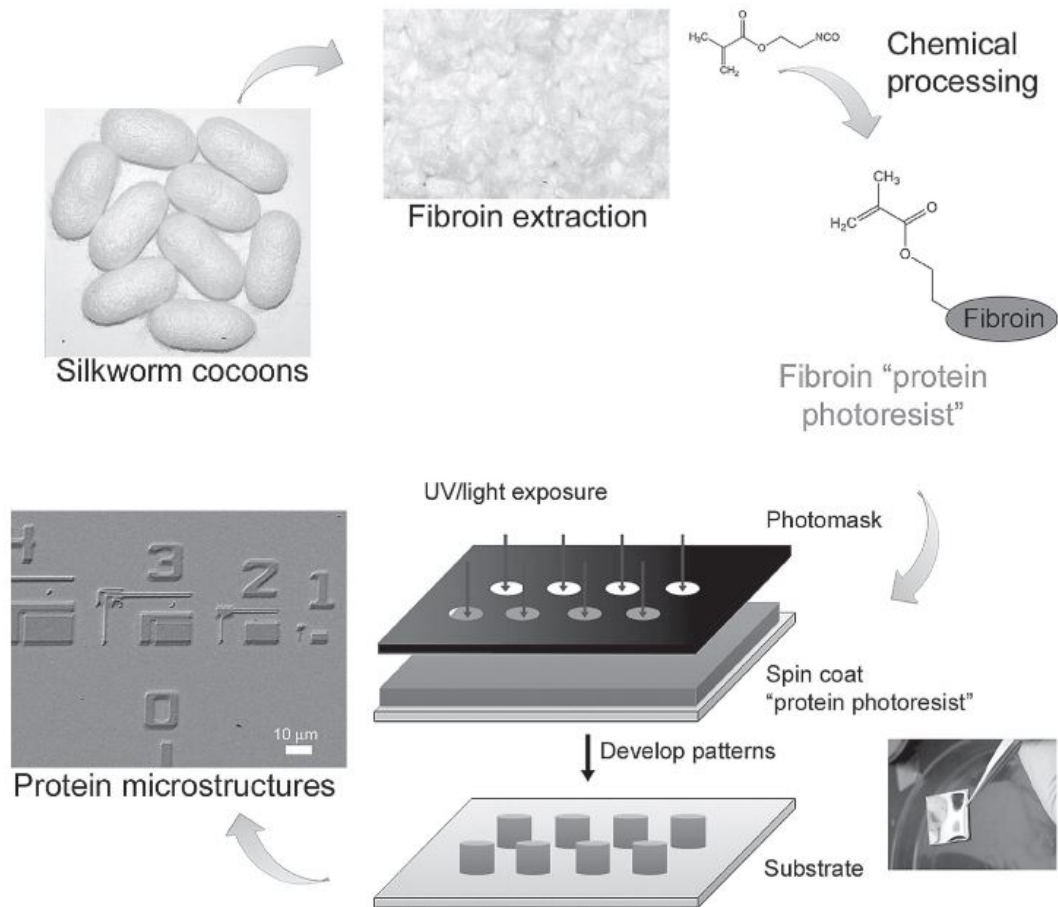
Figure 2.2 Photolithography process steps with synthesized "silk protein photoresist". Reprinted with permission from [3]. Copyright (2013) WILEY-VCH Verlag GmbH & Co. KGaA, Weinheim

Traditional photomask based photolithography has also been used to combine with plasma pretreatment to generate poly(hydroxyethyl mechacrylate) (PHEMA) patterns on

polypropylene films,[4] some even managed to pattern PEG layers on plastic substrates. [5]
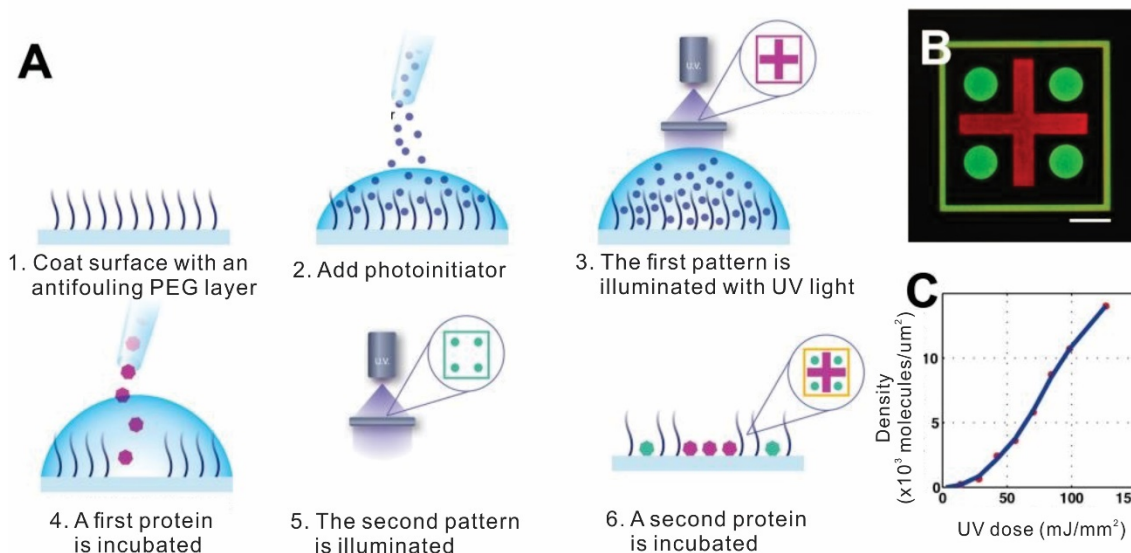
Figure 2.3 A) Schematics of the LIMAP patterning method. (1) Surface coating; (2) Photoinitiator added; (3) Patterning under UV exposure; (4) Protein incubated for attachment; (5) Exposure for next protein attachment; (6) Two protein patterning. B) Two-protein patterning fluorescent microscopy image, scale bar: 50 μm. C) Curve analysis of UV dose and protein immobilization density. Reprinted with permission from [7] . Copyright (2015) WILEY-VCH Verlag GmbH & Co. KGaA, Weinheim

Most photomask-based photolithography methods are constrained by the use of expensive masks. To get rid of it, maskless photolithography has been employed. Yang et al. and Strale et al. have chosen spatial light modulators such as digital micromirror devices (DMD) to direct write on photo sensitive layers on substrates. Yang and colleges used this technique to pattern a poly(ethylene) glycol diacrylate (PEGDA)-based hydrogel on glass, [6] while Strale et al. have used light-induced molecular adsorption (LIMAP) to pattern several molecules at one setup.[7] To achieve this, they relied on DMD to precisely control the exposure area. The photoinitiator was added into water environment which covered surfaces coated with antifouling PEG layers. Once exposure to UV light, activated

photoinitiator molecule would cleave PEG chains and leave the pattern, proteins could be deployed and incubated on surface. This procedure could be repeated for more than once if needed to pattern different proteins on same surface. The adsorbed molecular density is proportional to the dose of UV light, as shown in Figure 2.4(C), it could generate gradient or grayscale patterns of multiple molecules on same substrate. (Figure 2.5)
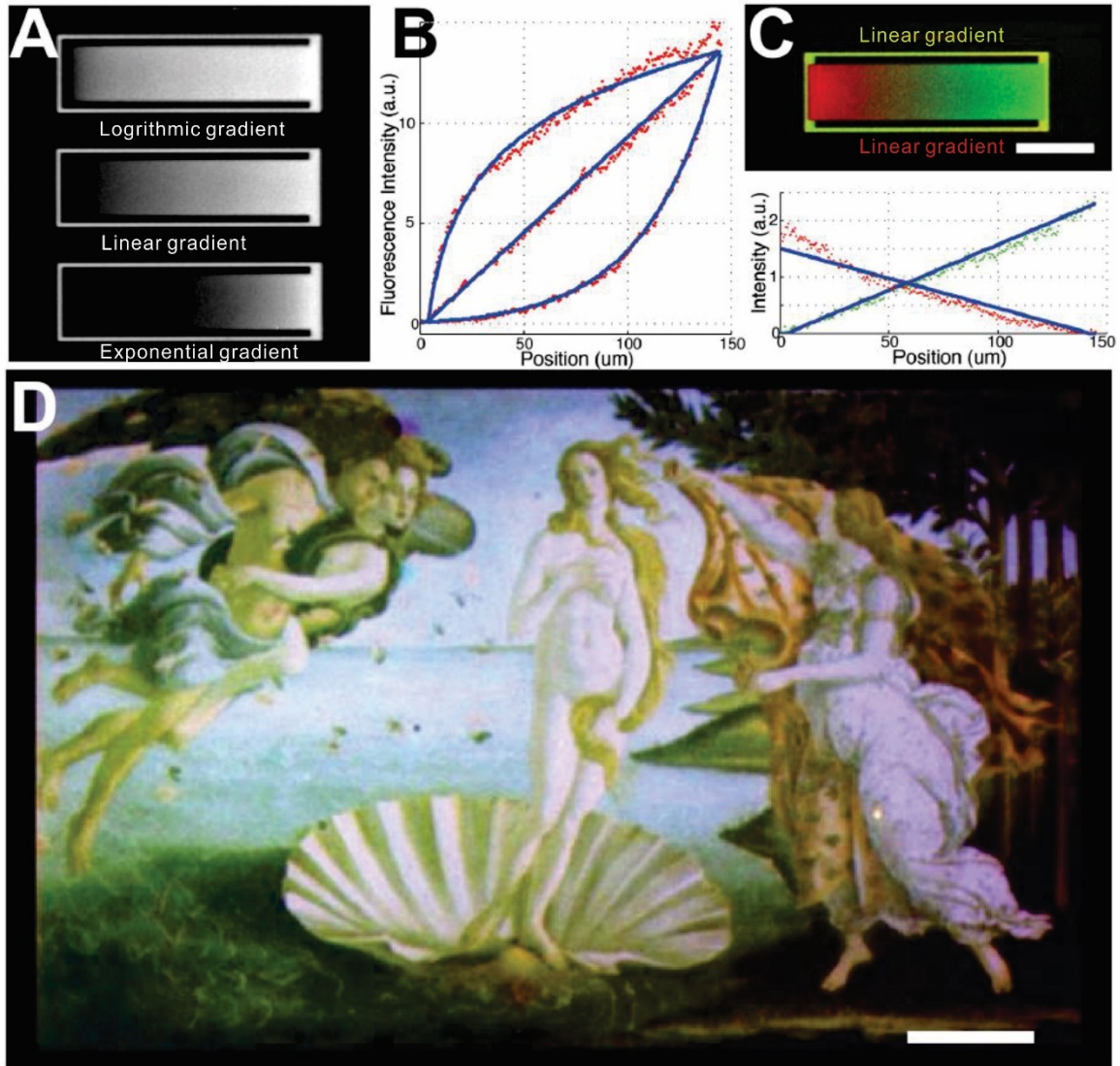
Figure 2.4 A) fluorescent microscopy images of different gradients and their B) curve analyses. C) Two protein gradients fluorescent microscopy images and curve analysis. D) Three-protein fluorescence microscopy image illustration with scale bar: 50 μm. Reprinted with permission from [7] . Copyright (2015) WILEY-VCH Verlag GmbH & Co. KGaA, Weinheim

The commercialized DMD system has been adopted and customized by Waldbaur and colleges, who have utilized protein adsorption by photobleaching (PAP) which incubated fluorescently tagged ligands onto protein-coated surface, and upon photobleaching the free-radical fluorophore on ligands would bind to the protein, to generate grayscale protein patterning, shown in Figure 2.6. [8]
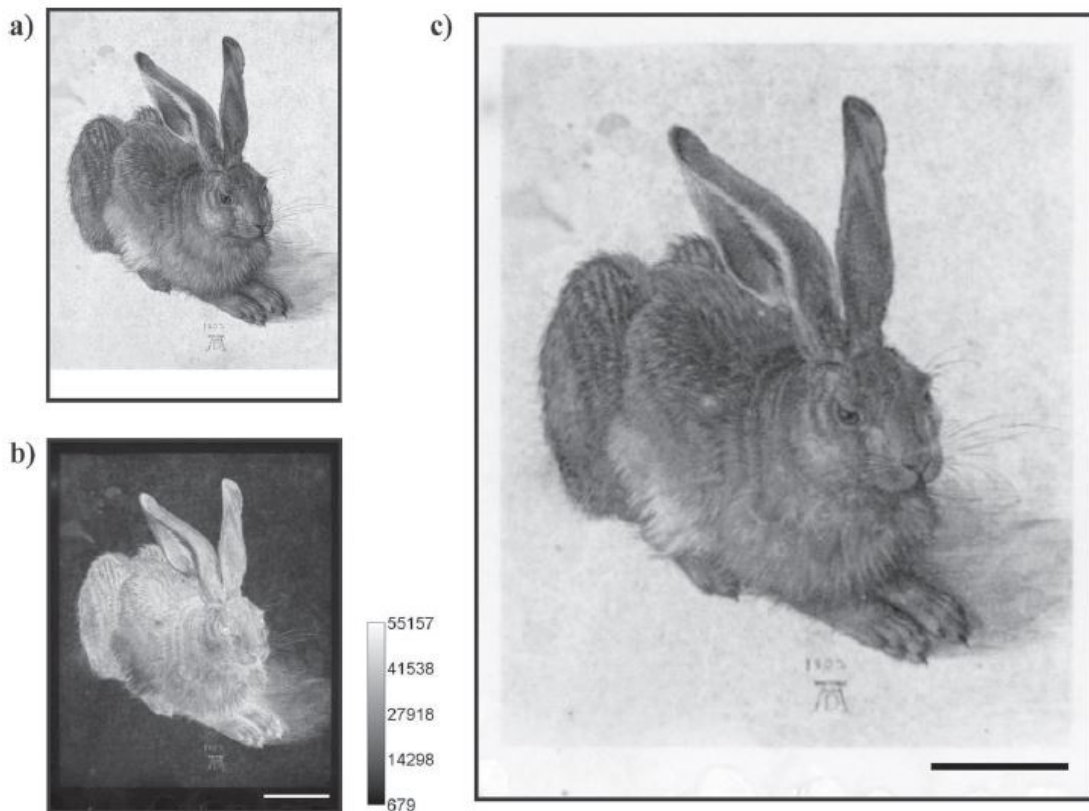
Figure 2.5 a) original image, b) fluorescent image, and c) inverted image of b), patterned with maskless DMD-based lithography method. Scale bar: 500 μm. Reprinted with permission from [8] . Copyright (2012) WILEY-VCH Verlag GmbH & Co. KGaA, Weinheim
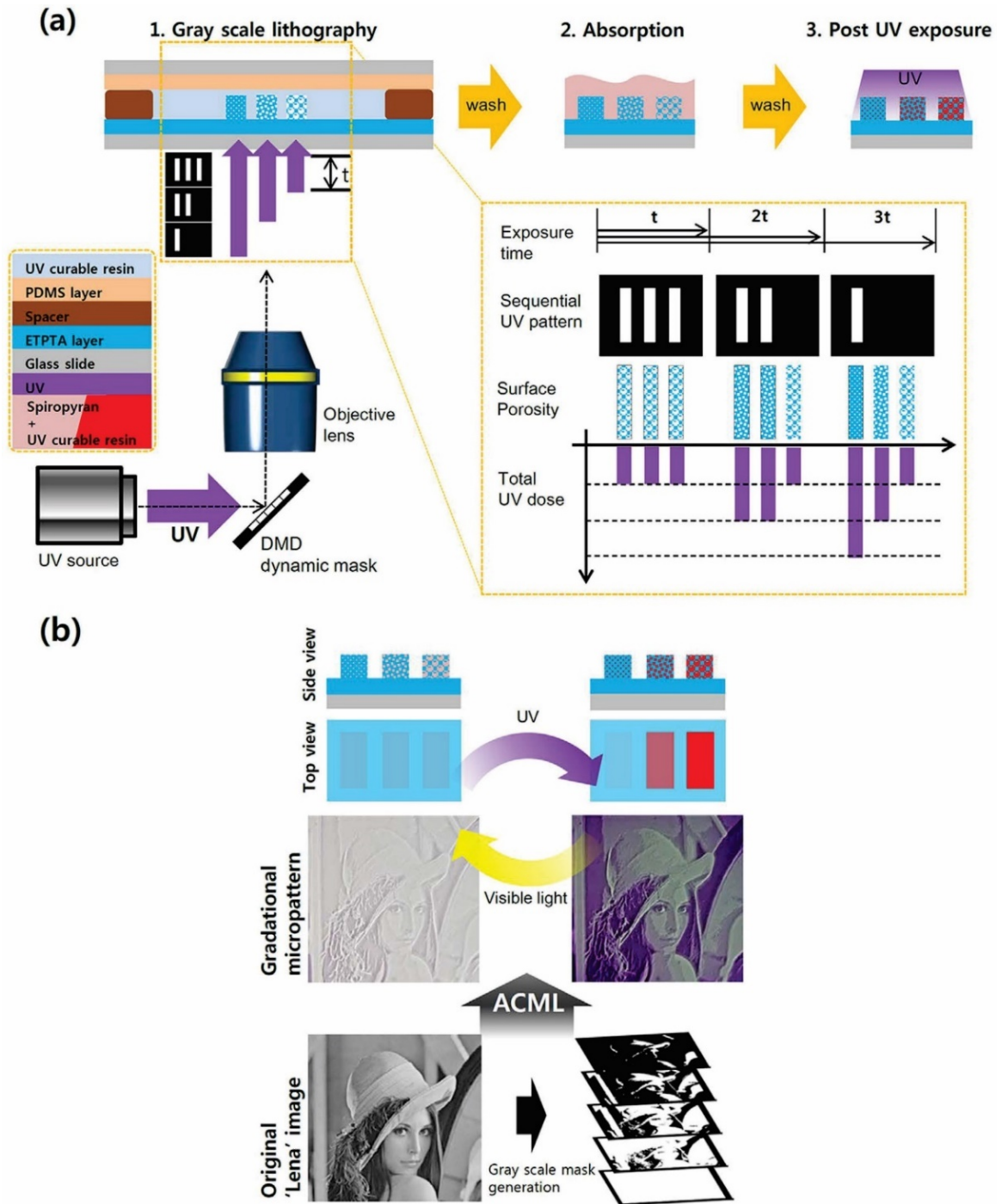
Figure 2.6 (a) Process flow of using MLCA 1) Grayscale polymerization with maskless DMD-based lithography, 2) absorption of functional material, 3) Post-UV exposure. (b) Image patterned using MLCA system. Reprinted with permission from [9]. Copyright (2015) Springer Nature.

Based on well-established Maskless Lithography systems, Jung et al. have developed Maskless Lithography Controlling Absorption (MLCA) technique as a modification to extend the benefit of DMD system. [9] Instead of direct patterning, they used the system to manipulate crosslinking densities of the polymer layer, then soaked it with selected functional material, spiropyran, to allow the adsorption. The pattern would form based on color transform of spiropyran under UV exposure, which demonstrated their proposed MLCA technique. (Figure 2.7) This method is focusing on photochromic material deposition with up to 2.5 µm resolution.

Both photomask based and maskless lithography system offers quick patterning with easy adjustable light energy control, while the latter could complete the same task in a simple manner, by software instead of physical photomasks. The operation environmental requirement and system platform size limited its applications. The equipment is expensive comparing to photomasks, especially the maskless lithography system. The patterning materials (or initial patterning) need to be photo sensitive. Other than these limitations, it could reach a resolution of 2.5 µm and offers complex grayscale surface patterning both in 2D and 3D in a quick manner, which is beneficial for a lot cases.[9]

2.2 Microcontact Printing

Soft-lithography is a non-photolithographic family of techniques for mold fabrication or replication. [10] The word "soft" indicates elastomeric materials being used in this process. Microcontact printing (µCP) is a soft-lithography based method, which aims at micro- and nano- scale surface patterning. µCP is very popular since it has been

developed due to its straight forward concept and ease of use, and has been widely adopted by many labs.

There are two main processes for using μCP. First is the elastomeric stamp fabrication to replicate pattern features, which usually involves use of photolithography to make patterned master. Second would be the printing consisting stamp, ink and the substrate, which is a flat surface. In simple words, a polymer stamp is used as an intermediary to transfer molecules in the ink to the substrate surface in a predefined pattern.

After this method has been introduced by George M. Whitesides et al. in the 1990s, its simplicity owned its popularity. [11] Researchers started to adopt this method for their own researches. Although there are variations from the first use for patterning self-assembled monolayers (SAMs) of alkanethiols on gold to function as a mask for a next-step etching, the core concept and procedures remain the same.

Figure 2.8 shows the comparison of feature patterning between photolithography and microcontact printing. Photolithography, also called UV lithography, is a process commonly used in microfabrication that uses lights to transfer geometric pattern from a photomask to photoresist material, which is sensitive to light energy. This however could also be treated as a typical flow chart for conventional μCP.

First, a master molds with pattern features is needed. This is normally varied by different desires, historically, these molds were typically fabricated using photolithographic methods. A photosensitive material (photoresist) would be applied to a silicon wafer and evenly distributed on the surface using a spin coating process. Then, this layer would be exposed to UV light through a patterned chrome-glass photomask, causing only the areas exposed to the UV light to cure. After this step, the rest of the uncured

photoresist layer could be washed away by a developer solution, thus forming the "master pattern" template shown in Figure 2.8.
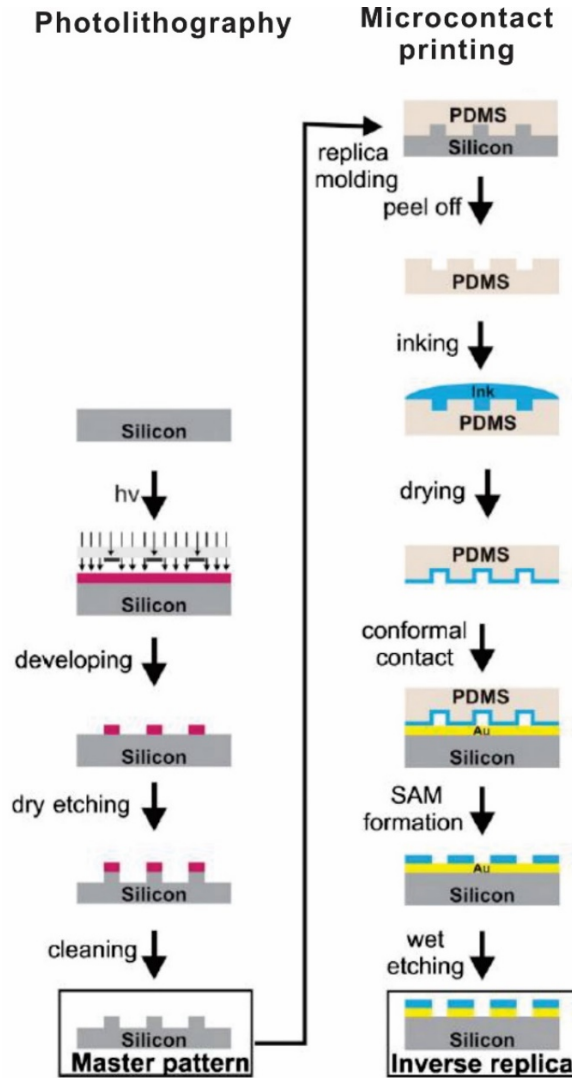
Figure 2.7 Schematics of microcontact printing. Photolithography is a prerequisite for master fabrication. Reprinted with permission from [12] . Copyright (2009) WILEY-VCH Verlag GmbH & Co. KGaA, Weinheim

Once the master template has been fabricated, the stamp material is usually poured onto this surface containing micro- or nano- structures to replicate surface patterns and generate a negative mold. Polydimethylsiloxane, abbreviated as PDMS, is the most widely

used elastomer to make µCP stamps. The cured PDMS is transparent and thus provide the convenience for later visual or microscopic inspections. It is obtained by pouring the ratio pre-determined mixture of polymer base solution and curing agent onto template surface, and thermally curing it. The process is rather easy and intuitive, and the involved lithography process guarantees its precision. The following step is to allow contact between the stamp surface and ink materials, so "ink" would be transferred onto stamp surface. After "ink" has been transferred onto stamp surface, it would be dried before use. Last step is to apply the stamp on desired surface to let "ink" transfer onto the substrate in a patterned form. After that, the stamp could be removed and leave the patterned surface ready.

Inking procedure includes two steps, soaking and releasing. Based on the patterning format, there is limited room for inking to be "improved" or "developed" other than being combined with other methods. A few years since its appearance, Emmanuel Delamarche et al. [13] has discussed three major different ink soaking methods, stamp soaking in ink solution (A), stamp with ink reservoir (B), and dip-N-stamp (C), as shown in Figure 2.9.
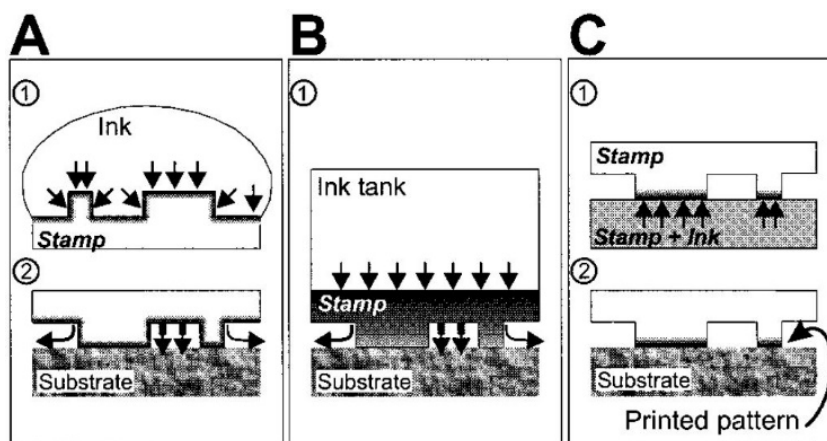
Figure 2.8 Three different ways for inking the stamp. A. (1) stamp pattern surface complete exposure to ink solution, (2) stamp contacting substrate to transfer ink; B. ink solution diffuse through stamp onto substrate to form patterns; C. (1) stamp pattern surface contacting with ink to absorb ink, (2) stamp pattern surface contacting substrate to release ink. Reprinted with permission from [13]. Copyright (1999) American Chemical Society

Method (A) and (C) have followed the steps closely, while method (B) integrated them together. Method (A) would expose stamp surface with features completely to the ink. This allows molecules to contact with both feature and non-feature regions. The major problem could be the interference from adjacent non-feature area, especially when feature height is low and the collapse of the feature area. Method (B) carries an ink tank that could supply high throughput for large amount of molecule deposition. It relies on molecular diffusion through thin stamp which makes local control difficult. Ink tank design also makes it relatively difficult to use repeatedly. Method (C) only allows featured region to contact with ink, which was pre-soaked in a polymer stamp. Release would be the same as method (A). This ink soaking process takes a long time, which makes it not so efficient timewise. Although lacking high throughput naturally, it provides the highest precision among the three. These basic inking formats have been utilized mostly for PDMS stamps and its similarities.

As mentioned earlier, µCP was first introduced by Whitesides et al. in 1993 in order to generate pattern of gold which has been pre-coated on silicon substrates. [11] In their work, it was demonstrated that with Novolac resin polymer stamp which is commercially available, and PDMS stamps which is lab prepared stamps, µCP could generate patterns of SAMs of alkanethiolates on the Au surface to prevent the etching from the combination of aqueous, alkaline cyanide ion and dioxygen. [14] SAMs form when organic molecules (organic thiols and disulfides) spontaneously chemisorb on solid surfaces (gold, silver, copper, etc.). [15] They are a fundamental component of micro- and nano-science, and extremely useful in chemical and bio-related researches. The schematic chart of this patterning is identical with Figure 2.8 that SAM formation has been absorbed onto PDMS

surface, then transferred onto gold substrate or substrates of other materials by PDMS stamp. Those SAMs would be utilized as protective "masks" to preserve under-covered substrate materials from being etched away. Comparing to some conventional SAMs patterning techniques, µCP has shown its great advantages of the simple concept, ease of operation, low cost, short preparation time, and modification potentials, and has soon become popular. Many researchers started to take advantages of this then innovative patterning method and brought enormous development to µCP.

Researchers have done µCP with SAMs after its born for a variety of purposes, from the attachment of proteins and cells to surface chemistry altering. Tian et al. have utilized SAMs with stamps, by modifying stamp surface wettability at the beginning. Selected ink material was absorbed onto feature surface of stamp first, then transferred onto substrate, as indicated in Figure 2.10 (b). [16] SAMs could also be used as barriers for substrates. In Benore et al.'s work, µCP was combined with selective wetting/dewetting to generate SAMs functioning as the "mask". After substrate absorbing polymers, SAMs were then removed to leave only polymer patterns. [17]
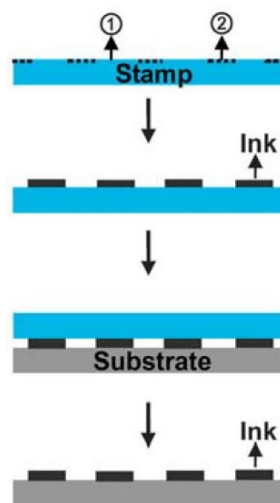
Figure 2.9 Schematics of modified microcontact printing with SAMs. (1) and (2) indicate opposite surface wettability. Ink would only adhere on one wettability state stamp surface,

and being transferred onto substrate. Reprinted with permission from [16]. Copyright (2013) The Royal Society of Chemistry.
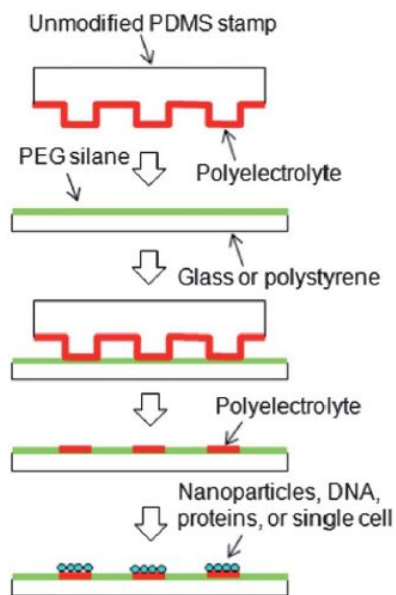
Figure 2.10 PEG silane surface coating enhanced surface attachment to polymers. Reprinted with permission from [18]. Copyright (2012) The Royal Society of Chemistry.

Concept of SAMs patterning has been extended to other molecules. Wang et al. have patterned polyelectrolyte on polyethylene glycol (PEG) silane coated glass or polystyrene for future nanoparticles attachment, such as proteins, DNA and cells. [18] Process schematics are similar with typical μCP, as shown in Figure 2.11. In a similar situation, C. Thibault et al. have directly patterned oligonucleotide on glass slides to form DNA arrays. [19] Pan et al. have generated rhodamine-labeled bovine serum albumin (BSA) pattern on aldehyde-functionalized titanium surfaces. [20] An improvement was brought by Chien et al. to use Polydopamine (PDA) as ink. [21] The benefit of this molecule is the versatile compatibility with multiple types of substrates, such as glass, silicon, gold, polystyrene, and poly(ethylene glycol) via microcontact printing. And it is capable of promoting protein absorption and cell adhesion.

The patterning of different ink materials by using default unmodified stamps have been greatly adopted due to its advantages. At its early stage, PDMS stamps were remained unmodified until researchers could not bear its limitations, which are noticeable and inevitable. The most common deformation problems may happen to PDMS stamps are feature collapse (including lateral collapse) and stamp sagging, as shown in Figure 2.12. Collapse would normally happen when feature height h is much larger than feature width w. Since the features are typically in micro scales or smaller, force applied to stamps is easily overwhelm its upper limit, thus generate the collapse. Figure 2.12 (B) and (C) are showing two typical collapse formats. Sagging is another issue, which is usually caused by large thin PDMS stamps. When a thin stamp has a large patterning surface region, chances are sagging would occur if without proper supporting design. Other than deformation issues, there are some limitations, such as contamination that prevents PDMS stamps from being used repeatedly.
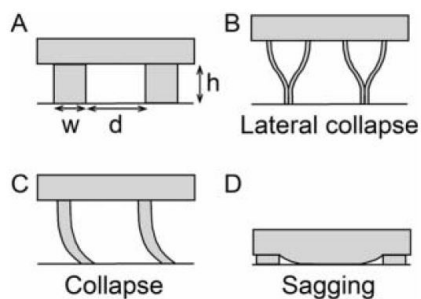
Figure 2.11 Diagrams illustrating commonly seen deformation types. Reprinted with permission from [22]. Copyright (2007) The Royal Society of Chemistry.

In order to implement those revealed issues, a variety of remedies have been proposed and tested or even evaluated. Some employed new materials or new strategies to reduce the limitation effects, some even exploited the limitation and turned it into benefits.

Filipponi et al. have created pyramidal PDMS stamps using this unique idea to yield remarkably low background noise for better fluorescence detection. [23] Pyramid-like microfeatures organized in arrays were collapsed when placed over flat substrates, which would give a more sensitive stamp feature. Tanaka et al. focus on the applied force which directly causes collapse, and developed an automated stamping system composed of a load cell and an automated actuator to fine control the applied stamping force with minimum of 0.1 N, for stamp stiffness calibration and cell sheet micropatterning. [24] Other than improvement done to unmodified PDMS based μCP, other solutions have been provided to minimize the limitations, such as different polymeric stamps. Li et al. have discovered several benefits from replacing PDMS with Polyurethane-acrylates (PUAs) as stamp material, which include higher surface energy permitting inking with hydrophilic materials, higher Young's modulus which represents a more rigid stamp than PDMS, and a more convenient way of controlling surface chemistry so extra coating step is no longer needed. [25]

Some other strategies for improvement include either new materials or new experimental steps. D'Arcangelo et al. have utilized Bovine serum albumin (BSA, the protein) to apply a coat of inactivation outside adhesive regions, so the adhesiveness to background noise ratio would be noticeably improved. [26] Pan et al. chose to pattern fibronectin on polystyrene (PS) surfaces for protein adhesion. [27] Castano et al. innovatively created protein patterns on hydrogels for later cell attachment, which has been pre-processed by freeze-drying. [28] Feng et al. brought "reactive" concept to μCP to replace traditional absorption by pre-coating substrate with reactive polystyrene-block-poly(tert-butylacrylate) deblock copolymer films. [29] Covalent binding would form much

more robust and strong attachment between molecules. Additional strategies described by

N. A. A. Rahman et al. and Zhu et al. combined μCP with other methods. [30, 31] The first

group used μCP and Electroporation (EP) for controlling cell function which could be led

to variety of medical applications. The second group mixed μCP with bottom-up

techniques (general concept of producing nanoparticles from atoms, from small to large)

for patterning thicker and multiplayer patterns.

As concentration gradients are useful for cell biology, e.g., chemotactic cells are

sensitive to concentration differences as low as 2%, [32] Researchers have been trying to

expand the use of μCP to this more complicated patterning. Michael Mayer et al. has again

introduced patterning of gradients of proteins in 2004, 10 years after μCP's debut. (Figure

2.13) [33]
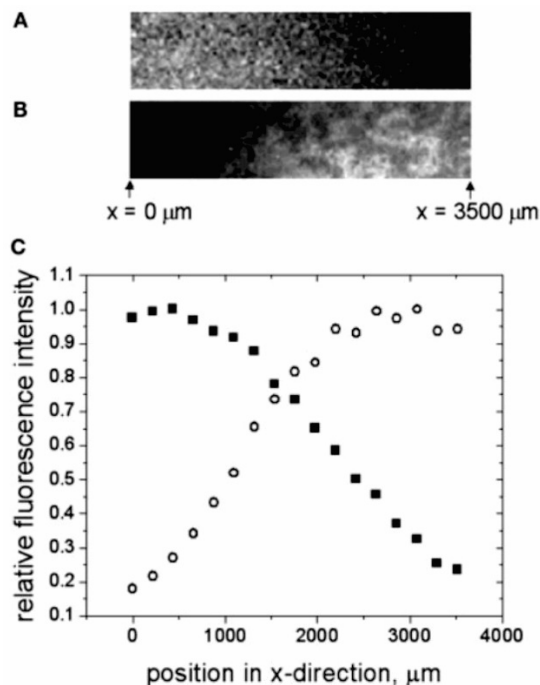
Figure 2.12 Two-fluorophore tagged protein diffused into flat agarose gel stamp and generated two gradients (A) and (B). (C) showed the analysis curves. Reprinted with permission from [33]. Copyright (2004) WILEY-VCH Verlag GmbH & Co. KGaA, Weinheim

The original embodiment has been modified with replacing PDMS stamp with agarose hydrogel. The purpose of adopting this hydrogel was to pre-generate gradient ink pattern before printing. The agarose hydrogel was casted against a prepared PDMS stamp. When the hydrogel was ready, FITC-BSA (Fluorescein isothiocyanate, a derivative fluorescein) and TRITC-BSA (Tetramethylrhodamine, a bright orange fluorescent dye) were allowed to diffuse into the hydrogel from opposite ends. The diffusion lasted for 4-7 hours depending on the stamp and features. When it was ready, the gradients of proteins would be transferred to a glass slide before examination. This gradient purely relies on molecular diffusion thus it took hours to finish the preparation. Also, because diffusion is non-stoppable, it would occur when the gradients were being transferred to substrates, which should be taken into consideration when designing hydrogel stamps.

Philipsborn and their group also looked into the "gradient" path, as they generated graded patterns of proteins with "lift-off" method. To achieve so, PDMS stamp with flat surface would be coated with protein molecules. A silicon master with patterns will contact with PDMS coated surface and etched away unwanted proteins. The negative pattern of proteins on PDMS surface would be transferred onto glass substrate by direct contact.[34] In this method, "higher concentration" would be expressed by higher density pattern arrays as seen from Figure 2.14. This type of patterning would be the closest-to-gradient patterning by using μCP without employing diffusion into the system.
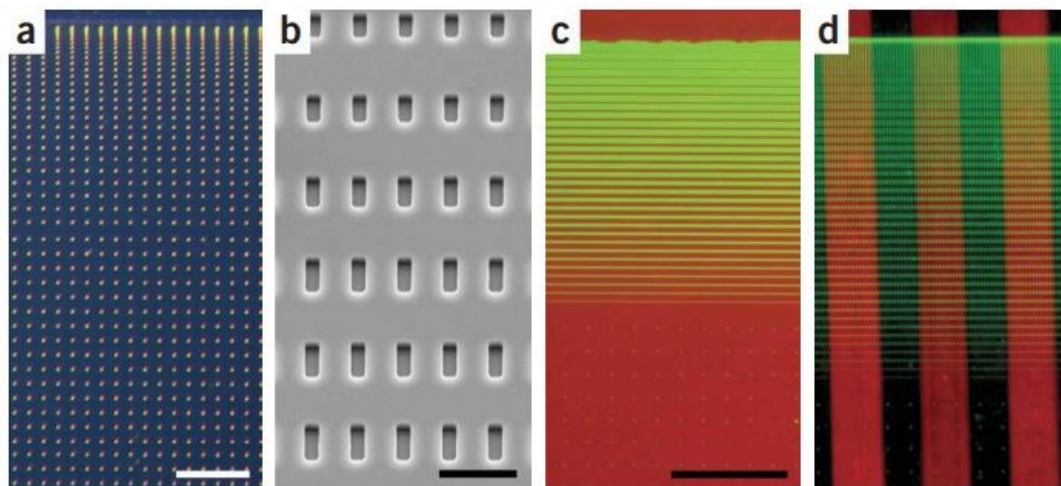
Figure 2.13 Gradational patterns of (a) Silicon master, (b) closer look at silicon master, (c) and (d) are protein patterns. Scale bars: a,c,d, 100 mm; b, 5 mm. Reprinted with permission from [34]. Copyright (2006) Springer Nature.

Overall, micro contact printing is a simple, relatively inexpensive way to create patterns with micro- or submicro-scale features. The stamps can be fabricated on a small budget without cleanroom environment and used repeatedly without fast degradation of performance to achieve a decent resolution. However, as stated above, some problems, such as shrinking and swelling of the stamps that could cause feature distortion, contamination and uncontrollable diffusion of special ink materials, were born with this method. The simple format also limited its applications within simple features like arrays of binary patterns, which was the main reason for researchers to use µCP. Researcher have done various attempts to perfect this mature patterning technique and expand its usage beyond large scale arrays or parallel printing. So far, there was no true grayscale patterning, the escalated gradient patterning, being accomplished yet after almost 3 decades since the initial existence of this famous patterning technique, even though sometimes the "gradient" has been referred as "grayscale".

2.3   Microfluidics Patterning

Microfluidics patterning (µFP) is another popular soft-lithography based patterning method, which relies on single or multiple sealed tunnels to deliver liquid contained molecules onto substrates. The word "microfluidics" refer to methods and devices that manipulate fluid flows by using small scale tunnels and chambers.

As being introduced by Delamarche et al, patterning with microfluidic networks (µFN), a new method using soft lithography, was developed originally to solve two limitations of the original µCP, milliliter quantities of ink solution usage and one molecule deposition at a time. [35] Although researchers have developed µCP to pattern multiple molecules on one surface, but it was still limited to once at each stamping. µFP solved this problem with its capability of patterning multiple molecules at one time, without interfering each other. µFP consists of two basic structures, the substrate which is ready to collect or absorb molecules from the fluid flow, and the channel for fluid flow to pass through that are embedded in elastomers by using soft-lithography methods. In order to fully expand its advantage, multiple channels (channel networks) are usually adopted in design.

The general form is shown in Figure 2.15, that fluid flow carrying molecules passes through the channels and the pre-selected substrate surface would bind molecules and generate patterns. Available substrate materials include glass (e.g. N-hydroxysuccinimide, NHS, attached glass slides), hydrophobic Silicon, polystyrene. [36] Channels can be formed in a variety of shapes, from simple parallel channels to much more complex geometry. When patterning is complete, unlike microfluidics devices focusing on utilizing the channels, the elastomers need to be removed to reveal the patterns.
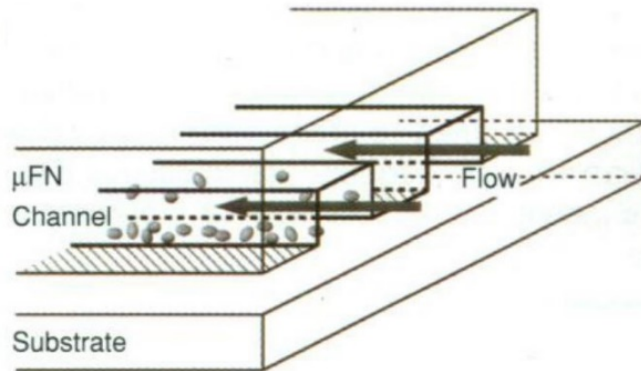
Figure 2.14 Silicon material with patterns formed microfluidic channels by contacting the substrate. Reprinted with permission from [35]. Copyright (1997) The American Association for the Advancement of Science.

Researchers have utilized µFP to conduct experiments in different fields. Delamarche et al. first developed this µFP method, and used it to successfully pattern proteins onto a surface. [36] Philipsborn et al. have combined µFP with µCP as an extra step to generate graded (close-to-gradient) protein patterns for signaling processes such as morphogenesis, cell migration and axon guidance. [37] They first use µFN to generate graded protein patterns on small elastomer cuboid surface, then µCP to transfer the pattern onto petri dish surface.

Two years after patterning use of µFN, Takayama et al. found an interesting phenomenon that laminar flows of multiple parallel liquid streams in rectangular capillaries would remain their parallelization and remain unmixed. [38] This was due to the fact that liquid flows in capillaries have low Reynolds number (Re) and thus the laminar flows. (Figure 2.16) This is an important discovery which realized multiple molecules deposition within one channel.
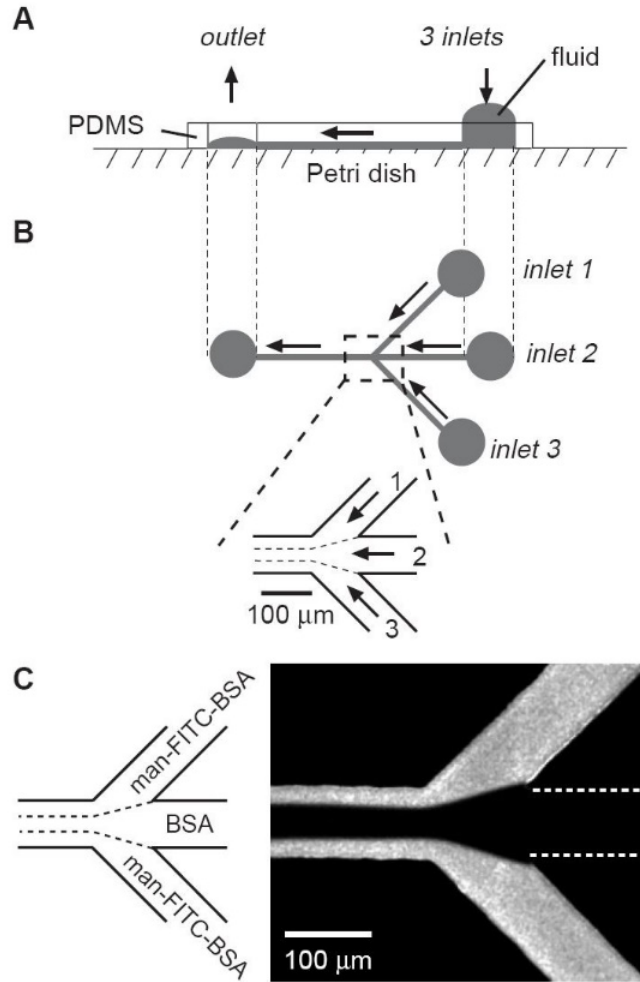
Figure 2.15 Schematics of laminar flow patterning. (A) Side view of channels; (B) Top view of channels; (C) Laminar flow illustration diagram and its formed patterns. Copyright (1999) National Academy of Sciences. U.S.A. Reprinted with permission from [38]. Copyright (1999) National Academy of Sciences.

After the reveal of laminar flow use, gradient patterning became much easier. Jeon et al. designed a classical 3 inlets – 1 outlet μFN combined with laminar flows to generate gradient pattern. [32] In Figure 2.17, it was just a branch to illustrate the basic concept. It could be expanded to 5 or more levels which makes it look like Christmas Tree, which has been referred by Whitesides et al. as "Christmas Tree Structure". [39] The fluorescence solution "gradient" can be check in Figure 2.18, which looks like several graded strips have been seamlessly stitched together.
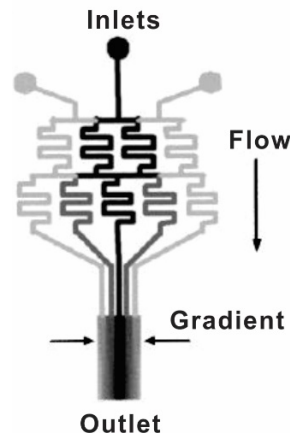
Figure 2.16 Diagram illustrating the "Christmas tree" channels. Reprinted with permission from [32]. Copyright (2000) American Chemical Society.
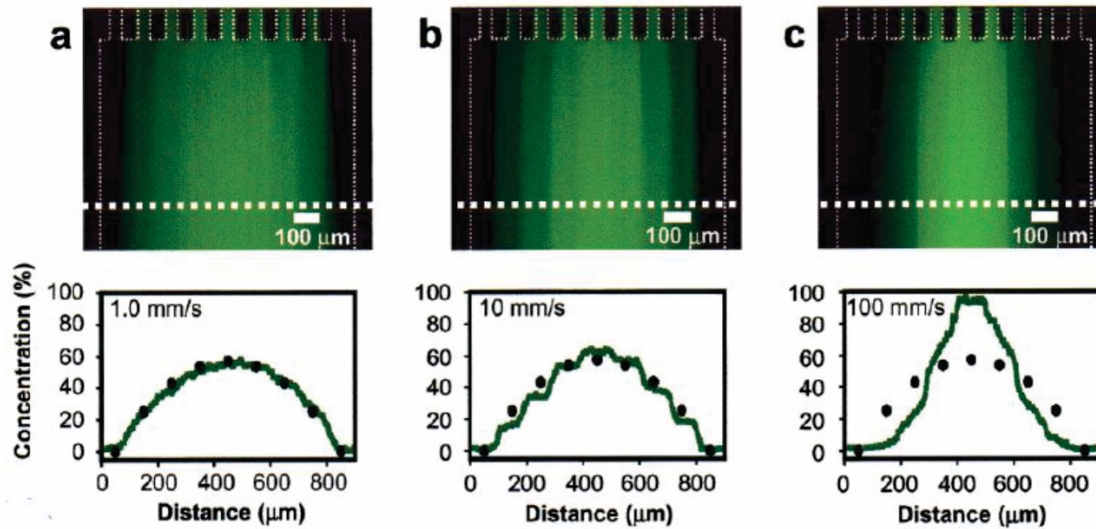
Figure 2.17 Fluorescence microscopy images of microfluidics patterning. Three images showed different gradient patterning curves with flow rates adjusted. Reprinted with permission from [32]. Copyright (2000) American Chemical Society.

The common μFP methods normally used syringes to drive the flows within the channels, which is pressure or vacuum driven. Since the final step of μFP is to remove the elastomer and reveal the surface pattern, the channel sealing must be reversible. According to Whitesides et al., irreversibly sealed structures can withstand pressures up to 50 psi, while conformally sealed structures can withstand up to 5 psi. [40] On the contrary, vacuum driven would be suitable for wider range of applications. There is also electrokinetic driven

25

for µFP, which utilizes voltage to drive the charged molecules to induce the flow movement.[40] The benefit is obvious that voltage altering makes fine control more flexible. The limitations include much more expensive equipment which involves complex operation, suitable buffer solutions and molecule materials. Based on the fact that electrokinetic driven µFP has too many limitations over its benefit, pressure or vacuum driven µFP is more popular and commonly seen.
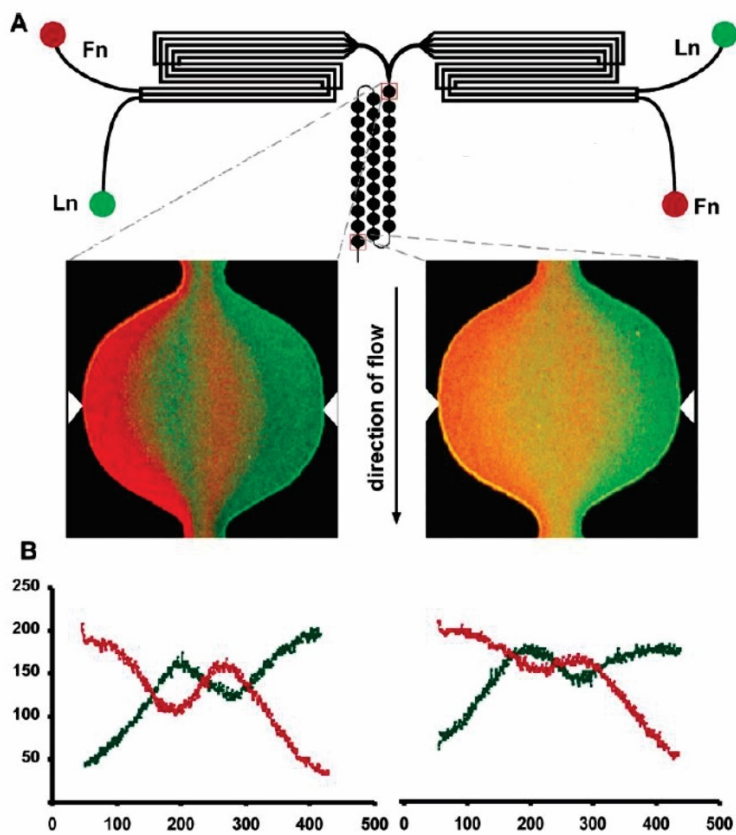
Figure 2.18 (A) Diagram illustrated experimental setup; (B) Gradient curves in dimension that is perpendicular to flow direction. Reprinted with permission from [41]. Copyright (2005) American Chemical Society.

Even though µFP is totally capable of producing gradients, they are perpendicular to the liquid flows direction, which limited its possibility of complexity. Jiang et al. have generated overlapping gradients of laminin (Ln) and fibronectin (Fn), which are in the same

dimension. (Figure 2.19) [41] There has no "real" complex 2-D surface patterning been spotted yet.

Overall, μFP method is another soft lithography-based method that is easy to use and modify. Although soft silicone material is an essential part of the method, μFP relies on a completely different structure than μCP. Small scale channels generally consume less than microliter solution and are suitable for scarce or precious reagents which produce relatively small amount of waste. PDMS has been greatly used for generating μFN for its simplicity, good surface feature replication capability, excellent bio-compatibility, and easy plasma bonding characteristic. However, because of the requirement of using ink in a solution format, μFP is only able to generate patterns as complicated as gradients. Grayscale patterns have not yet been observed by author to be generated by microfluidics channels.

2.4 Inkjet Printing

The aforementioned soft-lithography based patterning methods have been well defined, reliable, and widely used, they still require a prerequisite photolithographic process which uses photomasks, which are usually expensive and time consuming to fabricate/order, and cost more if any modification is further needed. Under such circumstance, "mask-less" patterning methods and their variants have been developed and serve as alternatives, such as ink-jet printing

Inkjet printing is a patterning method that uses modified versions of commercially available inkjet printers to deliver nanoliter volumes of liquids onto a substrate with help of programmable microcomputer chips and robotic components. Because of the adoption

of commercially available printers, it is relatively low cost, easy to use, and accessible to all.
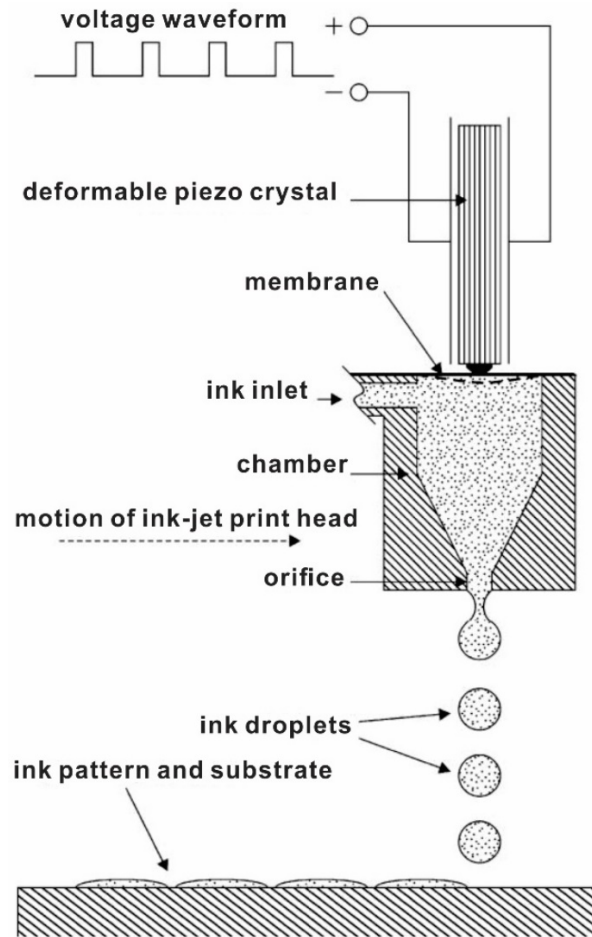
Figure 2.19 Diagram of the operation of ink-jet printing. Reprinted with permission from [42]. Copyright (2004) Elsevier B.V.

Neville and Sawyer modified this technique and turned it into a surface micro patterning instrument, which allows cell-adhesive patterns of collagen/poly-D-lysine (PDL) to be printed on glass surface which was pre-coated with covalently bonded poly(ethylene) glycol (PEG) as cell-repulsive background material. [42] As shown in Figure 2.20, inkjet printing generates ink drops when there is patterning signal coming in, which is called drop-on-demand mechanism. In their work, in order to succeed cell pattern

adhesion, both cell-repulsive and cell-adhesive materials must be used. To achieve this goal, they chose poly(ethylene) glycol (PEG) as the cell-repelling background and coated it on the glass coverslip. Then a collagen/poly-D-lysine (PDL) mixture has been patterned on the PEG coating through inkjet printing.

Similarly, inkjet printing has been adopted previously for applications like biosensor development, [43] DNA arrays, [44] micro deposition of active proteins on cellulose, [45] etc. Inkjet printing has also been used for non-bio related applications, such as light-emitting diode (LED) fabrication, [46] all-polymer transistor circuits printing, [47] and production of solar cells,[48] memory components,[49] sensors [50] and detectors.[51] The resolution of inkjet printing has been reported to reach 100 μm when dealing with protein patterning. [52] Sirringhaus et al have also mentioned 80 μm sessile droplet radius in their work of printing all polymer transistor circuits. [47] Due to the nozzle structure of inkjet printer, it is difficult to hugely reduce droplet/pattern sizes while still maintain a precise control.

Gradient patterning by inkjet printing has also been demonstrated by Miller and his colleagues. [53] They successfully printed fluorescently labeled bone morephogenetic protein-2 (BMP-2) and insulin-like growth factor-II (IGF-II) bio-inks on fibrin-coated glass surfaces. The method is shown in Figure 2.21. Instead of applying one layer, their group overprinted multiple layers of ink on the substrate in order to generate concentration differences. This concept is simple and easy to apply by designing and realizing with computer. This method could also generate grayscale patterning, although it has not been demonstrated in their work. The functional concentration gradient has been demonstrated to last for up to a week.
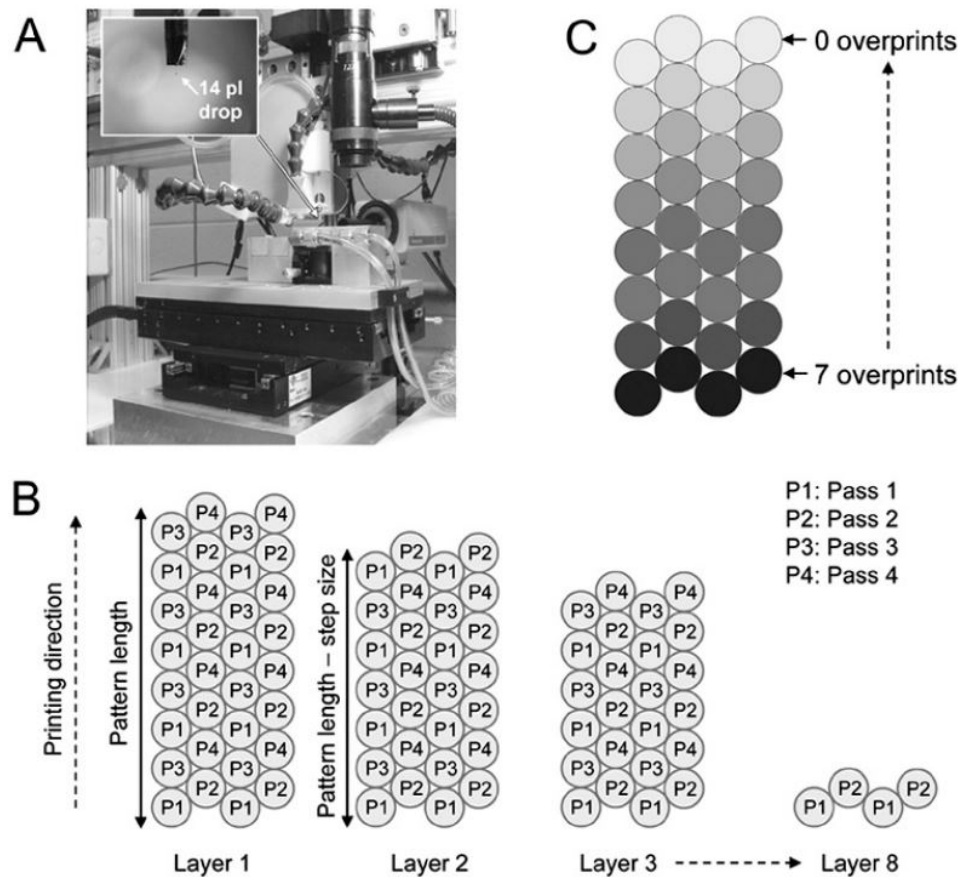
Figure 2.20 (A) Customized inkjet printer; (B) Schematics of overprint strategy for creating a linear gradient; (C) Illustration of the gradient pattern. Reprinted with permission from [53]. Copyright (2009) Bentham Science Publishers Ltd.

Kaiyong et al. have modified inkjet printer with ink container sanitized and cleaned. They also pre-determined the data sheet of relationship between pattern concentration and molecular gradient density and manipulated ink droplet volume for varying densities. Thus, for one time printing the gradient/grayscale patterning of 1mM 11-mercaptoundecanoic acid (MUA) could be generated onto gold-coated silicon wafer substrates. [54] Laminin protein molecules would be covalently linked with carboxylic acid groups to generate protein gradient for later cell culture use.

Inkjet printing costs less, has an easy operation system and highly reproducible design, its non-contact printing also prevents potential cross contamination. However,

concentration gradient patterning resolution of either overlap printing or droplet volume variation methods still relies on the native resolution of inkjet printer itself, and the relatively low spatial resolution constrained its adoption by sub-micron scale researches.

2.5   Scanning Probe Microscopy-based Methods

Scanning probe microscopy (SPM) is a microscopy that generates images from scanning results of interactions between physical probes and specimen. It has been used to investigate surface properties, which contains many different microscopies including Atomic Force Microscopy (AFM), scanning tunneling microscopy (STM), scanning thermal microscopy (SThM) etc. SPM based lithography (SPL) describes several nanolithographic methods such as Dip-pen nanolithography (DPN) and thermal-chemical scanning probe lithography (tc-SPL). This type of patterning method directly writes on the substrate without using masks, and could reach a resolution below 10nm. [55]

2.5.1 Dip-pen Nanolithography

Dip pen nanolithography (DPN) is a scanning probe lithography technique that utilizes atomic force microscope (AFM) tip to directly generate surface patterns. The sharp AFM tip, which could be as small as 1nm,[56] would carry the ink molecules and "write" them on "paper" so the molecules would be transferred to the substrate surfaces. Comparing to parallel patterning techniques such as µCP and µFP that could generate large scale surface patterns at one printing, DPN is a serial patterning technique like inkjet printing, which generates patterns one dot by one dot, thus is naturally slower in speed. Even though, DPN has its great advantage over other patterning methods that it delivers

small number of nano-size particles which could achieve extremely high spatial resolution without relying on other lithographic processes.
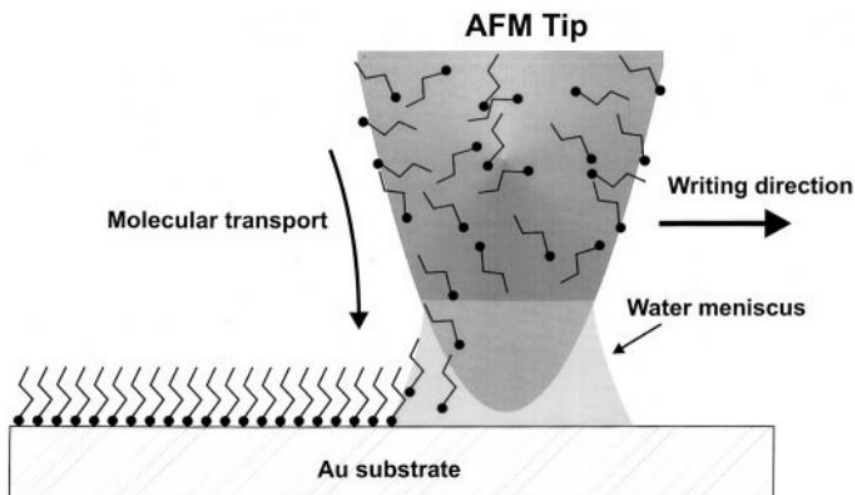
Figure 2.21 Schematic of DPN with water meniscus formation between AFM tip and substrate. Reprinted with permission from [57]. Copyright (1999) The American Association for the Advancement of Science.

Deposition through AFM tip was first discovered by Jaschke and Butt. [58] The AFM tip was first dipped into octadecanethiols (ODT) solution to load the molecules. The following step was to allow contact between loaded AFM tip and mica surface, so ODT would be transferred onto the surface to generate patterns. Richard et al. have further developed DPN by introducing water meniscus and utilized its size to control alkylthiols, 1-octadecanethiol (ODT), transport rate from "writing", effective tip contact area, and spatial resolution. [57] Figure 2.22 shows the working process of this modified DPN, where an AFM tip is deploying small amount of molecules onto the Au substrate. In a certain humidity environment, DPN is capable of generating 30 nm wide line, and it took 5 min to finish 1 μm length. Although the patterning time could be accelerated with adjusting humidity working environment of DPN, it still demonstrated the slow patterning speed.

2.5.2 Other SPL Methods

Scanning tunneling microscopy (STM) was first developed in 1980s by Binning and his colleges to obtain topographic pictures of surfaces on an atomic scale. [59] The working concept of STM is to monitor the current generated by voltage difference between the probe tip and the surface, when these two come close, which is called tunnel current. It varies when many factors change, and one is probe-surface distance. The same voltage manipulation could apply to surface patterning with SAMs replacement. Christopher and colleges have successfully replaced SAMs composed of dedecanethiolate (C12S-SAM) growing on an atomically flat gold facet with decanethiolate (C10S-SAM) thiolates. [60] As shown in Figure 2.23, dodecane solutions of thiol were chosen as the replacement media because of its nonpolar and very low dielectric characteristics. When voltage started to increase the thiol started to attach the surface and form the pattern. As the voltage kept increasing and exceeded a bias of 3v or slightly higher, replacement occurred that existing attached thiolate would be replaced by different thiolate in the solution. This characteristic has been used to create contrast image, the pattern.

It is also possible to use local oxidation reactions as a mechanism for surface patterning. Dagata et al. have demonstrated a localized pattern generation (chemical reaction) with STM working on Hydrogen-passivated silicon surfaces in air or oxygen environment. [61] Avouris et al used oxidation induced by a high density current with AFM tip and current-carrying sample surface to generate thin oxide tunneling barriers for less than 50 nm on semiconductors or metals. [62] By utilizing the strong interactions between AFM tips and surfaces, Liu et al have demonstrated nanoshaving and nanografting with AFM and STM. [63] Carroll et al. have used heated AFM tip for surface chemical reaction to generate grayscale images. (Figure 2.24) [64] The ThermoChemical NanoLithography

(TCNL) they applied could enable direct physical and chemical changes to polymer surfaces with sub-15 nm resolution.[65] They demonstrated localized gradients with spatial resolution of 20 nm and sub-180 nm resolution for the entire concentration profile.
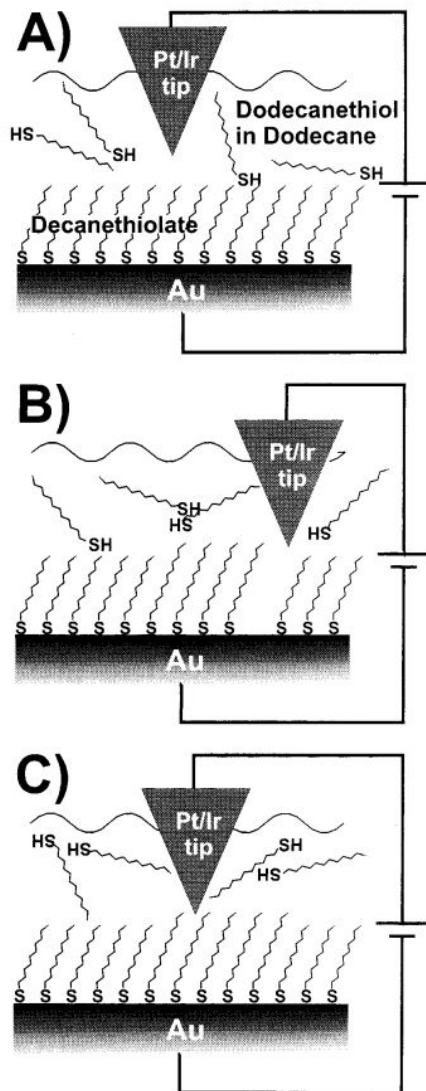
Figure 2.22 Schematics of the lithographic process of thiol replacement. Pre-attached thiolate chains (A) have been replaced with other thiolate chains (C) by the charged tip. Reprinted with permission from [60]. Copyright (2000) American Chemical Society.
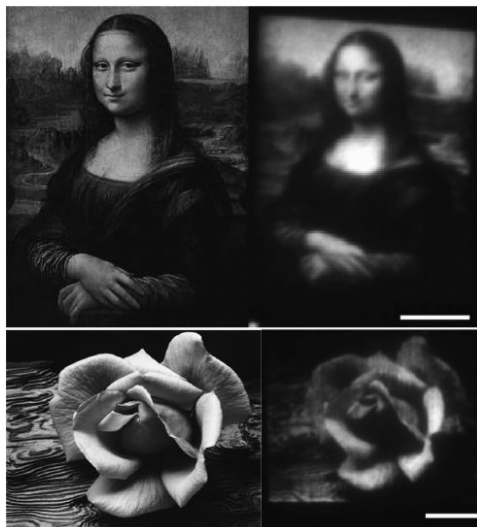
Figure 2.23 Images on the left side are original pictures. On the right side are patterned microscopy images. Scale bar: 10 μm. Reprinted with permission from [64]. Copyright (2013) American Chemical Society.

DPN and AFM based lithography methods have been widely used for its extremely high precision and resolution. Researchers have patterned on gold, germanium, silicon, and various oxides substrates with a variety of ink materials including alkylthiols, ferrocenylthiols, silazanes, proteins, DNA, metal salts, fluorescent dyes, conjugated polymers, alkynes, and alkoxysilanes. [66] The equipment is commercially available, the direct "writing" patterning style saves several procedures comparing to above mentioned parallel patterning methods. Hong et al. even developed parallel DPN to implement its slow speed limitation. The concept has been proposed with demonstration of 2-tip AFM along with adjustable substrate stage. [67] However, this adds to the complexity of the method, and even with multiple tips patterning is very slow.

The extraordinary resolution is the most important benefit researchers could earn from this type of lithography methods. However, there are still some major limitations, such as lack of high-throughput, and being unable to conduct gradient or grayscale patterning.

2.6   Laser-based Lithography

Laser-based lithography is a sequential lithography which takes significant longer time than lithographic methods that work in parallel such as UV photolithography and microcontact printing, to conduct a single patterning job for same scale. There are typically two types of patterning mechanisms. One is based on chemical reactions initiated by laser power which is similar with UV photolithography but in a much precise way, as it relies on coherently emitted laser beams, thus it could focus on smaller area than photolithographic patterning methods. The other utilizes high power of laser beam to ablate and generate 3D topography which will not be discussed here.

Laser based lithography includes a variety of methods. Multiphoton lithography is a direct laser lithography/writing method that has been popularly used with polymeric materials. This method could either directly generate small features with photosensitive materials that has similar patterning procedures with photolithography without using photomasks, or utilize the strong energy of laser beam to ablate the area it reaches. Jeon et al. have conducted arrays of 80 nm nanoscale features on 14 nm thick polymer brush layers with multiphoton lithography, shown in Figure 2.25. [68] This method has achieved great feature resolution. It has also been studied by Jeon and colleagues that minimum feature depended on polymer film thicknesses.
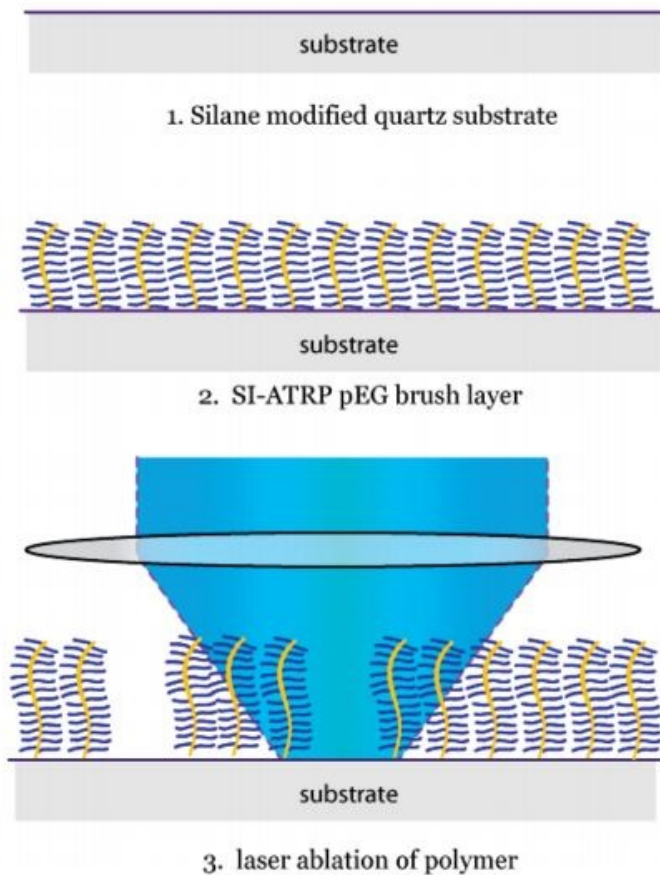
Figure 2.24 Schematic diagrams of laser ablation. Reprinted with permission from [68]. Copyright (2011) American Chemical Society.

Slater et al. have conducted patterning of cell adhesive ligands using Laser Scanning Lithography (LSL), a thermal desorption method.[69] The gold layer would increase temperature after being hit by laser beam, which will cause the desorption of alkanethiol SAMs. The SAMs not being desorbed would form the patterns. It has been demonstrated that ligand gradients can be achieved by either adjusting laser "writing" iteration numbers or tuning the angles between the surface and the focal plane. Hynes et al. have used this thermal desorption method, and expanded it to complex grayscale protein patterns.[70]

Belisle and colleagues used laser-assisted adsorption by photobleaching (LAPAP) to pattern grayscale proteins.[71] This would generates free radicals after fluorescein photobleaching, which would promote biotin binds to BSA layer that has been pre-coated on glass substrates. Protein concentration was still controlled by laser intensity thus grayscale patterning is possible and have demonstrated by Belisle and colleagues, shown in Figure 2.26.
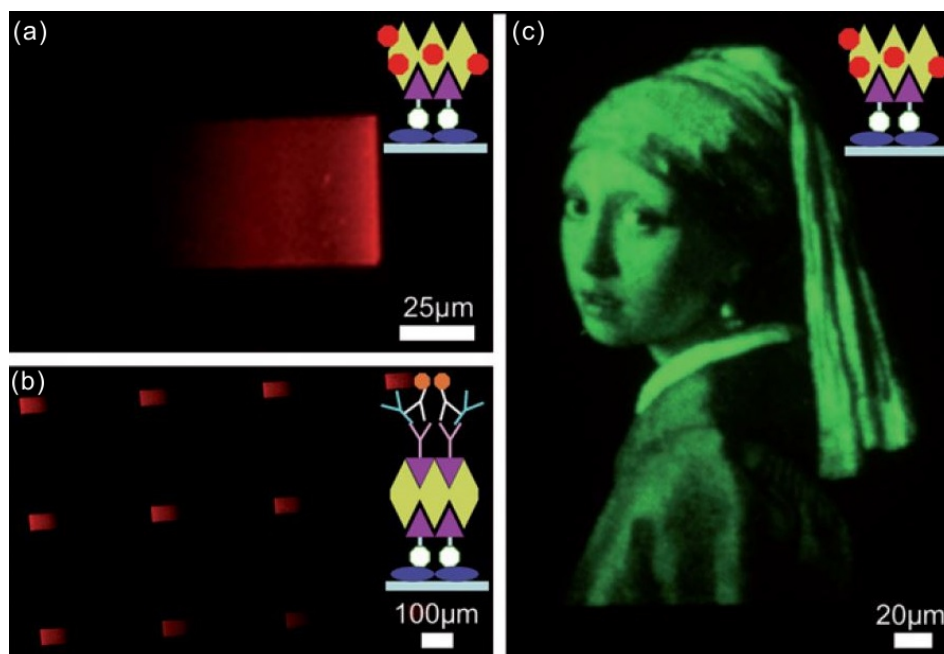
Figure 2.25　(a) Gradient patterning; (b) arrays of small gradients; (c) Fluorescent microscopy image of patterning. Reprinted with permission from [71]. Copyright (2008) The Royal Society of Chemistry.

Wiesbauer et al. have written arrays of 65 nm nanoanchors (acrylate patches) on glass substrates pre-coated with PEG 5000 silane. [72] The stimulated emission depletion (STED) lithography was a modification of 2-photon lithography, which used an extra outer rim of laser beam to inhibit the polymerization thus reduced the single feature diameter. By using this method, Wiesbauer and colleagues were able to achieve this subdiffraction-limited diameter and demonstrate more than 80% single antibody attachment. (Figure 2.27)

Similar photobleaching has been utilized by Sims et al. to immobilize Rhodamine (Rh6G0 dye on polymer coated glasses. [73]
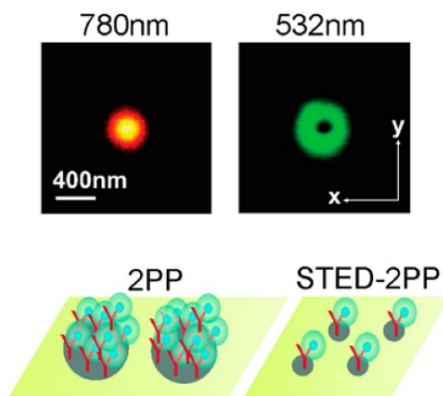
Figure 2.26 2PP excitation focus (left) and the STED lithography depletion donut-shape focus (right). Schematics of 2PP lithography and STED-2PP lithography generated anchors. Reprinted with permission from [72]. Copyright (2013) American Chemical Society.

Laser-based lithography methods were typically introduced for better resolution and smaller features, thus expected high precision was observed from above mentioned methods. The major drawback that came with high precision and serial patterning mechanism was the slow patterning rate due to small diameter of laser beams. However, there is no limitation on substrate topography and no photomask involvement, which makes it suitable for certain experiments where time is not the priority.

2.7 Other Patterning Methods
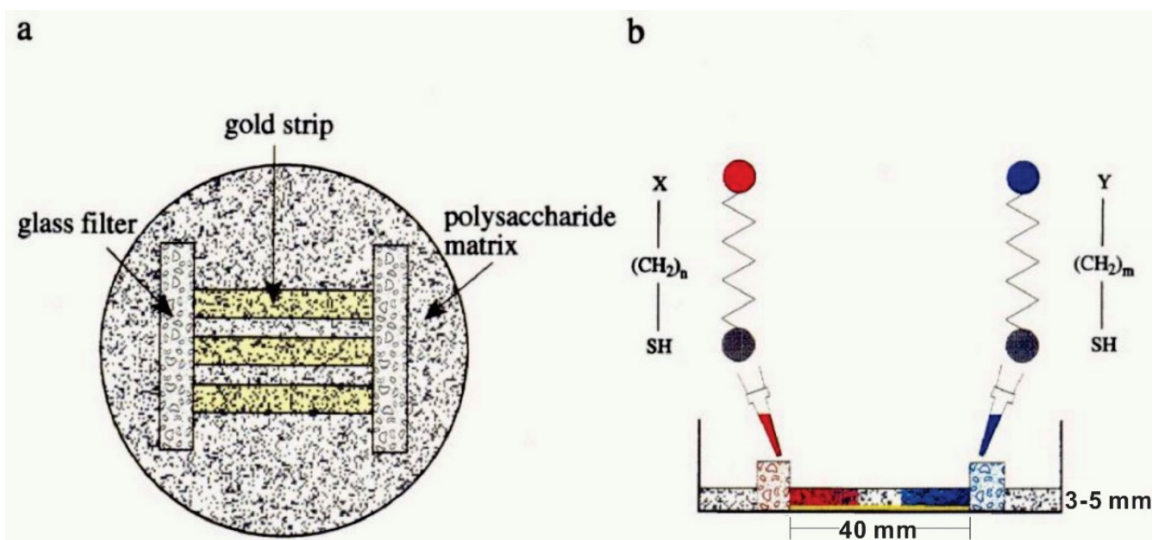
Figure 2.27 Schematic diagram of the (a) top and (b) side views of the cross-diffusion experimental setup. Reprinted with permission from [74]. Copyright (1995) American Chemical Society.

Liedberg and Tengvall have utilized alkanethiol-gold interaction to achieve one surface dimension chemical gradient with natural diffusion. [74] They demonstrated this concept with cross-diffusion setup, which consists filter glasses and diffusion matrix. The alkanethiol solutions would be pipetted into filter glasses on both ends of gold strip substrates. The matrix would provide an environment for thiols to diffuse through and contact with gold surfaces, illustrated in Figure 2.28. When diffusion started, surface areas that were closer to the filter glasses would be exposed to higher concentration of molecules and yielded higher concentration patterning. This method simply utilized molecular diffusion, so it is easy to understand or replicate. Although it was only demonstrated with one dimensional gradients generation, it has a potential to generate other slightly more complicated gradients.
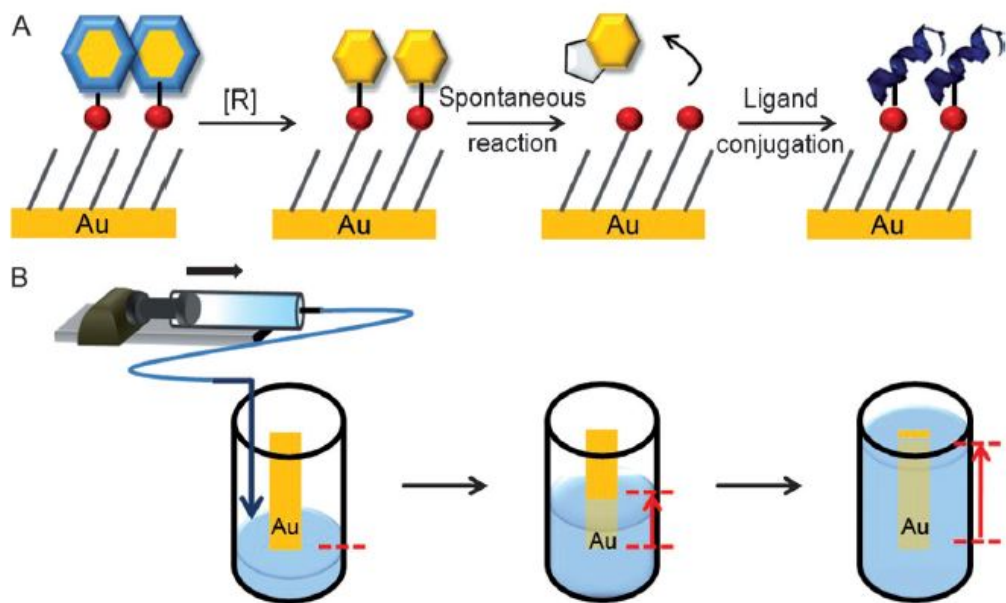
Figure 2.28 (A) Diagrams illustrating chemical reactions initiated by reducing agents; (B) Schematics of the experiment. Reprinted with permission from [75]. Copyright (2013) WILEY-VCH Verlag GmbH & Co. KGaA, Weinheim

Lee et al. submerged SAMs coated gold substrate into reducing agent solution, while the reducing reaction took a certain time, they were able to create surface gradients by controlling the submerging time. [75] To demonstrate this concept, they adopted an extremely simple form by slowly injecting this reducing agent solution into a container where the pre-treated substrate was placed in, shown in Figure 2.29. While the bottom of the substrate experienced longer time contacting with agent solution, more reactions took place and generated higher concentration of patterns. This method was straightforward, but were heavily constrained by its simple form and was unable to create more complex patterns other than unidirectional gradient.

Guan and colleges introduced a general approach to create multifunctional gradient bio-interface by controlling thermo-activated thiol-yne reaction on poly[(4-methylpropiolate-pxylylene)-co-(p-xylylene)] coated substrate surface. [76] The thermal

control was achieved by using two hot plates placed on each side of the substrate. (Figure 2.30) In Guan et al.'s work, two gradients were created to support their method. First gradient was achieved by thermos-activated thiol-yne reaction. After first gradient was formed, unreacted propiolate groups automatically formed the second gradient, and reacted with azide-terminated molecules to generate the second gradient whose concentration gradient was the opposite of first chemical gradient. The benefit of this method is the appearance of multiple molecules on same coating surface and is fairly easy to adopt. However, the limitation is obvious that two gradients can only be counter directional like diffusion activated methods. It relied on temperature gradient thus it is impossible to generate patterns other than thermal gradient shapes.
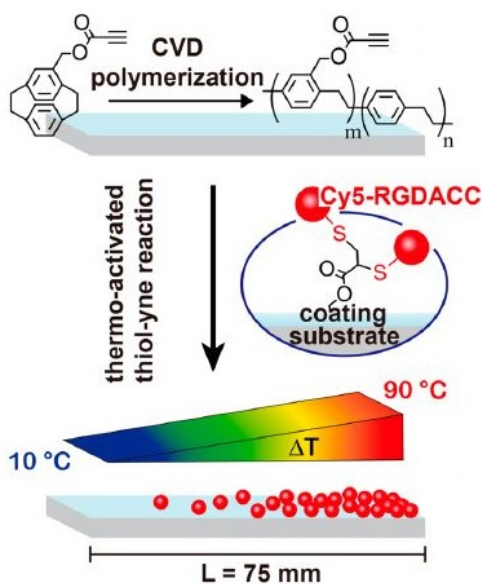
Figure 2.29 Schematics of thermos-activated thiol-yne patterning method. Reprinted with permission from [76]. Copyright (2016) American Chemical Society.

Han et al. developed a method named "space limited plasma oxidation" for gradient patterning on SAM modified surfaces by using plasma oxidation. [77] This method utilized oxygen plasma to convert inert methyl groups of SAMs to other functional groups. The

structure of this method is extremely simple as it requires only a glass slide, a spacer and the SAM coated glass substrate to create a "wedge" space, shown in Figure 2.31. When being placed in radio frequency (RF) plasma system, by limiting the reaction time, plasma being allowed to react with the surface was only contained by the wedge space, and thus generate the gradient. This method was innovative, quick to re-create and cost friendly, however, Han and colleagues showed the functional "wedge" angle limit (400 μm height spacer) for conducting this method, beyond which imperfect gradient curve would occur. This method is also another unidirectional gradient that is not capable of generating grayscale patterns.
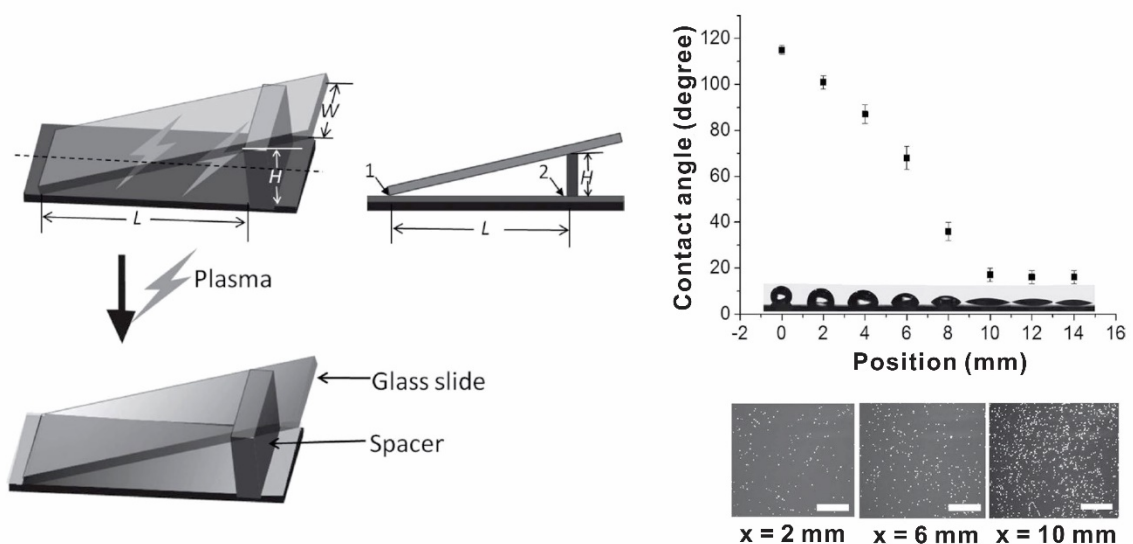
Figure 2.30 (A) The schematic diagram of the plasma oxidation patterning method; (B) Surface wettability analysis by water droplet contact angle; (C) Fluorescent microscopy images of patterned surface attached with amine functionalized beads. Scale bar is 200 μm. Reprinted with permission from [77]. Copyright (2012) WILEY-VCH Verlag GmbH & Co. KGaA, Weinheim

2.8   Summary

In this chapter, many surface chemical patterning methods including their advantages and limitations have been introduced. Photolithography methods often require

expensive photomasks or equipment but possess high resolution. With the help of photolithography, soft materials based microcontact printing and microfluidic patterning methods are widely adopted due to their high throughput. Inkjet printing utilizes the familiar commercially available inkjet printer to offer highly ease of use. Scanning probe microscopy-based methods and laser-based methods bring the pattern resolution to below 10 nm. Some other methods have either simple experimental setups or simple concepts to generate gradient patterns.

When reviewing the advantages and limitations, it is not difficult to find the perfect combination which are high throughput, ease of usage, inexpensive cost, and capability of generating complex patterns. However, all aforementioned patterning methods lack one or several of the mentioned characteristics. When it comes to bio-related fields, it often requires extra time for researchers to learn the operation of expensive equipment or within cleanroom environment. Methods such as inkjet printing do not have that barrier, but the limitation of lacking gradient or grayscale patterning constrained its application.

Therefore, it is beneficial for bio-related researchers to conduct surface patterning with protocols they are already familiar with. In this work, a surface patterning method capable of patterning grayscale that utilizes existing common bio-related lab equipment has been introduced, explained, and characterized. Both gradient and grayscale patterning would be demonstrated.

CHAPTER 3. THEORETICAL ANALYSIS AND DISCUSSION

In this chapter, mathematical model of this new patterning method will be introduced, based on assumptions that could be reasonably proposed. The simulation examples of patterning unidirectional gradient will be illustrated in figure form. Several types of possible noises will be discussed as well.

3.1   Electrophoretic Motion Through Heterogeneous Media

3.1.1 System Motion Developed

The surrounding environment of a particle can have a profound impact on the molecule's response to an applied force. When presented with the complex microenvironment inside a hydrogel material, a number of interactions can take place—size exclusion, charge-based interactions, hydrophobic interactions, etc.—that can slow a particle's velocity through this media. Classically this mechanism has been leveraged for separation of molecules, both in electrophoresis and chromatography, but here we utilize the ability to change particle mobility in order to deliver protein in controlled local quantities to a target surface.

The surface patterning mechanism developed in this work leverages the influence of media resistance on the steady-state velocity of electrophoretically-driven particles. For charged spherical particles in an electric field, this velocity can be derived using a force balance on the particle. The driving electrophoretic force (F_e) is a simple function of the strength of the electric field (E) and the charge on the particle (Q):

$$F_e = EQ \qquad\qquad (3.1)$$

If this particle exists in a viscous fluid, it will experience a drag force ($\boldsymbol{F_d}$) in the direction opposite of the particle motion. For dilute particles in a homogeneous medium with low Reynold's number, Stoke's law defines this force as being proportional to the particle velocity ($\boldsymbol{v}$), effective particle radius (r), and the dynamic viscosity of the surrounding media (η):

$$\boldsymbol{F_d} = -6\pi\eta r\boldsymbol{v} \tag{3.2}$$

At steady state these two forces will be equal and the particle will reach its steady-state velocity, $\boldsymbol{v_s}$:

$$\boldsymbol{v_s} = \frac{EQ}{6\pi\eta r} \tag{3.3}$$

Upon inspection of equations 3.1-3.3, it can be seen that under steady-state conditions, identical particles under the influence of the same electric field but in different surrounding media—i.e., different η values—will experience identical driving forces but reach different steady-state velocities.

While this simple model can be helpful for estimating particle motion in some cases, it has limitations in many practical applications. For simple Newtonian fluids, the steady-state velocity will be inversely proportional to the viscosity of the surrounding medium, but for more complex media such as hydrogels, interactions with polymer chains cause an increase in the effective resistance of the medium, hindering motion through the hydrogel. Additionally, deviation from spherical geometry changes the magnitude of the drag force on a particle and also alters the way the particle interacts with complex media such as hydrogels; a notable extreme of this effect can be seen in long-chain biopolymers such as DNA. Because of these complexities, it is often more expedient to discuss electrophoretic motion in terms of molecular mobility ($u \equiv \boldsymbol{v_s}/\boldsymbol{E}$) for a specific case. A

number of theoretical models exist to estimate this parameter in common applications [78, 79], or it can be determined empirically [80-83].

3.1.2 Flux Equation

If the electrophoretic mobility for a given particle/media combination is known, it is possible to calculate the number of particles passing through an arbitrary surface (S) orthogonal to the particle trajectory when the system is subjected to an electric field. This quantity, the flux (J, number of molecules per m^2 per second)) is calculated as

$$J = n * v_s = un|\boldsymbol{E}| \tag{3.4}$$

Assuming a volume filled with a known concentration of uniformly-distributed particles (n), the number of particles passing through this surface (N') between any two time points, t_1 and t_2 would be:

$$N' = \int_{t_1}^{t_2} \iint_S un|\boldsymbol{E}|dS\, dt \tag{3.5}$$
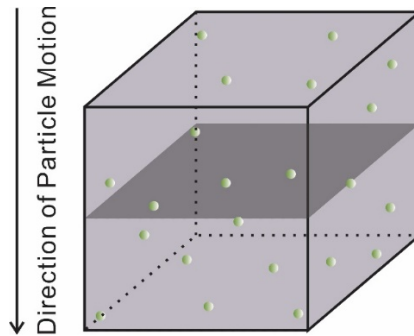
Figure 3.1 Molecules passing through arbitrary surface

3.1.3 Patterning Molecular Concentration Expression

In our application, proteins are electrophoretically driven through a hydrogel material and deposited onto a target surface at the hydrogel boundary. We can define the

lower boundary of the hydrogel as our surface of interest, having a local surface area A_s.
Utilizing the previous equation and assuming that all of the properties of interest are
invariant with respect to time, it is possible to estimate the local surface concentration of
particles deposited on the target paper (c):

$$c = N'/A_s = un|\boldsymbol{E}|(t_2 - t_1) \tag{3.6}$$

The evolution of c and the particle distribution within a hydrogel over time in a
high and low molecular mobility hydrogel can be seen in Figure 3.2a. For identical initial
volumetric concentration ($n_A = n_B$), the deposition rate of particles onto the target surface
is slower in the low mobility medium, resulting in a more gradual increase in surface
concentration. However, after a sufficient amount of time, both systems will result in an
identical surface concentration after the hydrogels are completely depleted of particles.
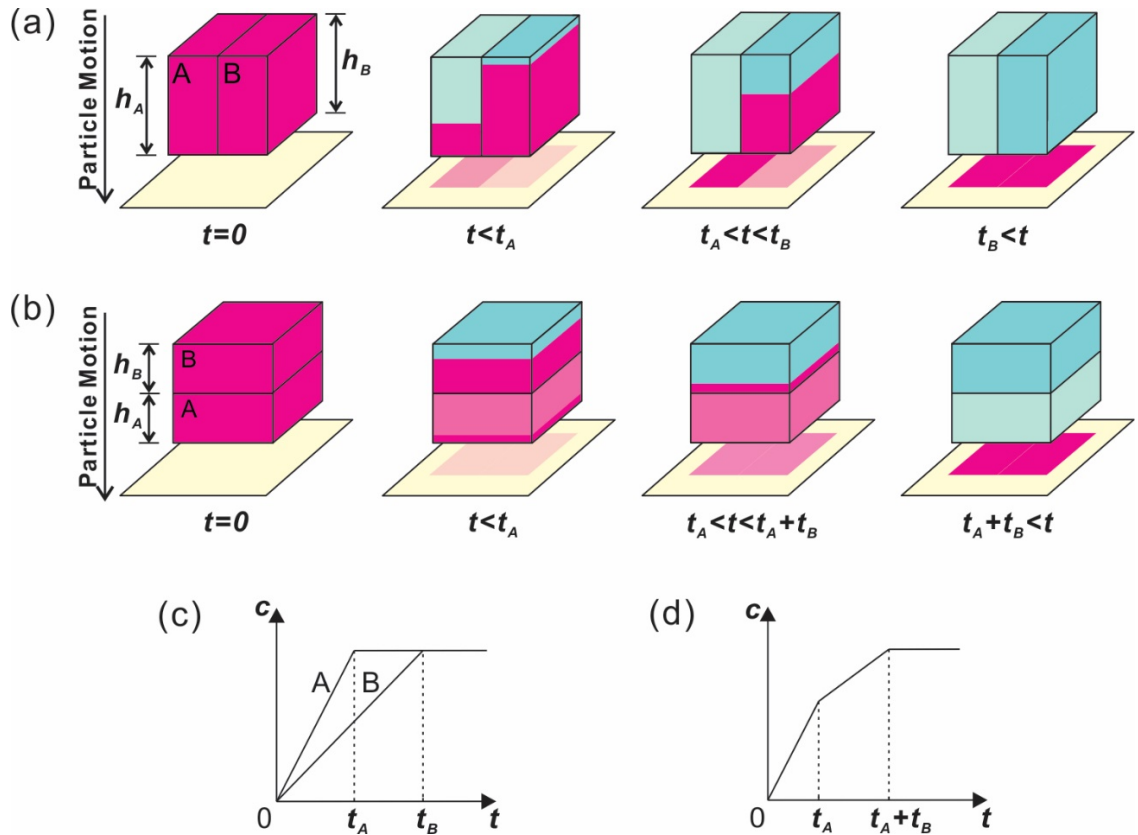
Figure 3.2 Deposition of molecules from different hydrogels positions

For a non-homogeneous case where a fluid medium has multiple distinct regions in sequence, particles will have different molecular mobility and different steady-state velocity in each region. Assuming constant particle velocity within each region, we can define t_i as the time required for all particles that originated in region i to move out of region i through the lower boundary of that region. This time is a function of the thickness of the region (h_i) and the magnitude of the steady-state velocity of particles within the region, $|v_{s,i}|$:

$$t_i = h_i/|v_{s,i}| = h_i/(u_i|E|) \tag{3.7}$$

For the specific case of a binary system that has two regions with distinct internal mobility (u_A and u_B) in series, if we assume uniform particle distribution within each region as an initial condition and then allow particle motion to progress over a specific operation time t, there are 3 different possibilities regarding deposition of particles onto the target surface. For short operation times ($t \leq t_A$), a fraction of the particles that originated in region A will be deposited on the target surface, but no particles from region B will reach the target surface. For very long deposition times ($t \geq t_A + t_B$), all particles from both regions will reach the target surface. And for intermediate operation times ($t_A \leq t \leq t_A + t_B$), all particles from region A and a fraction of the particles from region B will reach the target surface. Thus, surface concentration can be expressed as a piecewise function as follows:

$$c = \begin{cases} u_A n_A |E| t & \text{if } t \leq t_A \\ n_A h_A + u_B n_B |E|(t - t_A) & \text{if } t_A < t < t_A + t_B \\ n_A h_A + n_B h_B & \text{if } t \geq t_A + t_B \end{cases} \tag{3.8}$$

The evolution of c and the particle distribution within a hydrogel over time in this type of two-region hydrogel can be seen in Figure 3.2c; in this case, $u_A > u_B$. Initially the protein deposits quickly on the surface due to the high particle velocity in region A; but as this region becomes depleted of its original particles, it is being slowly replenished from particles that originated in the low mobility region B. This leads to a regional drop in volumetric concentration behind the original high-concentration front. The time that it takes to switch from a high-deposition rate to a low deposition rate is equal to t_A, and therefore is dependent on both the height of region A (h_A) and also on the steady-state velocity of the particles in region ($|v_A|$). Thus, by keeping the total height of a hydrogel constant ($h = h_A + h_B$), and regionally varying the proportion of the hydrogel height comprised of hydrogel A, it is possible to regionally control particle concentration deposited on the surface after a fixed amount of time. A similar effect can be attained by beginning with a higher initial concentration in region A ($n_A > n_B$), either in addition to or in lieu of a higher mobility in region A.

3.2   Generation of Grayscale Surface Patterning

In practice, one way to leverage this mechanism for surface patterning purposes is to create a patterned hydrogel with regions of different crosslinking density (thus, $u_A \neq u_B$) that has been incubated in a solution of constant volumetric concentration until it reaches equilibrium (thus, $n_A = n_B$). Based on the theoretical analysis provided in the previous section, if a dual-region hydrogel with varying h_A/h ratio is placed in a constant electrical field for a finite amount of time, the local concentration of particles transferred to the target surface should vary locally as a function of the h_A/h value of the hydrogel

stack immediately above it. For the case where $u_A > u_B$, in a section of the dual-region hydrogel where the h_A/h value is small (i.e., close to 0), the particle deposition rate will be high initially, but quickly switch to a low deposition rate as the particles originating in region A become rapidly depleted. In contrast, in sections of the dual-region hydrogel where the h_A/h value is large (i.e., close to 1), the particle deposition rate will remain high for a much longer period of time.
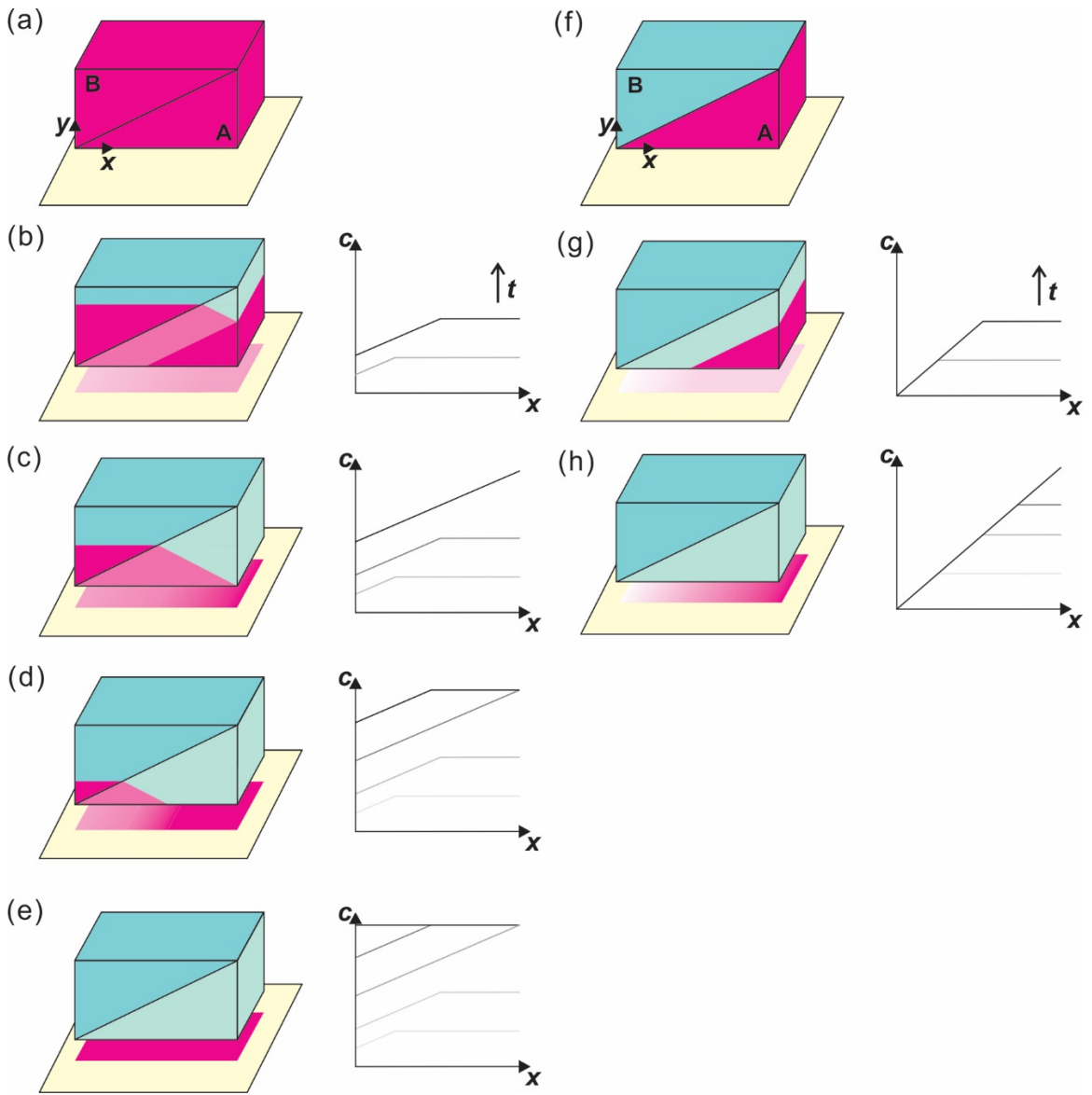
Figure 3.3 Gradient patterning simulated with two molecule loading mechanism

For any arbitrary geometry, equation (3.8) can be used to calculate the local surface concentration at any point in time. For a dual-region hydrogel where the h_A/h ratio increases linearly, such as that shown in Figure 3.3a, the surface concentration profile is largely uniform at the beginning of deposition (Figure 3.3b). During this time, most of the high mobility hydrogel still contains some of its original particles, so deposition is occurring at a relatively fast rate. Eventually a linear gradient will develop, peaking as the last of molecules originating in Region A deposits on the target surface (Figure 3.3c). Over time, the surface concentration becomes increasingly dependent on the contributions from particles originally in Region B (Figure 3.3d). Given enough time, complete depletion of both regions occurs, resulting in a uniform surface concentration (Figure 3.3e).

This embodiment of electrophoretic patterning is challenging because it requires excellent control of the deposition time in order to achieve optimal pattern resolution. Deposition times that are too short will result in an "underdeveloped" pattern (Figure 3.3b); in this case high h_A/h value regions and moderate h_A/h regions generate the same surface concentration. Deposition times that are too long will result in an "overdeveloped" pattern (Figure 3.3d); in this case low h_A/h value regions and moderate h_A/h regions generate the same surface concentration. In addition to the timing concerns, this method is limited because of an inability to produce patterns with regions where $c = 0$. Even if timed perfectly to get the ideal gradient (Figure 3.3c), there will be a nonzero offset the magnitude of which is proportionate to u_B/u_A.

This method can be made more robust by making $u_A \gg u_B$. If the high-resistance region is composed of a hydrogel that has a mesh size smaller than the particle size, it

prevents any diffusive or electrophoretic motion of the particles within that region of the hydrogel ($u_B \approx \infty$). This means that particles would be prevented from entering hydrogel during incubation step ($n_B = 0$), which in turn means that the entirety of the surface pattern would be caused by contributions from region A. This effectively prevents the "overdevelopment" case shown earlier and makes the deposition method much less time-sensitive (Figure 3.3 f-h). A similar effect can be obtained by introducing the proteins during the region A casting step. This method has the additional benefit of avoiding the time-intensive incubation step during fabrication, but does not allow for reuse of the binary hydrogels for repeated patterning. A similar surface patterning effect could be created by using a single hydrogel of varying height and providing an electric field for a long enough time to completely deplete the particles within the hydrogel. However, in practice, the second hydrogel is necessary in order to provide mechanical stability and parallel surfaces, which in turn helps ensure a uniform internal electrical field.

3.3   Other Considerations During Electrophoretic Patterning

3.3.1 Realistic Predictions of Electrophoretic Mobility

Equation 3.8 gives the surface deposition calculation under ideal conditions of perfect spherical molecules moving within homogeneous medium, which means certain assumptions must be made to satisfy this estimation, since in reality, both protein molecules and hydrogels related parameters are non-ideal. Some parameters such as the heights of both gels are known values, electric field strength can be calculated through simple measurements. However, the electrophoretic mobilities of BSA however is unknown, which is also the key parameter of the whole deposition. In our experiment, it is the

electrophoretic mobilities of BSA molecules traveling through polyacrylamide hydrogels that has 2.6 crosslinking ratio (%C) at monomer concentrations (%T) of 10% and 15% respectively.

From previous literature reviews, we have obtained some important messages about PA gels in order to obtain BSA mobilities. When considering the internal structures of PA gels, "pore" size, which is the space that polymer chains generated, has been first introduced while discussing molecular sieving, [84] and commonly accepted, referred and improved. The average "pore" size of the gel varies with the change of polymer concentration. Stellwagon [85] also suggested the prediction from Ogston theory that the decreasing of average pore sizes is not linearly related with the increasing of polymer concentration (%T) but as $T^{-1/2}$. [85] This can be indirectly supported by Kremer and Blattler from their data. [86, 87]

Later, as some researchers discovered the electrophoretic molecular sieving similarities between liquid polymer solutions and crosslinked PA gels, more complex hydrodynamic activities were considered other than the pure static pore theory. Bode [79] introduced theoretical demonstrations including the new parameter verified with Morris' [88] empirical data on this new concept. Crosslinked gels are separated into two compartments and fractional resistance would be paid great attention to. From equation 3.3 we know the electrophoretic mobility can be calculated with the polymer viscosity. However, because Bode's parameter still relied on existing empirical data for the third parameter's estimation, the extra introduced error is not worth the detour.

From definition, the electrophoretic mobility of the protein can be expressed as

$$u_{pT} = dE^{-1}t^{-1} \tag{3.9}$$

where u_{pT} is the mobility at temperature T, d is the distance that molecule travels, t is the time. [85] From this equation (3.9), we could measure the molecular travel distance, the electric field strength, and the run time for calculation of mobilities. Since most other parameters we used are at 20°C, such as equivalent radius of BSA molecules, we convert the mobility following equation

$$u_p = u_{pT} \cdot [(20 + 30/(T + 30)] \tag{3.10}$$

where u_p is the mobility of the molecule at a common temperature of 20°C. [89] The unit for temperature is °C. With equations 3.9 and 3.10, we could run the test experiment and measure the required mobilities for certain molecule-medium combinations. Direct measurement requires dedicated equipment for electric fields measurement which would make the experiment really complicated. In this case, the most likely situation is to estimate the electric field. The error introduced would benefit the final estimation of deposition, but make the original purpose of the mobility test experiment meaningless. Thus, we chose to estimate the BSA electrophoretic mobilities in a reasonable manner.

Another intuitive way is to directly use the empirical data from previous experiments of other researchers. Since we couldn't find the molecular electrophoretic mobilities of exact concentrations of PA gels and BSA molecules, we will directly estimate the BSA mobilities within 10% and 15% PA gels from Morris' actual measurements of BSA mobilities for different %C and %T. [88] They have included data of 8 molecules travelling through 20 different polyacrylamide hydrogels. However, the certain combination selected by our experiment doesn't show up in their data sheet, which means we have to estimate the mobilities in a reasonable way.
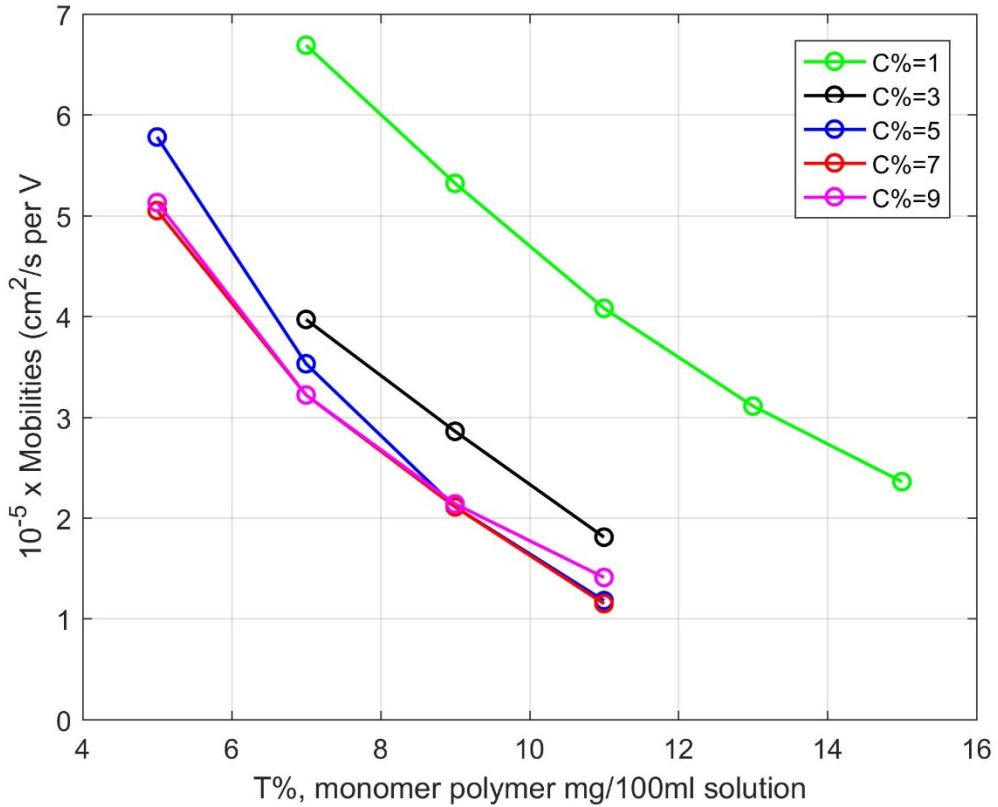
Figure 3.4 Re-plot Morris empirical data [88] of u_{rel} regarding C% and T%.

To begin with, we first generated a new plot using Morris data. In our experiment, PA gel that has Bis-Acrylamide/Acrylamide=37.5 (C%=2.6) has been selected, T=10 and T=15 monomer concentrations have been used to fabricate PA gels for containing BSA molecules. Kremer [87] and Blattler [86] have shown the exponential variation on either C% or T% value changes. After locating the estimations for C=1 and C=3 for both Ts, following Table I, we could use selected data and estimation for deposition simulation.

Table 3.1 Estimated u_{10} and u_{15} from Morris data plot [88]

BSA molecules		T% g monomer / 100ml solution	
Estimated u_{rel}		u_{10}	u_{15}
	1	4.6	2.36
C% g bisacrylamide /	3	2.3	0.8
100g total acrylamide	2.6	2.8	1

Directly from the Morris data plot, we have $u_{10} = 2.8 * 10^{-9} \ [m^2/(v \cdot sec)]$ and $u_{15} = 1 * 10^{-9} \ [m^2/(v \cdot sec)]$. These two mobilities then would be plugged into equation 3.8 to estimate the surface deposition concentrations with each gel which could be compared with empirical results.

3.3.2 Nonuniform Compression of Hydrogel Material

Excessive pressure that causes mechanical deformation of the PA gel could be another factor to the experimental results. Due to the nature of the hydrogel, when there are more polymer chains to crosslink, the PA gel is stiffer; this manifests as the material having a higher Young's modulus in the direction of compression (E_x). Hydrogels that contains proteins are less crosslinked and have a lower Young's modulus.

From Hooke's Law and Young's modulus expressions, we can determine the force (F) required to deflect a material a certain amount (Δx), given that we know the Young's modulus, the surface area perpendicular to the force (A_r) and thickness in the direction of the deflection (x):

$$F = \frac{E_x A_r}{x} \cdot \Delta x \qquad (3.9)$$

From this, we can derive a stiffness coefficient (k) for a hydrogel of known height

(h) as being

$$k = \frac{E_x A_r}{h} \qquad (3.10)$$
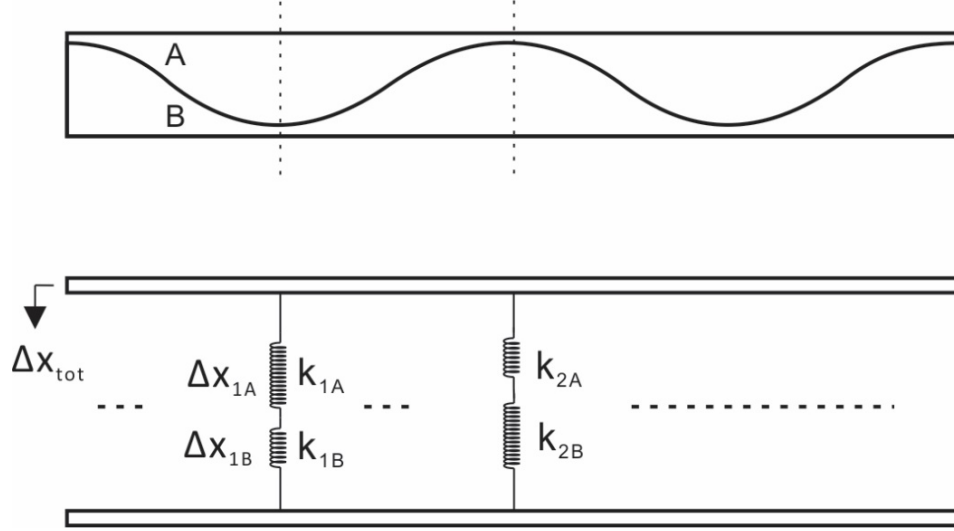
Figure 3.5 Side view of the waveform feature, which contains two gels with different Young's modulus. Combination of the gels could be treated as two spring system, while the total displacement of gel is considered equal.

At different locations, gels have variant height ratios, thus the stiffness coefficients would be different. The total deformation of the gel in every location is the same, $\Delta h_{tot} = \Delta h_{1A} + \Delta h_{1B} = \Delta h_{2A} + \Delta h_{2B} = \cdots$.

If we look at position 1, since the force that two gels experienced are the same, we have

$$F = \frac{E_{xA} A_r}{h_{1A}} \cdot \Delta h_{1A} = \frac{E_{xB} A_r}{h_{1B}} \cdot \Delta h_{1B} \qquad (3.11)$$

Reorganize the equation and have the following form

$$\frac{E_{xA}}{E_{xB}} \cdot \frac{\Delta h_{1A}}{\Delta h_{1B}} = \frac{h_{1A}}{h_{1B}} \qquad (3.12)$$

In this equation, h_{1A} and h_{1B} are denoted gel heights. Gels' Young's moduli are constant once the gel materials are determined, which means for the same gel, higher gel would result higher deformation, regardless Young's modulus of the gel.

From Figure 1 (Young's modulus of the polyacrylamide gels as a function of the crosslink concentration) in Benguigui [90], the Young's moduli of the PA gels used can be estimated directly as $E_{xA} = 5 \times 10^5 \ Pa, \ E_{xB} = 1.5 \times 10^5 \ Pa$.
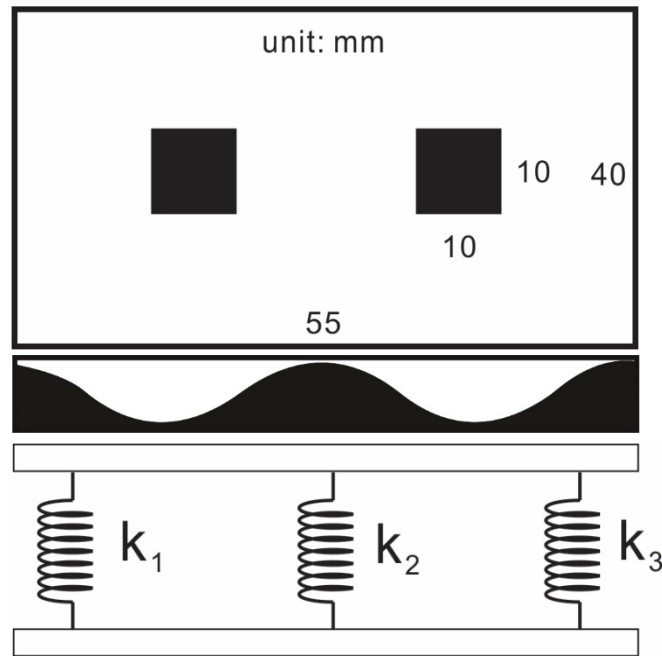
Figure 3.6 Illustration of heterogeneous hydrogel structure (top view) and waveform feature shape (side view). Their dimensions are shown in the figure.

In our experiment, the compression force is estimated as $5 \ N$, the total gel height is $1.1 \ mm$. If we simplify the gel structure it becomes a multi-spring system, one large supporting gel, and two feature gel area. The feature gel area is less than 5% of the total gel, so we simply use $2.2 \times 10^{-3} \ m^2$ as the surface area. Plug all values into equation

59

(3.14) we obtain the total deformation $5\ \mu m$. Because of the flat surfaces on both sides, this distance would also be the deformation for feature area.

Reconsider the triple spring model in Figure 3.7. Since we have the additivity of the deformation distances of each gel, and the equalities of compression forces and total deformation, from those equations we can derive the following expression

$$\frac{\Delta h_B}{\Delta h} = \frac{E_{xA} \cdot \frac{h_B}{h}}{E_{xB} + (E_{xA} - E_{xB}) \cdot \frac{h_B}{h}} \tag{3.13}$$

Insert Young's moduli for both gels so we can obtain the relationship between $\frac{\Delta h_B}{\Delta h}$ and $\frac{h_B}{h}$, shown in Figure 3.8. The ratio of the deformation of feature gel to total deformation would increase in a fast manner when the ratio of its height to total gel height gets boosted up to 50%, but in general these two ratios have very similar to linear relationship.
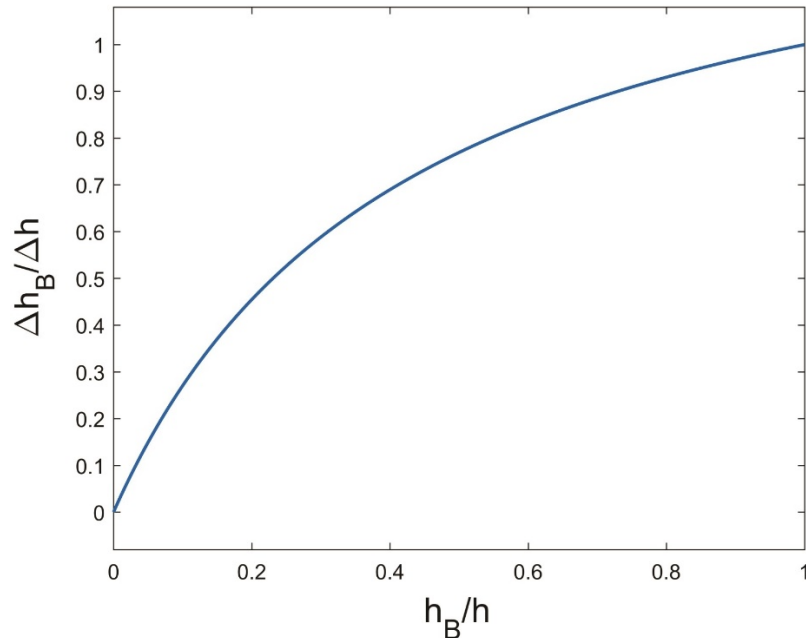
Figure 3.7 Relationship between deformation ratio and height ratio of feature gel to total gel.

From the above figure, we can easily obtain the sideview ratio relationship plot which is shown in Figure 3.9 in below. In the relationship curve we can observe more deformation from less crosslinked PA gel when the feature height reached its highest value than locations where lower feature gel existed. There should be more solution containing protein molecules being pushed out of the gel at higher gel locations, which should result higher instant deposition when gel being loaded into the apparatus before running the experiment.
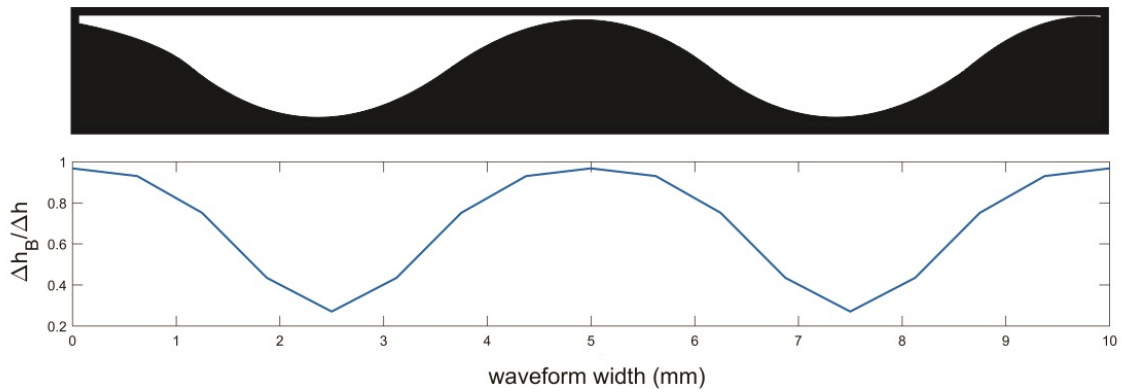
Figure 3.8 ratio of the deformation of feature gel to total deformation corresponding to waveform feature shape sideview.

To conclude, based on the total deformation, we can safely neglect the height shortage from mechanical deformation while analyzing the patterning results. The molecules being pushed out when gel being loaded is inevitable and will cause the pre-patterning before running the experiment. However, experimental result returned an inversed image where at lower gels the intensity from instant contact is higher. This interesting phenomenon would be looked into and explained at a later time. $\Delta h_B / \Delta h$

3.3.3 Free Diffusion of Molecules During Patterning

Molecules in the hybrid hydrogel structures will experience diffusion both prior to and during electrophoretic patterning, which can have a negative impact on the fidelity of the resulting surface pattern. Free solution diffusion coefficient can be calculated according to Stokes-Einstein equation under certain assumptions:

$$D^{soln} = \frac{k_B T}{6\pi\mu r} \tag{3.14}$$

k_B is Boltzmann's constant, T is the absolute temperature, μ is the viscosity, and r is the radius of the spherical particle. Diffusion coefficient in PA gel would be substantially reduced because of the crosslinking of polymer fibers. Brickmann [91] and Tong et al [92] has given the expression of hindered diffusion coefficient as

$$\frac{D^{gel}}{D^{soln}} = \frac{1}{1 + \kappa r + \frac{1}{3}(\kappa r)^2} \tag{3.15}$$

where κ^{-2} is Darcy permeability of the specific hydrogel, r is the molecular radius, D^{gel} is the molecular diffusion coefficients in hydrogels. Because of the way that we are preloading the hydrogel with proteins, only one gel out of the two is preloaded, thus the diffusion is inevitable. When considering this boundary diffusion, we could use the one-dimensional semi-infinite diffusion model with n as the volumetric concentration to estimate the process.
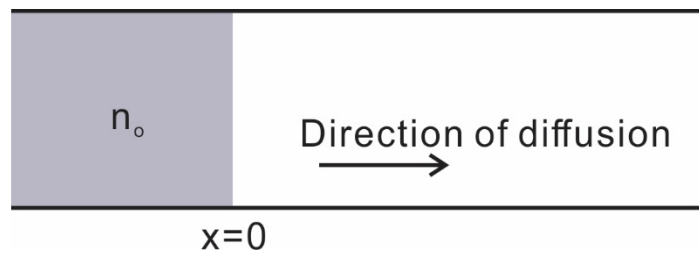
Figure 3.9 Diagram for semi-infinite diffusion. n_o is the initial concentration, the diffusion is assumed only towards right direction.

Boundary diffusion can be simplified as the diagram showed in Figure 3.10. The

loaded protein concentration is $n(x,t) = f(x,t)$, which is a function of the diffusion

distance (x) and experimental time (t). Diffused concentration at any time t is given

$$\frac{\partial f}{\partial t} = D^{gel} \frac{\partial^2 f}{\partial x^2} \tag{3.16}$$

The initial and boundary conditions are defined as: $f(x,0) = 0$, $f(0,t) = n_o$, and

$f(x \to \infty, t) = 0$. To solve this PDE, we bring the variable $\eta = \frac{x}{2\sqrt{D^{gel}t}}$ to transform (3.20)

to an ODE:

$$\frac{d^2 f}{d\eta^2} + 2\eta \frac{df}{d\eta} = 0 \tag{3.17}$$

Solve it for the concentration

$$n(x,t) = f(x,t) = n_o \left(1 - \frac{2}{\sqrt{\pi}} \int_0^\infty e^{-\eta^2} d\eta\right) \tag{3.18}$$

The whole minus term in the brackets is the form of error function, so re-write it as

$$n(x,t) = f(x,t) = n_o erfc\left(\frac{x}{2\sqrt{D^{gel}t}}\right) \tag{3.19}$$

Since the boundary diffusion is between two gels, the effect of the partition

coefficient needs to be considered, which can be defined using Ogston's model [92]:

$$K = \frac{c^{gel}}{c^{soln}} = \exp\left[-\phi\left(1 + \frac{r}{r_f}\right)^2\right] \tag{3.20}$$

ϕ is the volume fraction of fibers, r is the radius of the molecule, r_f is the radius of the

fiber chain. Tong's data [92] yields $K_{10\%} = 0.014$ and $K_{15\%} = 0.0016$, that we found

partition coefficient of 15% PA is approximately 11% of the value of that of 10% PA,

which implies the total molecular concentration of 15% PA would be at most 11% of the

concentration of 10% PA, if diffusion is the only method being used for introducing

molecules into PA gels. This means that only up to 11% of the proteins pre-loaded in 10% PA gel can diffuse into 15% PA gel once they contact and sufficient time is given. In such case, the diffusion effect between gels before patterning would be limited.

Patterning has been tested with multiple time intervals, so if we insert estimated values into equation (3.20) we should obtain the diffusion curves for different situations as shown in Figure 3.11. TRITC-BSA has a diffusion coefficient of $12.6 \pm 1.5 \ \mu m^2/sec$ [93] in water, and according to equation (3.20) the hindered diffusion coefficient in 15% PA gel has dropped to $0.598 \ \mu m^2/sec$. Initial protein concentration is 0.01 mg/ml, so the diffusion curves from free solution to 15% PA gel are shown in Figure 3.11.
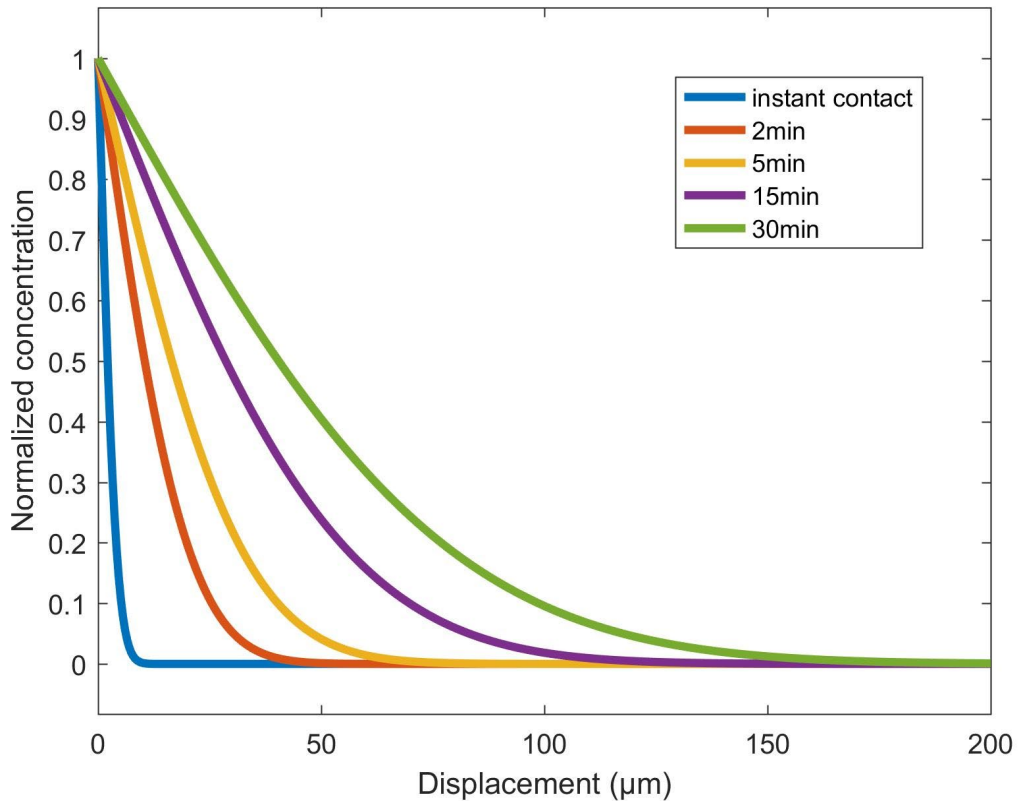
Figure 3.10 Semi-infinite diffusion at different experiment time intervals

As we see, even for 30 min, which is the longer time interval in our experiments, the diffusion would hardly affect distances beyond 150 μm. Yet there are still two conditions not considered.

First, because of the effect of the partition coefficient, the protein molecules entering from 10% PA gel to 15% PA gel would be limited. We could rebuild the model as 11% of the original initial concentration, which would significantly reduce the effect of diffusion. Or we could combine the boundary effect with diffusion and estimate with lower diffusion coefficient, which would generate the similar result. Secondly, the diffusion trajectory needs to be considered. During electrophoretic waveform patterning, the diffusion problem becomes more complex. As electrophoretic force drives the BSA towards the target paper, regions of l0% PA become depleted of BSA which results in a high concentration gradient within the 10% PA hydrogel, providing a strong driving force for diffusion. Exactly how this impacts the final pattern is largely dependent on geometry. The strongest driving force for diffusion will be in the direction orthogonal to the boundary separating the +BSA and –BSA regions. For waveform patterning, the slope is relatively shallow shown in Figure 3.9, so the diffusion in lateral direction would be a small portion of the total diffusion, which implies the small influence on electrophoresis.

Therefore, the diffusion influence of the pre-loaded proteins can be neglected either before the patterning or during the electrophoretic motion.

CHAPTER 4. EXPERIMENTAL RESULTS AND DISCUSSION

In order to validate the theory presented in the previous chapter, a variety of protein surface patterns were created using the electrophoretic patterning method, including a binary pattern (letters), gradients in one direction (linear gradient and periodic waveform pattern), and surfaces with variability in multiple directions (a complex horse pattern). This chapter discusses the materials used, the experimental procedures and the results of these experiments in detail. It also discusses how the methods of mold fabrication and experimental processes evolved from the initial, simple binary patterning experiments to eventually produce complex greyscale surface patterns.

4.1 Binary Patterning

The main purpose of the binary patterning experiments described in this section was to demonstrate the ability to generate two concentrations of proteins on the same surface simultaneously. In order to do this, it was necessary to create a hydrogel composed of two individual hydrogels (A and B) with different internal mobility, as described in the previous chapter. Based on the theory from Chapter 3, if a hydrogel with two different h_A/h values were incubated in a protein solution and then subjected to an electric field that would drive the protein from the hydrogel onto a target surface, it should produce a surface pattern with regions of high and low protein concentration.

4.1.1 Binary Mold Fabrication
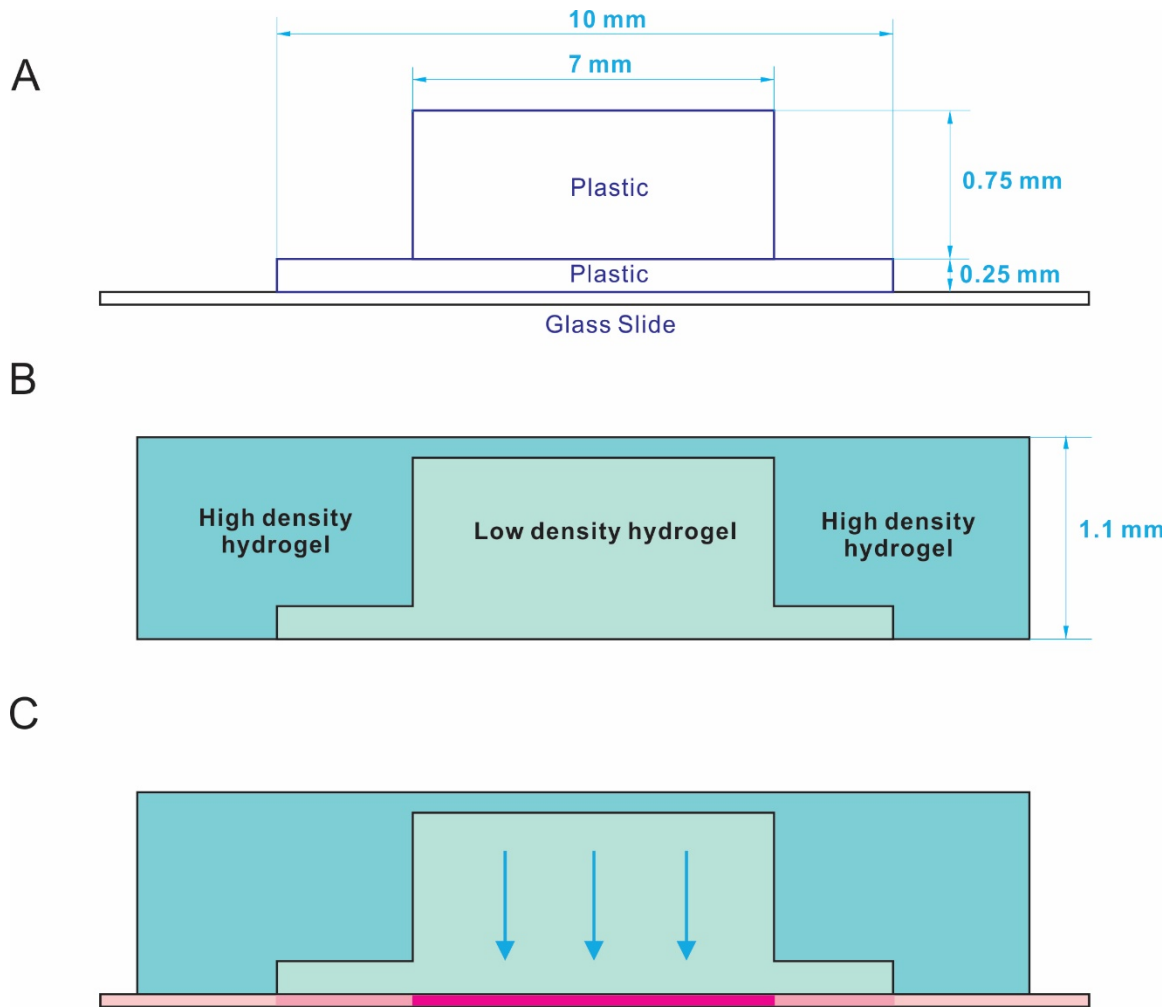
Figure 4.1 A: Thickness distribution in completed mold; B: Binary cast from mold; C: Orientation of hydrogel and protein direction during electrophoretic patterning. Not drawn to scale.

In order to produce hydrogel with two distinct h_A/h values, it was necessary to create a binary mold, as shown in Figure 4.1. In this design, the mold is composed of two layers of plastic shims with different thicknesses which were cut to shape using scissors. The shims were then glued using super glue (Control Gel Super Glue, Loctite) onto a glass microscope slide (Figure 4.1A). Controlling the thickness of the glue was difficult, which added some height variability to molds produced using this method; this was one of the

reasons that the stacked-shim molds were replaced with different fabrication methods in later designs. Two-layer hydrogels fabricated using this mold had the cross-section shown in Figure 4.1B. The hydrogels had a total height (h) of 1.1 mm, which was the thickness of acrylic gasket used in the casting step described in the next section. During electrophoretic patterning, the lower boundary in Figure 4.1C would be in contact with the target paper that would receive the protein molecules.

4.1.2 Binary Hydrogel Fabrication

The heterogeneous hydrogel was fabricated using the method shown in Figure 4.2. First, a 15% polyacrylamide (PA) gel solution—which was prepared from 2.4 mL double-distilled water (ddH$_2$O), 5.0 mL 30% degassed Acrylamide/Bis-Acrylamide 37.5:1 (AM/Bis, Bio-Rad), 2.5 mL gel buffer (1.5 M Tris-HCl buffer, pH 8.8, Bio-Rad), 50 µL 10% ammonium persulfate (APS, Bio-Rad), and 15 µL tetramethylethylenediamine (TEMED, Bio-Rad)—was poured into an assembly made of a glass microscope slide, a laser-cut U-shaped acrylic gasket, and the binary mold described in the previous section. Binder clips were used to clamp the three parts of the assembly together. A layer of deionized water (ddH$_2$O) was gently added as the "lid" to promote a flat gel edge. This "water-lid" method was necessary due to the volume change that occurs during the hydrogel gelation process, which would cause defects if the hydrogels were cured in a rigid enclosed space.

After solidification for 15 min at room temperature, the binary mold was carefully removed without damaging the 15% PA gel. A 8% PA gel solution, **prepared from 4.7 mL ddH$_2$O, 2.7 mL 30% degassed AM/Bis 37.5:1, 2.5 mL gel buffer (1.5 M**

Tris-HCl buffer, pH 8.8), 50 μL 10% APS, and 15 μL TEMED, was poured into

the area left by the mold, and then a clean glass microscope slide was applied to cover the

gel solution. Care was taken to ensure that no air bubbles were trapped between the

hydrogel and the glass microscope slide. Blinder clips were used again to clamp three edges

of the new assembly together, and a layer of ddH$_2$O was added to the open surface. After

15 min of solidification at room temperature, all glass slides and the gasket were carefully

removed under a rinse of a small amount of ddH$_2$O to avoid tearing the gel due to adhesion

between the cured gel and glass surfaces.
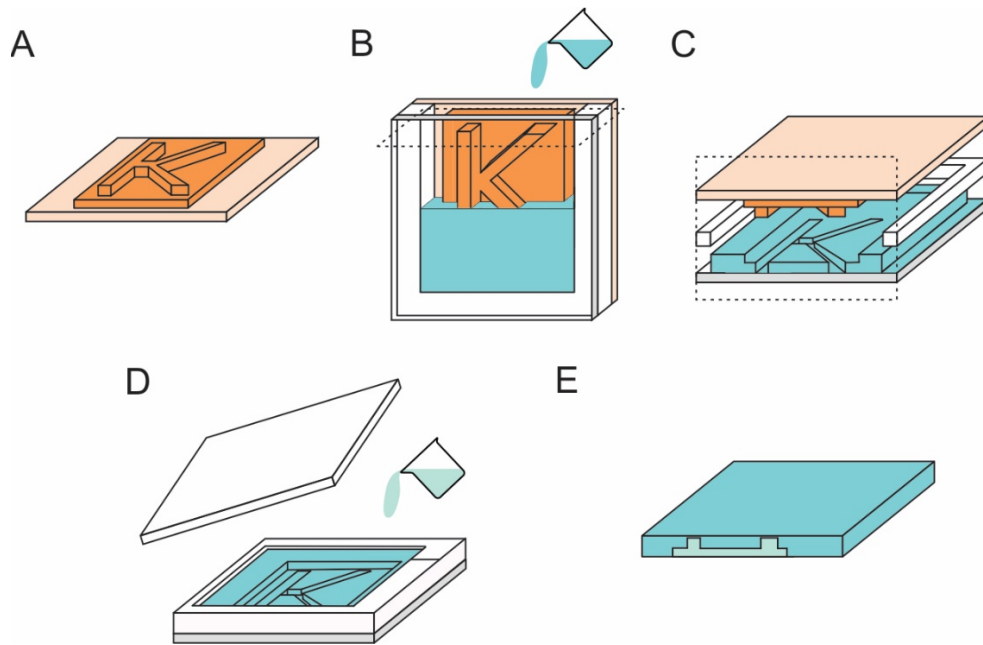
Figure 4.2 Fabrication of binary hydrogel. A reusable SU-8/glass mold (A) was assembled with a glass microscope slide and u-shaped gasket before pouring high density hydrogel (15% PA) into the enclosed space (B). After curing, the mold was removed from the hydrogel (C) and a low density hydrogel (8% PA) was poured into the voids formed by the original mold (D). This assembly was covered with a plain glass slide and cured, after which the hydrogel was removed from the assembly (E).

4.1.3 Protein Loading and Patterning

The hydrogels were loaded with proteins by soaking them in a 0.1 mg/ml bovine serum albumin (BSA) solution, inside a 37°C incubator for 24 hours for the molecular concentration to reach equilibrium. The BSA solution was created by mixing BSA powder (Sigma-Aldrich, A7906-500G, pH 7, ≥98%) and 1x PBS buffer (Mediatech Inc, B003L13PK, Phosphate Buffered Saline, 1X). After incubation, the BSA-laden hydrogels were rinsed with ddH$_2$O, prewetted with a buffer solution, sandwiched between layers of filter paper (Cotton blotting filter paper, 0.84 mm thick, Sigma-Aldrich) and target paper (Amersham™ Protran® Western blotting membranes, nitrocellulose, GE Healthcare), and loaded into a plastic cassette (Mini Gel Holder Cassette, Bio-Rad), as shown in Figure 4.3. The buffer solution was prepared by mixing 52.2 g Glycine (Research Products International) and 10.89 g Tris base powder (Research Products International) into 3.6 L of ddH$_2$O.
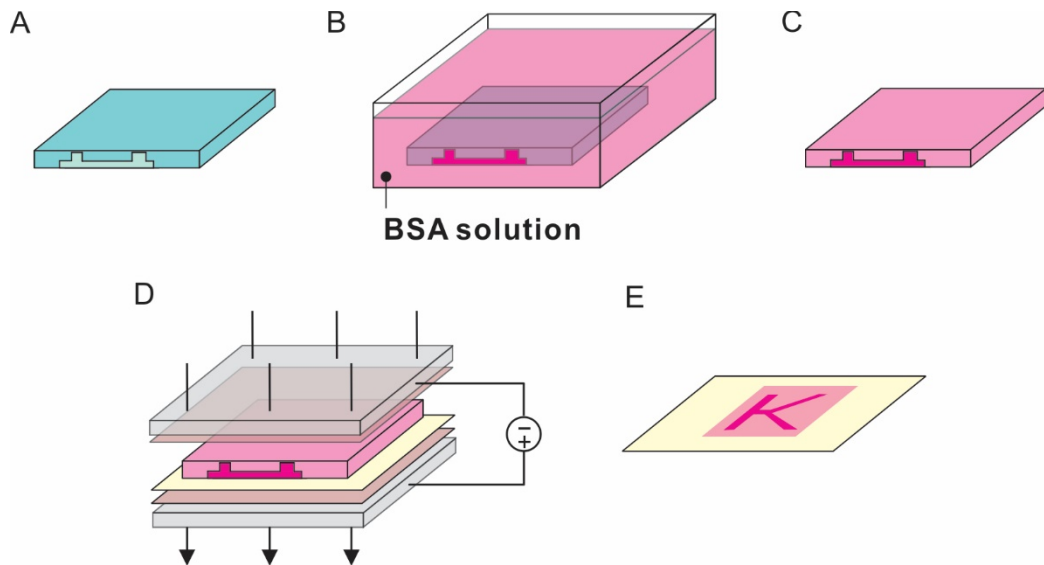
Figure 4.3 Protein loading and electrophoretic patterning to create binary protein surface pattern

The commercial equipment used for electrophoretic patterning is shown in Figure 4.4. All components were purchased from BioRad, and the transfer kit used was the Mini Trans-Blot® Cell. Once the cassette was assembled with heterogeneous hydrogel being wrapped in between target paper, filter papers, and foam pads, it was placed into the Bracket component, which was in turn placed inside the Buffer Container. The Buffer Container was filled with buffer solution, accompanied by a pre-frozen flask of coolant. The Buffer Container was then placed in a refrigerator or heat insulated box surrounded by ice cubes. This low temperature setup was necessary to absorb the heat generated during electrophoresis in order to protect the hydrogel from being damaged and protein molecules from being denatured.
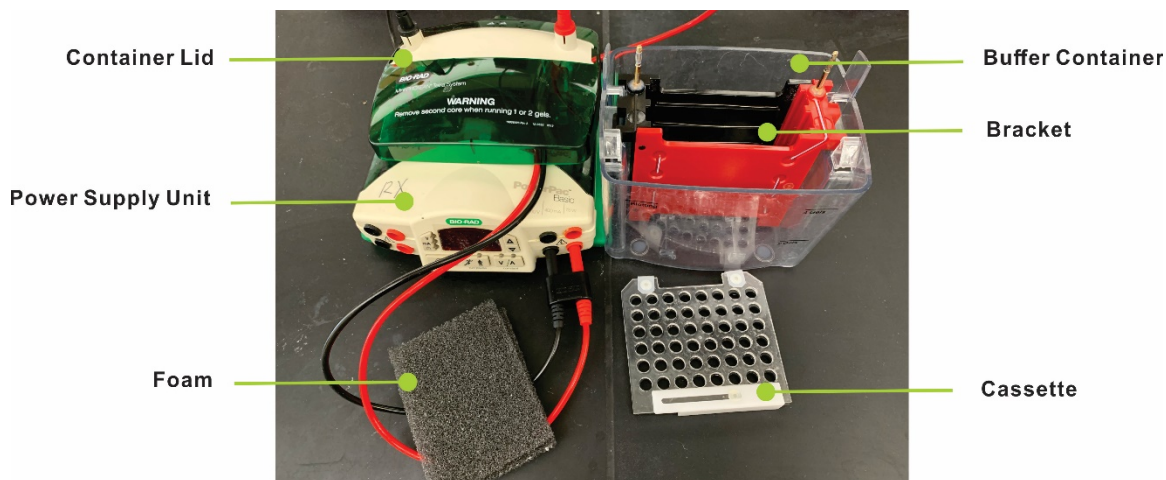
Figure 4.4 Commercial western blot equipment from BioRad, containing a power supply unit and transfer kit.

After preparation, the anode and cathode in the lid of the Buffer Container were connected to the power supply unit (PowerPac™ HC High-Current Power Supply), which could be used to maintain a fixed voltage, current, or power output. In this set of experiments, a fixed voltage of 80 V was applied for 40 min. Once finished, the assembly was disassembled and the target paper was placed in a low wall container.

The protein pattern on the target paper was visualized using Ponceau S, which is a light red dye that non-selectively binds to proteins. Ponceau S staining solution (0.1% Ponceau S w/v in 5% acetic acid, Sigma-Aldrich) was poured into the shallow container so that it fully covered the target paper. The container was gently rocked for about 20 seconds to allow the solution to thoroughly cover the paper; then the Ponceau solution was disposed of and ddH$_2$O was added to the container to rinse the target paper. The target paper was rinsed 20 seconds before disposing of the ddH$_2$O, and then repeating the rinse step 3 times until there was no pink color in the water. Then the target paper was dried by picking up the corner with two fingers and gently waving; after drying it was stored in a sealed dark container preserve the color.

4.1.4 Results and Discussion
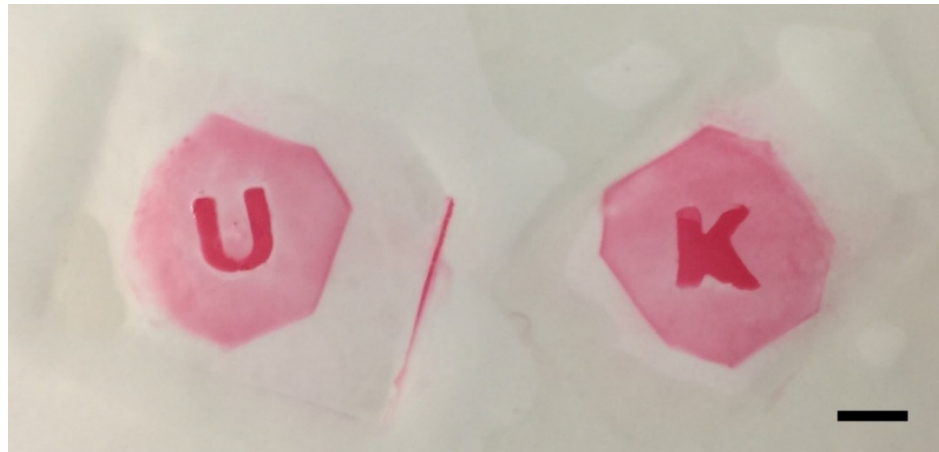
Figure 4.5 Binary pattern of "U" and "K" letters in Ponceau-stained BSA. Scale bar: 10 mm.

Figure 4.5 shows a photograph of two letter patterns created using the binary patterning experimental procedures described above. Images of the results were taken using an 8-megapixel digital camera, but due to the influence of ambient light and camera

parameter settings, it was difficult to get quantitative data from these results. However, this represented the first successful creation of surface patterns with multiple distinct surface concentrations using the electrophoretic patterning method. While there are imperfections in the pattern (the letter "K" has an imperfect shape due to the gel ripping during the gel fabrication process) and the edges are somewhat uneven (the use of epoxy glue to make the molds yielded uneven edges), these binary patterns demonstrated the ability to control surface pattern concentration regionally by controlling h_A/h values within a hydrogel, as suggested by the theory in the previous chapter.

4.2   Linear Gradient Patterning

After the success of the binary patterning proof-of-concept experiments, the next set of experiments was designed to extend this concept to create a protein pattern with a linear concentration gradient.

4.2.1 Linear Gradient Mold Fabrication

In order to generate a pattern with a linear concentration gradient, it was necessary to create a hydrogel with the geometry shown in Figure 4.5A. This, in turn, required a mold with a smooth surface slope, similar to that in Figure 4.5B; because the layered plastic shim method used to make the binary patterning molds was incompatible with this new geometry, we starting seeking out new materials and methods for mold fabrication.

We initially explored Polydimethylsiloxane (PDMS) as a material for the molds, as it is an elastic polymer commonly used in biological and chemical laboratories and it is known for its ability to replicate features with submicron resolution. However, after early tests, it became clear that PDMS inhibited PA hydrogel polymerization. This is due to the

73

fact that PDMS is permeable to gas, so ambient oxygen diffused through the PDMS mold walls and interfered with PA gelation. Instead, we chose to use a combination of glass, acrylic and SU-8 photoresist (Microchem) as the mold materials, since all three were compatible with PA gelation, and SU-8 is convenient to cast into shape and cure with UV light.
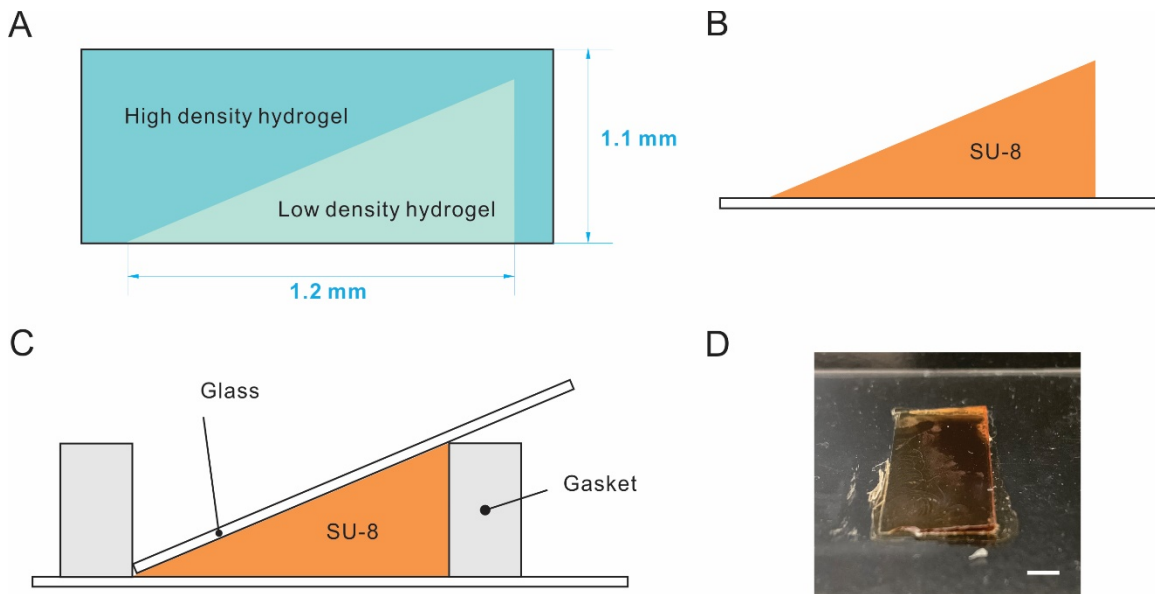
Figure 4.6 Side views of (A) gradient heterogeneous hydrogel, (B) feature mold design, (C) method for fabricating gradient mold, and (D) image of final mold. Scale bar: 5 mm.

The mold was fabricated by starting with a clean glass microscope slide and attaching a laser-cut rectangular acrylic gasket using binder clips. SU-8 3050 was gently poured onto the reservoir formed by the glass and acrylic, being careful to prevent inclusion of any air bubbles. A glass microscope slide (25 x 75 mm, McMaster-Carr) was placed so that one edge rested on the microscope slide base and the other rested on the edge of the acrylic gasket, forcing the SU-8 into a wedge shape as shown in Figure 4.6C. The whole assembly was immobilized and exposed to a portable UV lamp with an intensity of 0.4 mW/cm^2 until the SU-8 was partially cured, by shining the UV light for approximately

45 minutes through each side of the assembly. Before the SU-8 was completely hardened, the angled microscope slide and gasket were removed from the assembly. At this time, any imperfections in the SU-8 portion of the mold could be trimmed before a second UV exposure of 30 min, which would finalize the SU-8 cure. The glass slide with SU-8 mold was then thoroughly rinsed and cleaned using IPA and ddH$_2$O before use.

4.2.2 Linear Gradient Hydrogel Fabrication, Protein Loading and Patterning

The linear gradient heterogeneous hydrogels were cast, preloaded with BSA and electrophoretically patterned using the same materials and methods used in the binary feature experiments (Sections 4.1.2 and 4.1.3).

4.2.3 Results and Discussion

Images of Ponceau stained surface patterns were taken by the same camera as used in previous experiments and used to generate image intensity maps using Matlab (Figure 4.7).
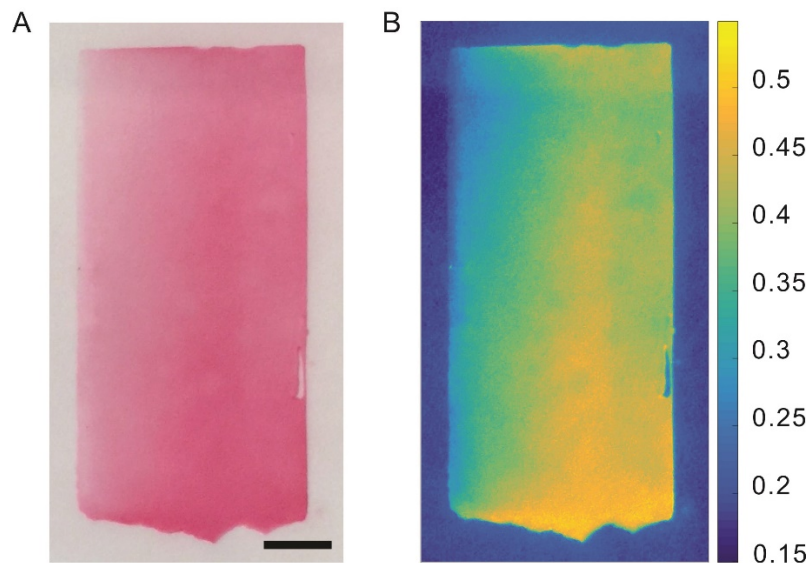
Figure 4.7 Protein patterning with ponceau detection (A) and corresponding intensity map generated by Matlab (B). Scale bar: 5 mm.

From this intensity map, two major gradients can be seen: one in the horizontal direction—which was intended—and a second, unintentional gradient in the vertical direction. The vertical gradient was most likely caused by unevenness in the original SU-8 mold. Despite the unwanted effect in the vertical direction, a clear linear gradient is seen in the horizontal direction, providing a basic demonstration of grayscale patterning. To emphasize this, when looking at part of the overall pattern, as shown in Figure 4.8, it is possible to see a distinct horizontal gradient, as confirmed by the intensity plot included in the same figure.
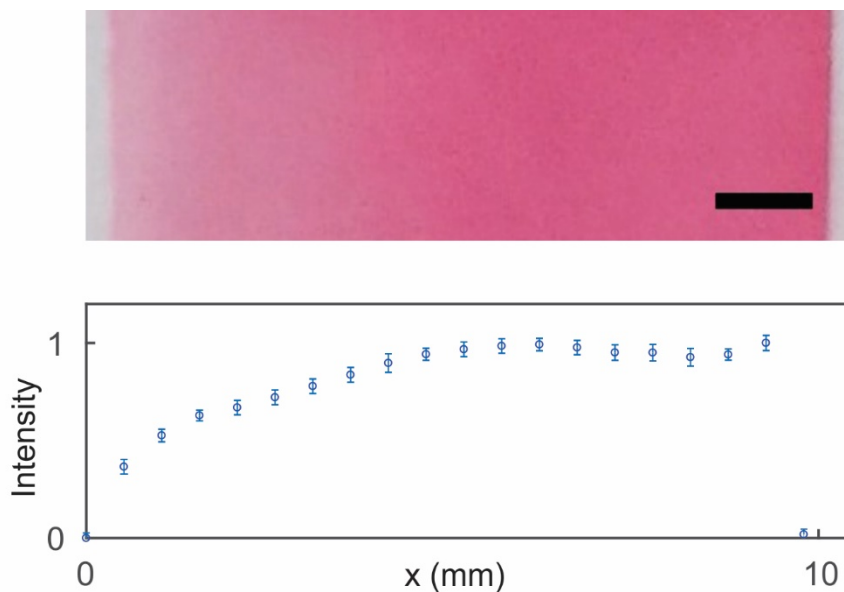
Figure 4.8 Partial image of previous result with Matlab-generated intensity plot. Scale bar: 2 mm.

The intensity plot shown in Figure 4.8 represents the mean and standard deviation of 8 lines of data taken at separate, evenly spaced traces across the whole image. The small standard deviation suggests that over smaller areas where the mold geometry is relatively

well controlled, it may be possible to reduce variability in the pattern produced. Also of note is the fact that the traces are not exactly linear, as the theory in Chapter 3 would have predicted. This is due in part to the semi-qualitative correlation between Ponceau stain intensity and protein concentration as well as some other factors that are discussed later in this chapter.

One thing that became clear during this series of experiments was the difficulty associated with maintaining consistent quality when fabricating the heterogeneous hydrogel, particularly in regions where the first hydrogel cast (15% PA) was very thin and covered a large surface area. Figure 4.9 shows the results of some experiments where problems occurred. In these cases, the 15% PA hydrogel was so thin that it tore or wrinkled when the mold was removed during fabrication. The effect of these wrinkles is reflected on the pattern deposition, where it formed uneven spots.
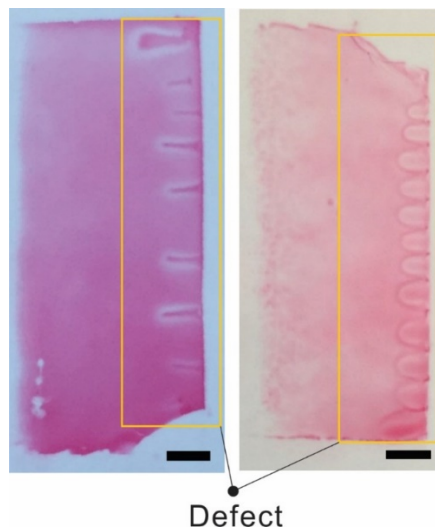
Figure 4.9 Patterns resulting from defective hydrogels. Scale bar: 3 mm.

In addition to showing the effects of defective hydrogels on patterning, Figure 4.9 also demonstrates the problem with using the digital camera and image intensity analysis method for quantifying results. Despite the fact that these images were taken using the same materials and equipment, lighting and camera settings have a significant impact on the absolute intensity captured in the images. This makes it very challenging to make quantitative comparisons between experiments and is one reason that this method of image analysis was replaced in later experiments.

4.3 Waveform Patterning

The results of the linear gradient patterning demonstrated potential of this method, but also highlighted problems with controllable mold fabrication, pattern detection, and uneven pressure gradients during patterning. The following series of experiments was intended to mitigate these problems. The first problem was addressed with the introduction of 3D printing for mold fabrication; in addition to addressing repeatability issues, the updated mold fabrication protocol could create much more complex features that would have been impossible with the previous methods. In addition, two methods of protein pattern detection were explored: the Ponceau staining technique and a fluorescent detection method. Finally, the method for loading the hydrogel into the holding cassette was modified in order to produce more even, repeatable pressure over the surface of the hydrogel during patterning.

4.3.1 Waveform Mold Fabrication Using 3D Printing

Because of the strong interest in 3D printing technology over the past few years, the cost for printing has dropped significantly, while the resolution steadily increased. This

made 3D printing a viable option for making the 3D molds used in this research. After some test printing, the FormLabs 1+ 3D printer was selected for mold generation (Figure 4.10A). This printer had a minimum layer size of 25 μm which was acceptable for generating features for the hydrogel molds. The molds were created by generating a 3D model with Solidworks and exporting it as a STL file. This file was then imported into FormLabs software for rendering and printing. The FormLabs SLA 3D printer relies on curing of a photoresponsive resin solution under the exposure of laser UV, and printing time was 2-3 hours on average for the molds used here; the feature area was generally 10 x 10 x 1 mm with a 75 mm x 50 mm x 2 mm thick base (Figure 4.10B). Additionally, supportive structures were automatically generated by the printer software. Once the printing was completed, the resin mold was removed and rinsed with IPA, resulting in a mold such as the one shown in Figure 4.10C.
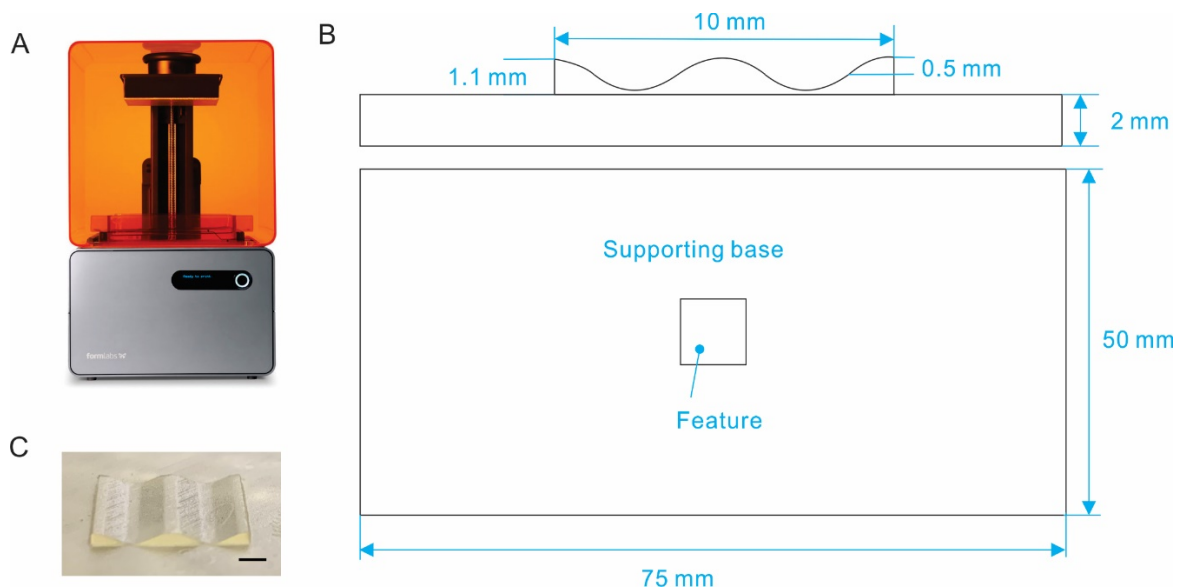
Figure 4.10 A: FormLabs 1+ SLA 3D printer; B: Geometry of waveform feature mold and base and C: SLA mold of waveform feature. Scale bar is 2 mm.

The raw resin molds produced using the FormLabs printer have two main issues for direct use as hydrogel fabrication molds. First, the waveform feature shown in Figure 4.10 printed more accurately when the entire mold was printed tilted at an angle to the base of the FormLabs machine. However, this resulted in an increase of surface roughness on the base of the mold, as shown in Figure 4.11A. Second, the resin base would slowly warp when exposed to the ambient environment, as shown in Figure 4.11B. Increasing the thickness of the base decreased the severity of the curvature, however even for a 4 mm thick base—which caused an extreme increase in printing time compared to the original 2 mm base—some curvature would still exist. The combination of these two effects made it impossible to create a watertight seal when assembling the mold for hydrogel casting.
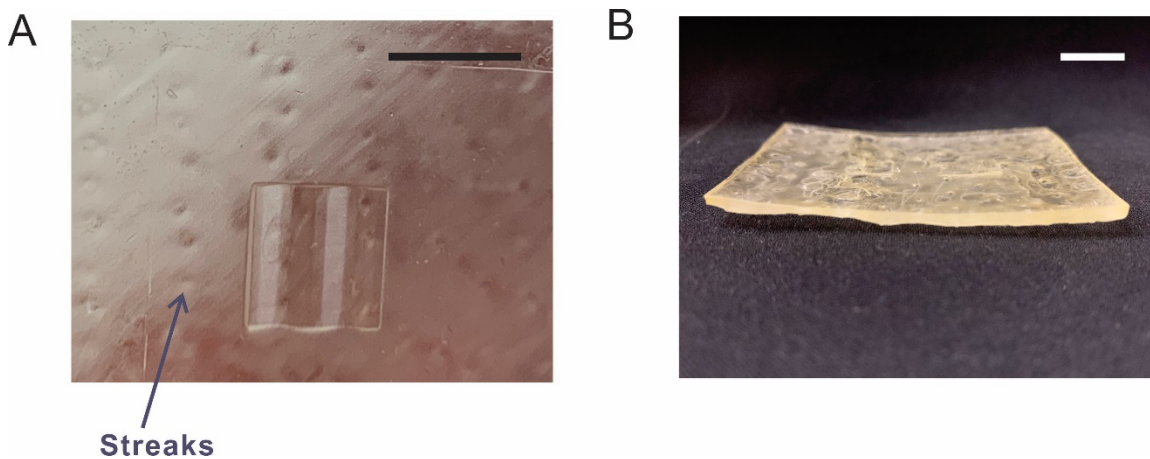
Figure 4.11 A: Close view of SLA resin mold showing surface roughness generated by the 3-D printer; B: Resin mold curvature example. Scale bar: 10 mm.

To mitigate this problem, new molds were made out of SU-8 and glass by using a two-step casting process and the original SLA mold. First, the negative of the SLA mold was cast in PDMS by pouring liquid PDMS over the SLA mold, degassing it in a vacuum and curing it in an oven at 150 °F for 90 min. Once cured, the SLA and PDMS was removed

from the oven and allowed to return to room temperature and then the two components were separated. The negative PDMS mold was then used to cast the final SU-8 mold by pouring SU-8 3050 into the PDMS mold cavity, sealing it with a clean glass microscope slide, and using a portable UV light source to cure the SU-8 through the glass. Because the PDMS interfered with UV light passing through, the SU-8 mold could only be cured through the glass side of the assembly, so for our feature height it typically took more than 100 min to cure than the linear gradient SU-8 mold.

The intermediate mold was made from PDMS in part because it is easy to work with and the flexible nature of PDMS made it easy to remove from the final SU-8/glass mold. However, because the SU-8 casting step required the PDMS mold be clamped to the glass microscope slide with a relatively large amount of force (to prevent liquid SU-8 from leaking out before curing), it caused the PDMS to deform during this step. In order to measure the magnitude of this deformation, the final SU-8 mold was cast in another layer of clear PDMS. This PDMS was removed from the SU-8 and backfilled with another layer of PDMS that had been dyed to be opaque using a small amount of food coloring. After this PDMS/PDMS composite was cured, it was cut using a razor blade and the cross-section imaged using a Nikon microscope (Figure 4.12). By analyzing this image, it is possible to see the true minimum and maximum feature heights of the SU-8 mold, which are 350 μm and 950 μm, respectively.

Figure 4.12 Cross-section of PDMS casting made from SU-8/glass waveform mold. Scale bar: 1 mm.

The SU-8 mold was sent to Micro/Nano Technology Center at University of Louisville for 3-D contact profiling using a Veeco contact profilometer. The raw data included 33 tracing lines and was processed using Excel and Matlab, resulting in the graphs shown in Figure 4.13. The surface plot shows that the geometry closely matches the original CAD file used to generate the SLA mold, however there is a slight gradient in the y-axis direction caused by the SLA to PDMS to SU-8 casting steps.
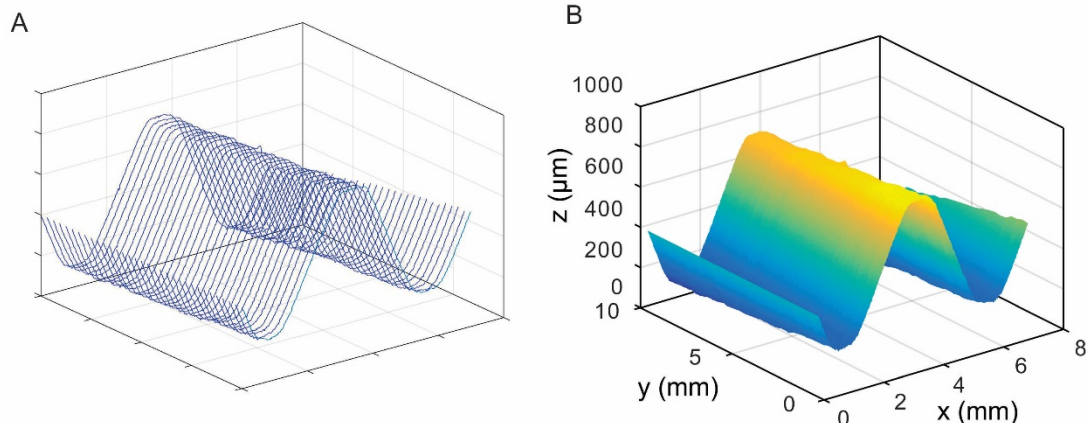
Figure 4.13 SU-8 mold surface: (A) raw data from stylus profilometer (33 traces) and (B) surface plot generated by extrapolating raw data. Both images generated in Matlab.

4.3.2 Results and Discussion – Ponceau and Incubation Experiments

After the SU-8 waveform mold was fabricated, the rest of the experiment was performed in the same manner as the linear gradient patterning. Image results were taken with the same lab camera (Figure 4.14A) and analyzed with Matlab. A section of the SU-8 waveform mold surface profile and the intensity of the corresponding Ponceau pattern

are shown side-by-side in Figure 4.14B and C. In this comparison, there is a strong correlation between the intensity curve and the SU-8 mold surface profile.
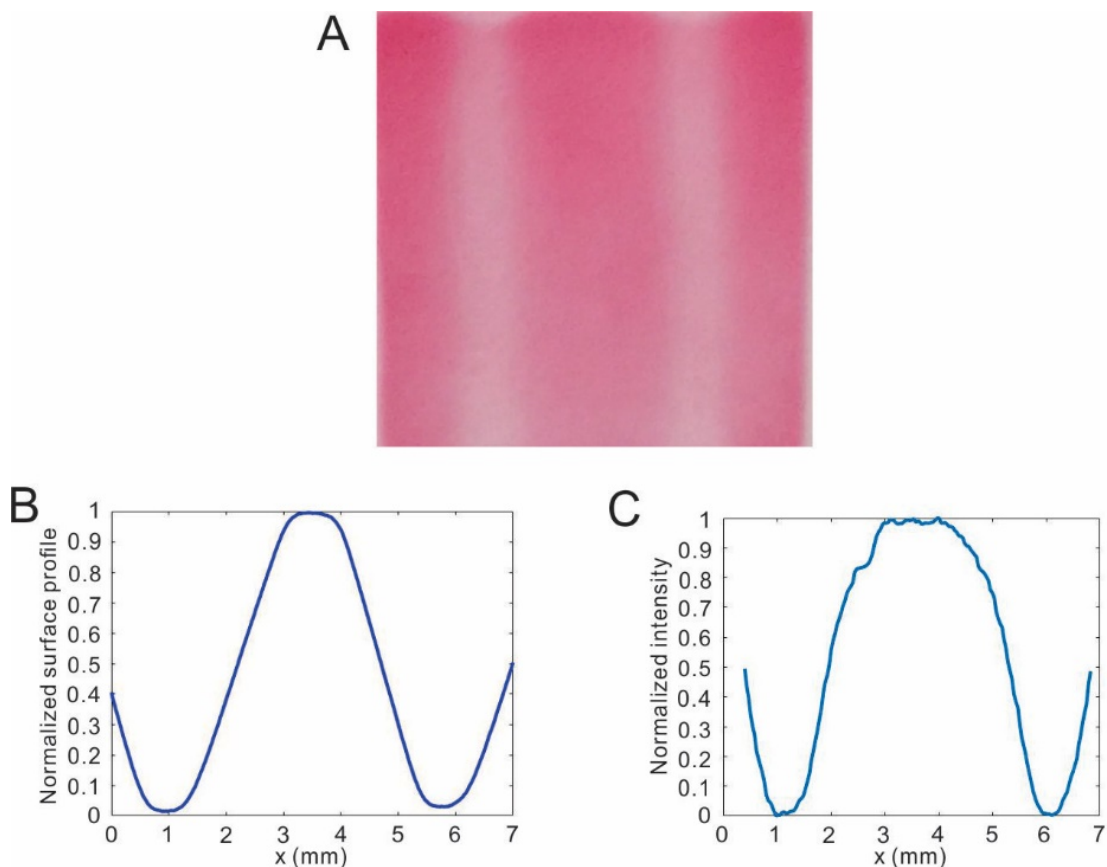
Figure 4.14 A: Waveform patterning image with Ponceau stain; B: Surface profile plot of SU-8 mold; C: Selected area protein concentration plot from A. Scale bar: 2 mm.

Ponceau S stain has been a popular protein detection tool in biological laboratories because of its convenience and ability to stain virtually any protein. However, this chemical relies on reversible bounding with proteins and can deteriorate over time, leading to problems with long-term storage of patterning results. Additionally, because of the non-specific nature of the stain binding to proteins, it provides only a semi-quantitative visualization of the results [94]. For these reasons, all of the following experiments instead use fluorescently-tagged BSA molecules (TRITC-BSA, Protein Mods, LLC).

4.3.3 Results and Discussion – Fluorescent Detection and Cure-in-Place Experiments

The incubation-based protein loading method used in previous experiments is time intensive as it requires soaking the hydrogel in protein solution until it equilibrates—typically on the order of 12-24 hours. In order to combat this problem, a "cure in-place" protein loading method was developed. In this method, proteins were mixed into the hydrogel solution when it was still in liquid form, poured into the mold, and cured in place. The entire experimental process is shown in Figure 4.15, with the cure-in-place step represented in Figure 4.15d. And as mentioned in the previous section, fluorescently-tagged BSA molecules were used instead of unlabeled BSA so that fluorescent detection could be used instead of colormetric image intensity analysis. The combination of these two changes made the patterning method much more time efficient—by eliminating what was, by far, the longest step—and reduced errors in detection that had been stemming from the semi-quantitative Ponceau stain and inconsistencies with image lighting and acquisition using a standard camera.
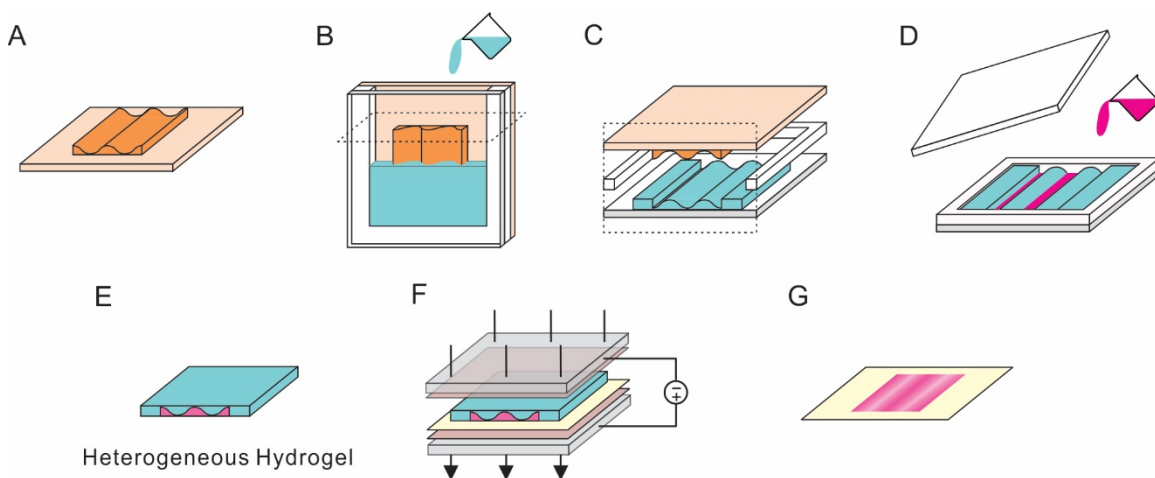
Figure 4.15 Fabrication and patterning of 3D heterogeneous hydrogel. A reusable SU-8/glass mold (A) was assembled with a glass microscope slide and u-shaped gasket before pouring high density hydrogel (15% PA) into the enclosed space (B). After curing, the mold was removed from the hydrogel (C) and a low density hydrogel (8% PA) mixed with TRITC-BSA was poured into the voids formed by the original mold (D). This assembly

was covered with a plain glass slide and cured, after which the hydrogel was removed from the assembly (E). The hydrogel was sandwiched between target and filter papers and placed in an electric field for a predetermined amount of time (F), causing the proteins to be deposited onto the target paper in the desired pattern (G).

The methods used in these experiments are similar to those in previous sections, but with a few notable changes (including those listed above). Two-layer waveform hydrogels were made by sequentially casting 15% PA and 10% PA hydrogel using the mold. First, a mold was cleaned with isopropyl alcohol (IPA), rinsed with ddH$_2$O, and dried using compressed air; then this mold was assembled with a plain microscope slide and the same 1.1 mm thick laser-cut u-shaped acrylic gasket such that one end of the assembly remained open to air. The 15% PA solution was prepared from 2.4 mL ddH$_2$O, 5.0 mL 30% degassed Acrylamide/Bis-Acrylamide 37.5:1 (AM/Bis), 2.5 mL gel buffer (1.5 M Tris-HCl buffer, pH 8.8), 50 µL 10% ammonium persulfate (APS), and 15 µL tetramethylethylenediamine (TEMED). This solution was poured into the mold/gasket assembly and carefully covered with a layer of ddH$_2$O and allowed to gel at room temperature for 15 minutes (Figure 4.15A,B). Once the 15% PA hydrogel polymerized, the mold/gasket assembly was carefully disassembled so that the mold could be replaced with a plain microscope slide (Figure 4.15C). A 10% PA hydrogel + TRITC-BSA solution was created by 5 mL of PA hydrogel solution (made in bulk by mixing 5.2 mL ddH$_2$O, 2.2 mL 30% degassed AM/Bis 37.5:1, 2.5 mL gel buffer, 50 µL 10% APS, and 15 µL TEMED) and adding 5 µL of 10 mg/mL tetramethylrhodamine-labeled bovine serum albumin (TRITC-BSA, Protein Mods, LLC) in 1x phosphate-buffered saline (PBS). This solution was poured into the hydrogel/gasket assembly and carefully covered with a layer of ddH$_2$O and allowed to gel at room temperature for 15 minutes (Figure 4.15D). After gelation, the

two-layer hydrogel was removed from the glass and gasket assembly (Figure 4.15E) and briefly rinsed with ddH$_2$O to remove any residual proteins on the surface.

BSA-laden hydrogels were prepared for electrophoretic patterning by sandwiching them between layers of filter paper and target paper, both of which were prewetted with buffer solution prior to assembly. This assembly was then loaded into a commercially-available electrophoretic transfer cell. Once assembled, a voltage of 80 V was applied for a specified time to cause partial or complete transfer of the BSA from the hydrogel to the target paper (Figure 4.15F,G).

After patterning, the target paper was removed and protein transfer was measured by imaging target paper using fluorescent microscopy on a Nikon Ti-E microscope. All images were acquired using the same exposure settings and intensity values were normalized between values of 0 (no signal) and 1 (saturation). Error bars in all figures represent standard deviation in measured data sets. Intensity analysis of images was performed using Matlab software.

Results from an experiment that was run for 15 minutes is shown in Figure 4.16, along with a graph comparing the florescent intensity to the local mold height used to generate the hydrogel. The fluorescent intensity of the resulting TRITC-BSA pattern shows good general agreement with the 2D topography of the mold. Some variability was observed in this experiment and similar ones, most likely caused by geometric distortion of the hydrogel during fabrication and lateral diffusion of BSA proteins during the printing process.
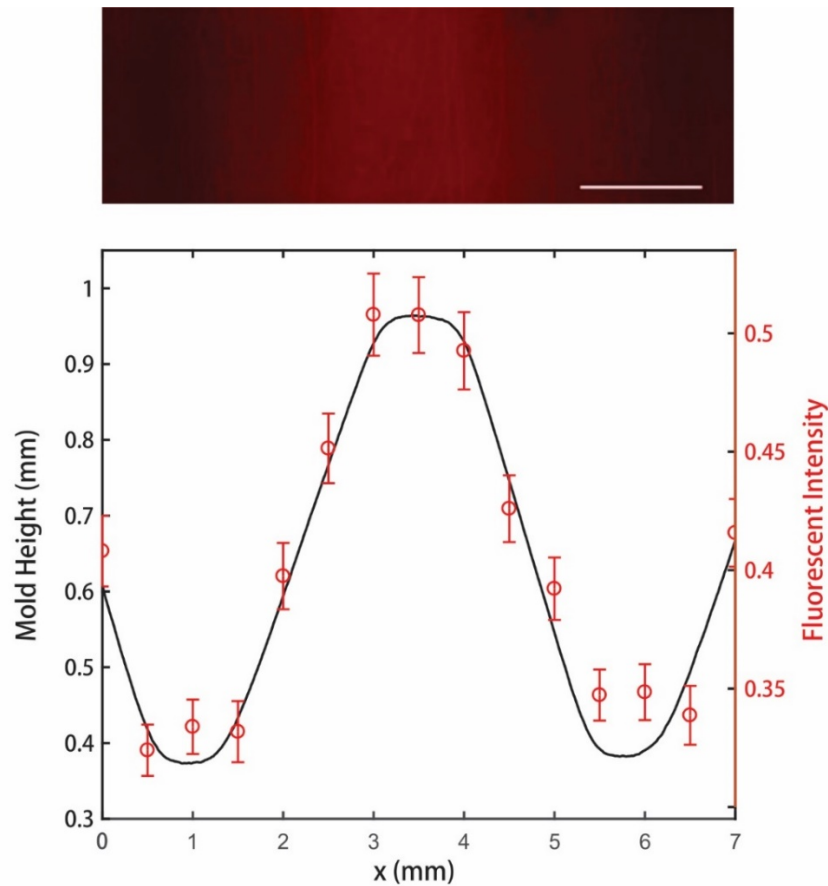
Figure 4.16 Fluorescent micrograph of TRITC-BSA pattern generated using waveform mold (top) and normalized fluorescent intensity from image compared to measured waveform mold height (bottom). Scale bar: 2 mm.

Experiments were also run using hydrogels preloaded with different volumetric concentrations of protein during the curing process (0.005, 0.010 or 0.015 mg/mL). All three samples were run for 15 minutes, and the fluorescent intensity was measured at the same place on each of the three resulting patterns (at a location that correlates to $h_A = 650$ μm). Figure 4.17 shows the results; it can be seen here that there is a linear correlation between initial protein concentration and average intensity, indicating that fluorescent intensity could be used as a quantitative estimate of protein concentration in this range.
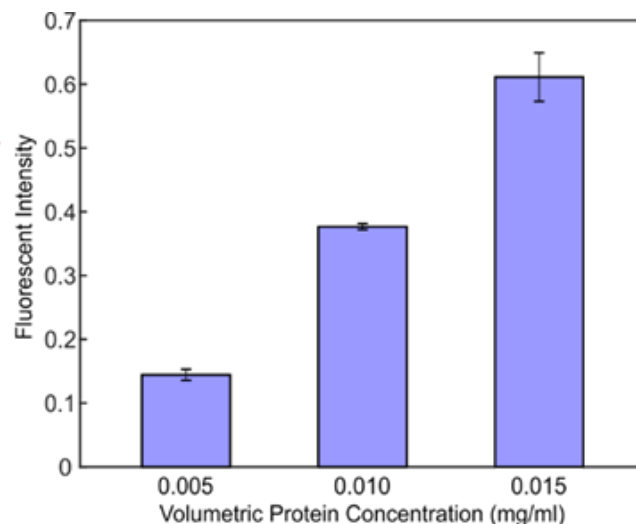
Figure 4.17 Fluorescent intensity of pattern produced using different protein concentration, measured at the same location in each pattern.

This experiment was also repeated for different electrophoresis times: 2, 5, 15, 30 and 40 minutes. The resulting images are shown in Figure 4.18; from this, it is possible to see the intensity increase in the first few images (2, 5, and 15 minutes), and then it eventually plateaus (15 to 30 minutes) and then eventually decreases slightly (30 to 40 minutes).
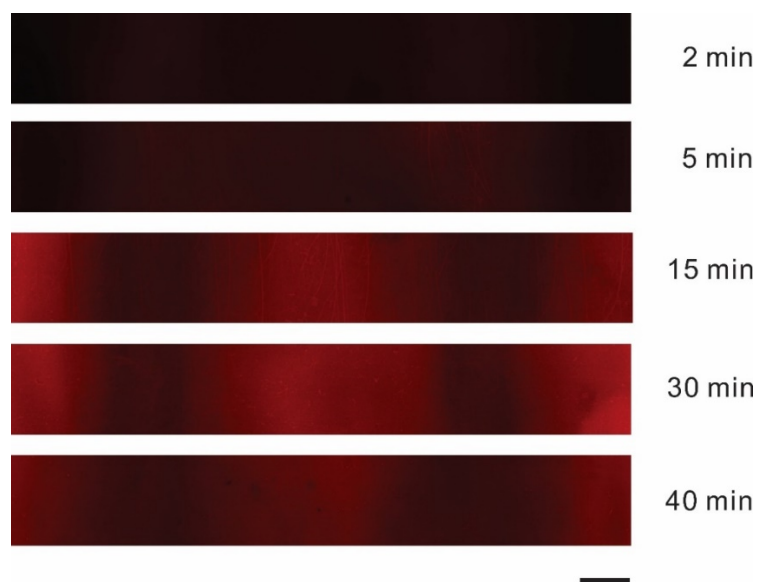
Figure 4.18 Fluorescent micrograph of TRITC-BSA pattern generated using waveform mold at different patterning times. Scale bar: 1 mm.

Figure 4.19 shows fluorescent intensity measured in two regions of these surface patterns: one region corresponding to a 10%PA+TRITC-BSA hydrogel thickness (h_A) of 400 μm and another of 950 μm. These show the same trend that can be observed qualitatively from the images themselves: short deposition times show incomplete deposition, characterized by an increase in intensity at longer times for both thicknesses, but the intensity value plateaus earlier and at a lower intensity value for the low h_A value (h_A = 400 μm), while the higher h_A region of the hydrogel (h_A = 950 μm) takes longer to fully deplete, which is consistent with the theoretical predictions in chapter 3.
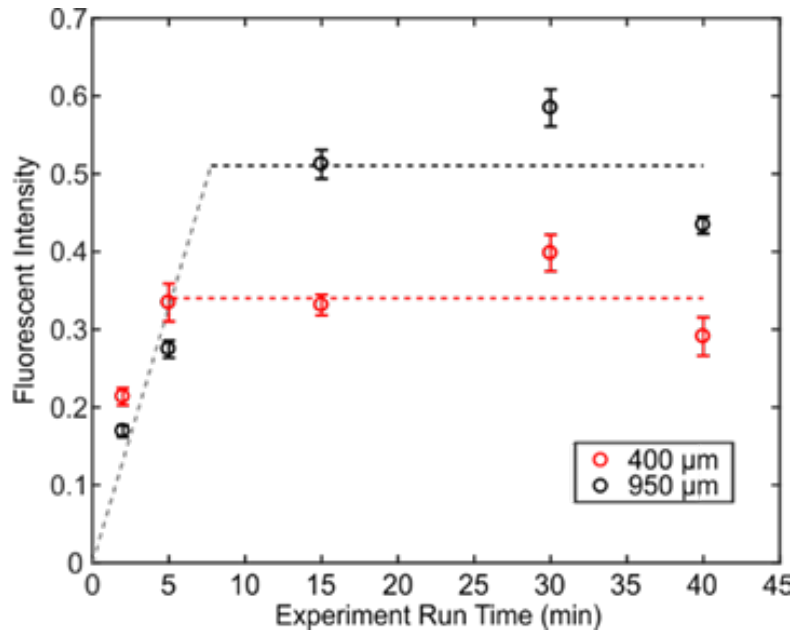
Figure 4.19 Pattern intensity as a function of time measured at two regions with the waveform mold

A linear fit of the incomplete deposition points was calculated and is shown as a grey dashed line in Figure 4.19, while the average values of the intensity at each height after full depletion are represented as black and red dashed lines. The intersection of these lines can be used as a rough estimate of full depletion time at each h_A value: approximately 7.6 min for the 950 μm thick hydrogel (intersection of black and grey dashed lines) and 5.1

min for the 400 μm thick hydrogel (intersection of red and grey dashed lines). In addition, experiments run for extended periods of time—more than 3x the full depletion time— exhibited a decrease in intensity, which may be caused by degradation of fluorophore or electrophoretic force driving the protein further into the porous structure of the target paper.

4.4   Complex Grayscale Feature Patterning

In order to demonstrate electrophoretic patterning for more complex surface patterns, several other surface patterns were generated, largely using the processes described in the previous section.

4.4.1 Coin Patterning

In order to generate a complex 3D structure without having to print an SLA mold, the relief surface present on the back of a quarter was used as a starting point. A negative mold of this surface was cast in PDMS and then transferred to a positive mold in SU-8 on glass (Figure 4-20A), using the methods described in the previous section. A heterogeneous hydrogel of 15%PA with 10%PA+TRITC-BSA was cast and run for 15 minutes at 80 V, resulting in the pattern shown in Figure 4-20B. Overall, there was good consistency between the mold and BSA pattern, but because the peak-to-valley height of the features on the mold was relatively low (around 150 μm), not much intensity difference was seen between the regions corresponding to tall features in the mold and those corresponding to shorter features in the mold.
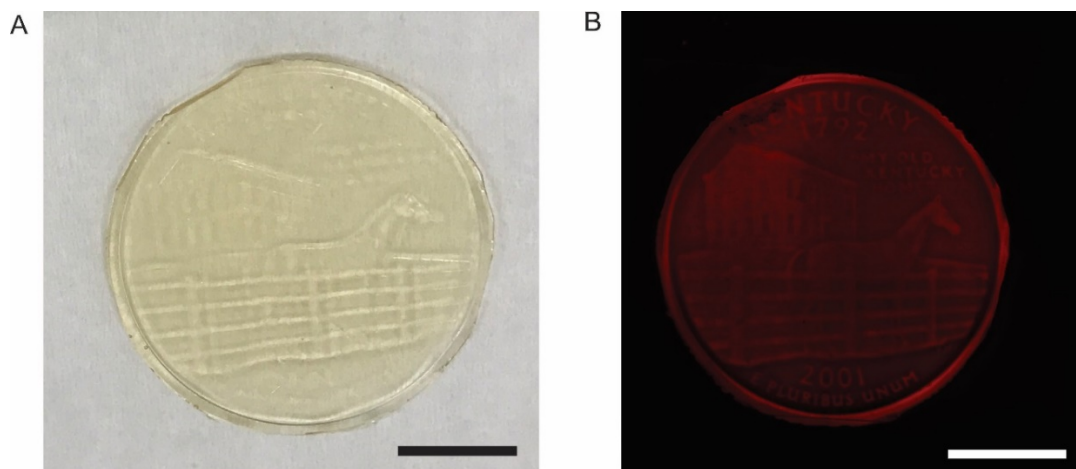
Figure 4.20 A: SU-8 mold created from a quarter; B: fluorescent image of the resulting pattern. Scale bar: 8 mm.

4.4.2 Horse Feature Patterning
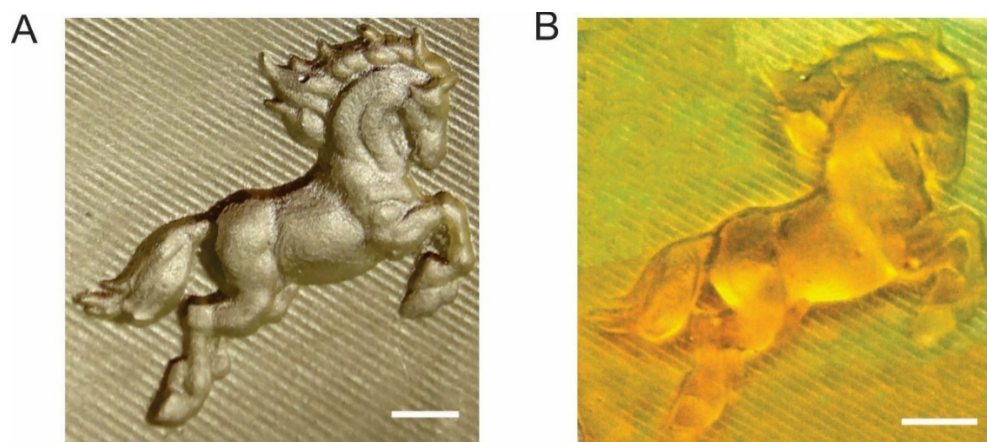
Figure 4.21 A: PDMS negative mold sputter coated with gold for visualization and surface measurement. B: Positive mold created by casting SU-8 against 3D printed SLA negative mold Scale bars: 2 mm.

An open source 3D SLA file [horse by poggia 10, MakerBot's Thingiverse] was scaled and printed using stereolithography and replicated in PDMS (Figure 4.21A) and then SU-8 (Figure 4.21B). SU-8 molds were used to create 10%PA+TRITC-BSA and 15%PA binary hydrogels as described in section 4.3.4, and then run in an electrophoretic

transfer cell for 15 minutes at 80 V voltage. After use, the PDMS mold in Figure 4.19A was sputter coated with a 300 nm thick layer of gold for optical surface profiling by a Zygo interferometer.

Figure 4.22 shows a 3-D confocal scan of one of the heterogenous hydrogels before patterning. It can be seen from the well-defined pattern in this image that the fluorescent TRITC-BSA is only contained in the 10%PA hydrogel and does not diffuse into the 15% PA hydrogel after the hydrogel is fabricated.
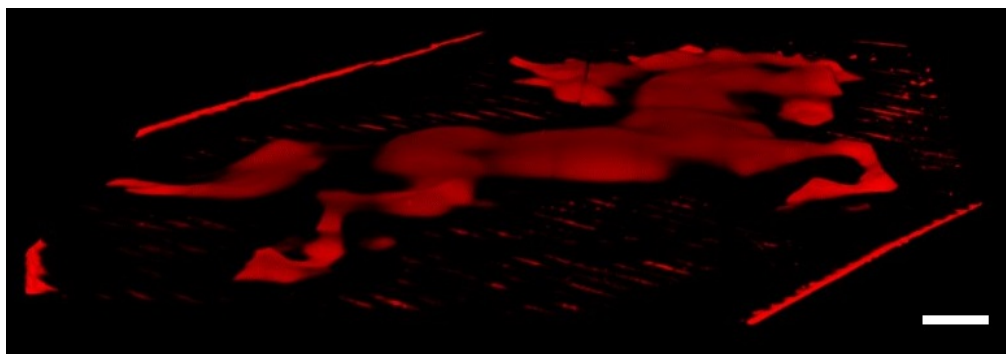
Figure 4.22 Confocal microscope image scan of 15%PA/10%PA-TRITC-BSA hydrogel. Scale bar: 2 mm.

Confocal images were also taken of the hydrogels before and after electrophoretic patterning. Figure 4.23 shows the comparison before (left) and after (middle, right) running a 15 min electrophoresis experiment. In the "after" image, the fluorescent signal was so low that LUTs settings had to be adjusted in order to get any signal, resulting in the grainy image quality. The stark difference between the min/max values in the before versus after images suggest that most or all of the fluorophore tagged proteins were extracted from the hydrogel during the electrophoretic patterning process. Therefore, it is safe to claim that after 15 min all protein was deposited.
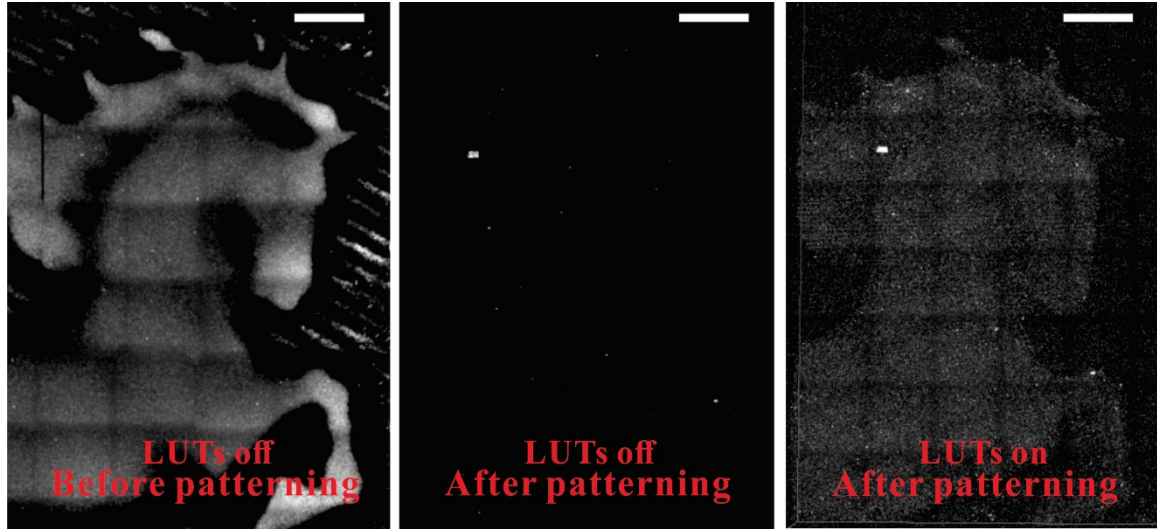
Figure 4.23 Region of two layer hydrogel before (left) and after (middle, right) 15 minutes of electrophoresis. Scale bar: 2 mm.

The local surface height of the mold was sampled at 40 random points and compared to the local fluorescent intensity in the resulting fluorescent image for a sample run for 15 minutes (Figure 4.24). The results demonstrate a general linear correlation between the local mold height and local fluorescent intensity at low to medium mold heights (dashed line), as predicted by theory. However, above 450-500 μm the correlation becomes increasingly nonlinear, an effect caused by diffusion of BSA molecules away from geometric peaks within the patterned hydrogel. Since the diffusion trajectory is normal to the boundary between the 10% and 15% PA hydrogels, in complex patterns where the molds have geometry with steep local slopes—such as horse pattern—the diffusion effect is more pronounced than in the waveform pattern, which has a much more gradual slope. Therefore, when molds have "sharper" peaks, resulting patterning tends to have a more pronounced "blurring" effect.

93
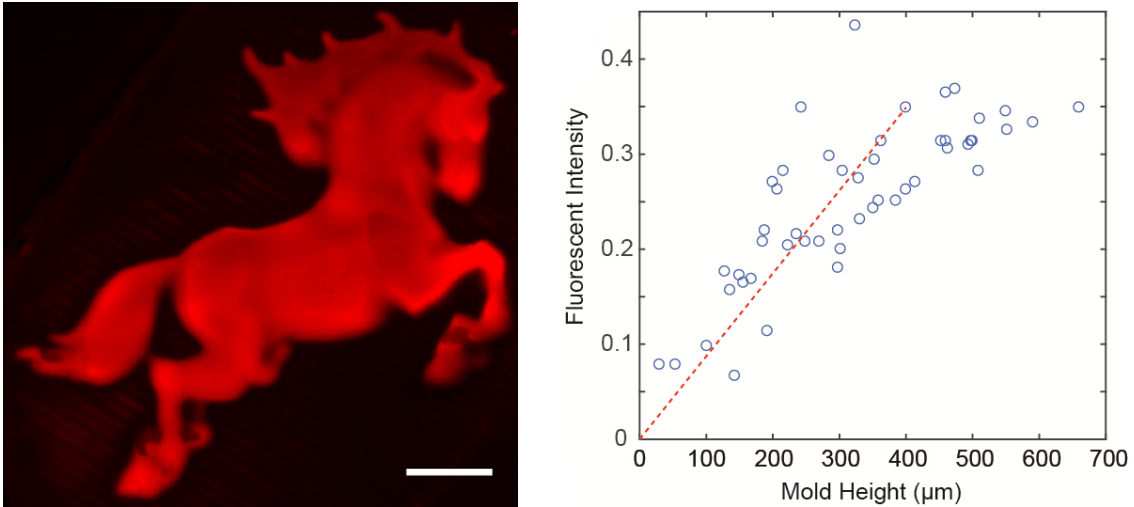
Figure 4.24 Fluorescent image of TRITC-BSA surface pattern (left) and comparison of regional mold height to fluorescent intensity on deposited surface pattern for randomly-selected points in the pattern (right). Scale bar: 2 mm.

4.5   Other Considerations

4.5.1 Pressure Effects and Uniformity in Patterning

The cassette used to assemble the target paper, filter paper and hydrogel for patterning had a basic hinge and locking mechanism and was made out of thin, relatively flexible plastic. Because of this, the cassette generated uneven pressure on the hydrogel (Figure 4.25). In order to minimize the effect of the non-uniform pressure on the patterning results, a 2 mm thick piece of acrylic was laser cut such that the outside dimensions were the same as the dimensions of the cassette, but it had a rectangular cut out of 75 x 50 mm (the same size as the hydrogel) in the center. This stencil was used to improve repeatability of hydrogel placement within the cassette from experiment to experiment, and was removed before the cassette was closed and used in electrophoretic patterning.
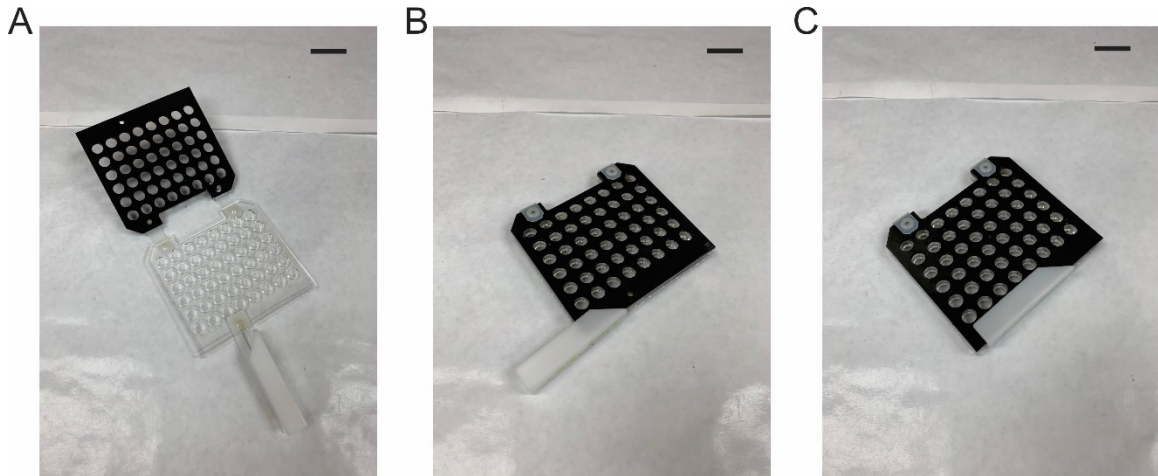
Figure 4.25 A: Cassette with hinge used in patterning experiments. From open status (A) to closed (B) then to locked (C). Scale bars: 20 mm.

To explore the effect of the pressure and other uniformity effects on patterning, we used a flat, homogeneous hydrogel (10% PA gel) incubated in BSA and subjected it to electrophoretic patterning. Figure 4.26A shows the result after patterning and Ponceau staining; a Matlab analysis of the pattern (Figure 4.26C) shows a slight overall gradient along the y-axis and also a small amount of local variability, likely caused by regional variation in the hydrogel composition and density. Overall, the total variability caused by these effects is small compared to the effect of the hydrogel height in patterning (i.e., intensity varies from 0.18 to 0.48 for selected gradient pattern in Figure 4.26, but only from 0.35 to 0.39 in the homogeneous hydrogel image).
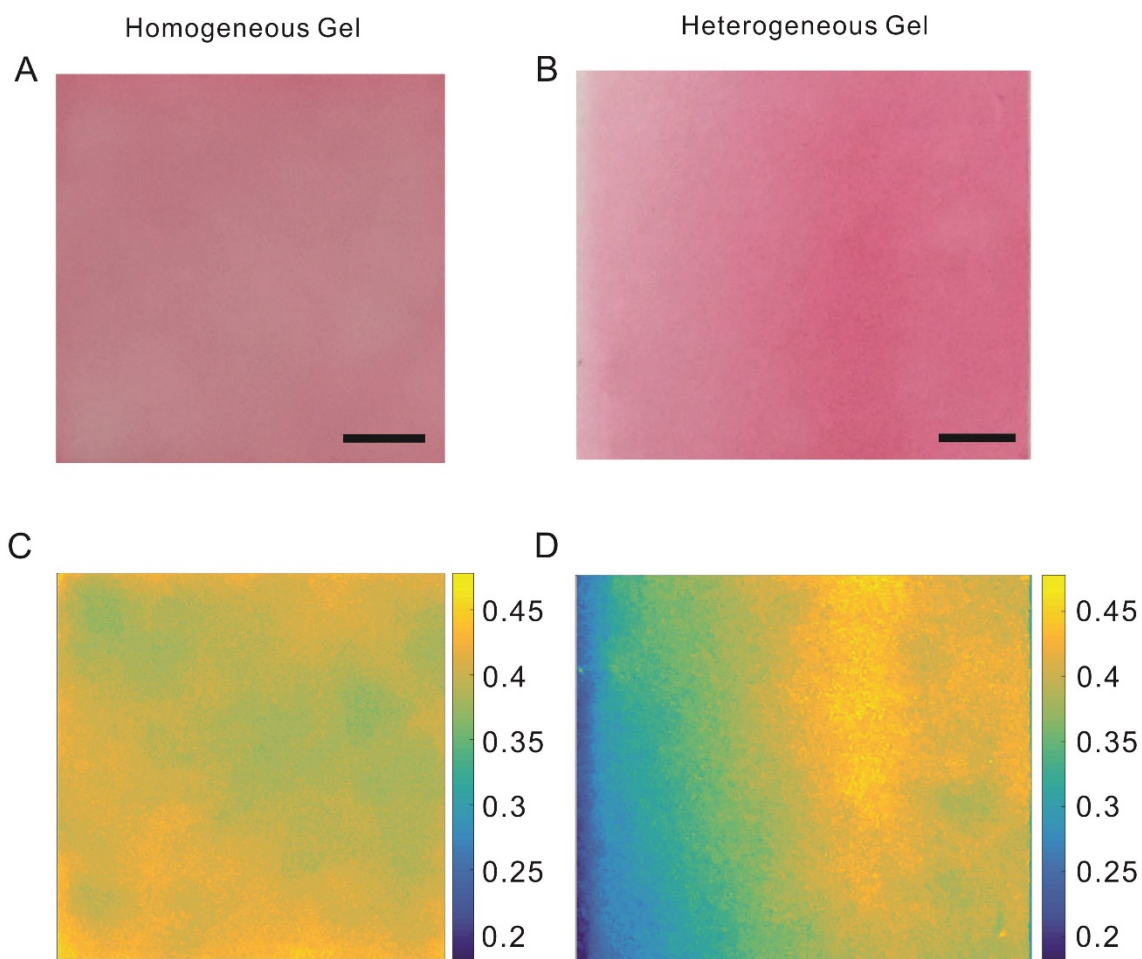
Figure 4.26 Ponceau-stained filter paper pattern from homogeneous hydrogel (A) compared to linear gradient (B). Matlab intensity analysis each image (C, D). Scale bar: 2 mm.

4.5.2 Electrophoresis-Free Transfer

To further examine the effects of diffusion and pressure in patterning, heterogeneous hydrogels were fabricated as previously described in sections 4.3.3 and 4.4 and assembled in the cassette with target paper and filter paper. Then the assembled cassette was allowed to incubate in the electrophoretic transfer chamber for a set period of time without applying an electric field. Because the cassette applies a constant, but uncontrollable, amount of force, a separate apparatus was also built that used a manual *z-*

stage to apply a controllable amount of pressure/displacement to the hydrogel/target-paper/filter-paper stack.

Figure 4.27 shows the results of the same waveform hydrogel pattern run using three different experimental conditions: (A) assembled in the cassette and run for 40 minutes at 80 V (+pressure, +electrophoresis), (B) assembled in the cassette and incubated for 40 minutes with no applied voltage (+pressure, -electrophoresis), and (C) assembled in the *z*-stage apparatus where the hydrogel and target paper were brought into contact but no pressure was applied and incubated for 40 minutes (-pressure, -electrophoresis).

A

+pressure +Electrophoresis

B

+pressure -Electrophoresis

C

-pressure -Electrophoresis
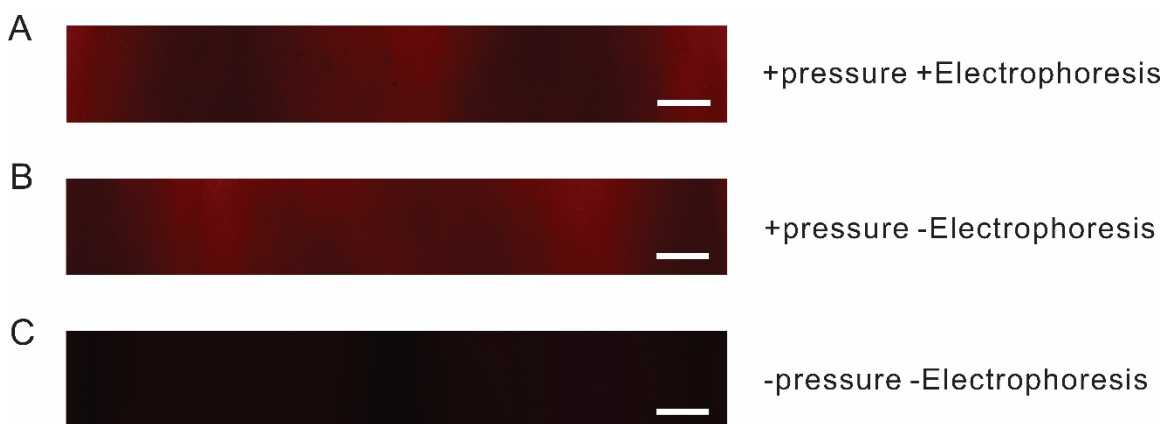
Figure 4.27 Patterning results after 40 minutes using (A) 80V electrophoresis patterning, (B) non electrophoresis using cassette assembly and (C) non electrophoresis using *z*-stage to bring target paper into contact with hydrogel. Scale bar: 2 mm.

The results from (B) show a surprising inversion of the original intended pattern (i.e., high protein deposition in places where low deposition was intended and vice-versa). But in experiments when the pressure was removed (C), very little protein transfer occurred at all.

The electrophoresis-free patterning experiment was repeated using the *z*-stage to apply a higher amount of pressure during patterning using contact. The results are shown

in Figure 4.28, along with results using electrophoresis. These also show a significant inversion in the intended pattern, although it is difficult to make concrete comparisons between the two because of the image and pattern quality. In addition, the –electrophoresis experiments in Figure 4.28 were run using an unknown concentration of TRITC-BSA in the hydrogel.
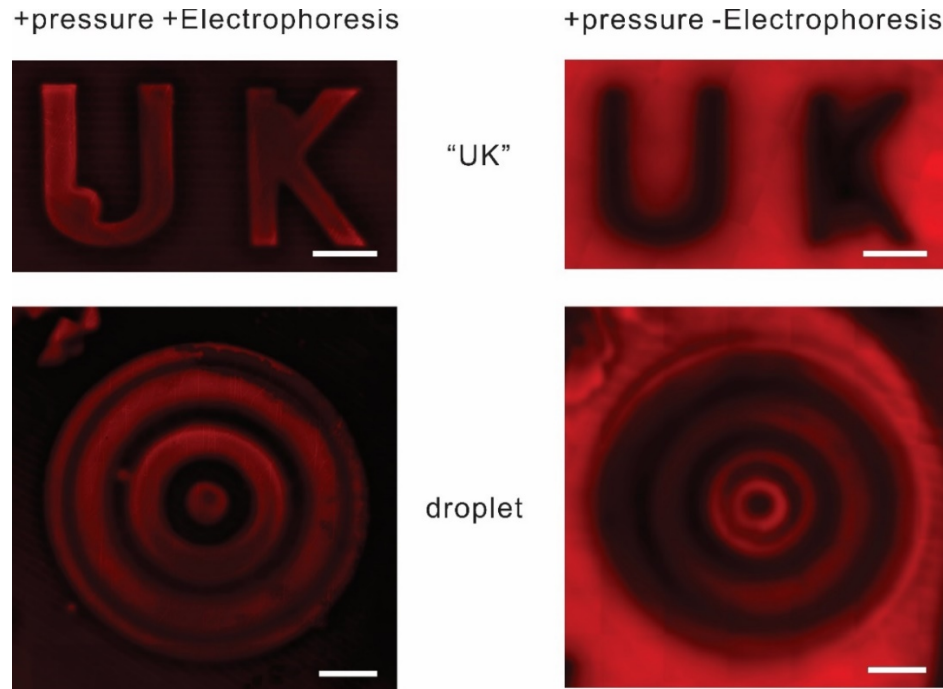
Figure 4.28 Patterns produced using electrophoretic patterning (left) compared to diffusion/pressure based patterning using a *z*-stage to apply controlled pressure. Scale bars: 2 mm.

The pattern inversion shown in the previous figures appears to be a repeatable, and interesting effect. In the future, it would be of interest to characterize this effect further and explore the mechanisms causing it.

CHAPTER 5. CONCLUSIONS AND FUTURE WORK

5.1   Conclusion

In this work, we demonstrated a method of generating grayscale protein surface patterns by combining equipment and techniques commonly found within most microbiology labs—a commercially available electrophoretic transfer cell and fabrication of polyacrylamide hydrogels—with a technology that has recently become broadly accessible: desktop 3D printing. By starting with molds derived from 3D-printed master geometry, we were able to create polyacrylamide hydrogels that had patterned regions of high and low polymer density. When these heterogeneous hydrogels were loaded with proteins, they were preferentially retained in the low-density regions. Subjecting these hydrogels to an electric field caused proteins to move quickly onto a target surface, resulting in grayscale surface patterns.

By using this method, we successfully created multiple patterns of increasing complexity: a binary pattern, a one dimensional linear gradient, a waveform gradient pattern, and more complex patterns including a coin, concentric circles, and a horse. All equipment and materials used in this dissertation are commonly seen and found in biological laboratories, thus achieving the original goal of using a universal commercial apparatus to generate complex surface patterns.

5.2   Future Work

5.2.1 Improvements to Electrophoresis Patterning Process

While using commercially available equipment is advantageous because it broadens access to this technique, using equipment for purposes other than those for which

it was explicitly designed does present some drawbacks that became apparent during these experiments. One thing that could be done to alleviate some of these problems would be to create a new cassette for holding the hydrogel. The current cassette generates uncontrolled and non-uniform pressure; replacing this system with one that contains brackets to hold the gel assembly properly might reduce or eliminate pressure variability and minimize distortion of the hydrogel shapes. In addition, a redesigned cassette holder could help to deliver a more uniform electric field. Finally, the low Young's modulus of the hydrogels made them difficult to handle consistently; designing a special set of tools to aid in transfer of the hydrogel from mold to cassette could lower the damage rate and make the process easier.

5.2.2 Testing with Other Biochemical Species

This analysis and patterning method discussed in this dissertation can theoretically be extended to any particle that can be propelled by electrophoretic force, given that appropriate hydrogel combinations can be found to sufficiently control particle sequestration and motion. One of the next steps would be to demonstrate patterning with other biochemical species or even try patterning multiple types of biochemicals at the same time. Mobility of molecules in specific hydrogel formulations can be determined empirically, and in some cases estimated from the literature; these values can be combined with the analysis presented here to estimate patterning results.

5.2.3 Pressure Induced Inverse Patterning

Pressure induced inverse patterning was an interesting discovery during the development of this patterning method. Initial results demonstrated the potential of this

method, as it was capable of producing a large intensity variation between different sections of the pattern. This method needs to be further characterized to determine fidelity of the patterned features to the mold and determine the repeatability of this method.

Additionally, the mechanics of the heterogeneous hydrogel and other properties need to be further studied to help determine the governing mechanisms behind the inverse patterning phenomenon, so that it can be used to predict resulting patterns. The z-stage mechanism developed in this work provides a simple way to precisely control of the pressure applied on a hydrogel stack. A modified version of this mechanism—reducing the bulk of the device and adding the ability so submerge the hydrogel in buffer solution— could be useful in these studies and eventually in the creation of new patterns.

REFERENCES

1. Rabih Zaouk, B.Y.P., Marc J. Madou, *Introduction to Microfabrication Techniques.* Microfluidic Techniques, 2006. **321**: p. 5-15.
2. V.S. Goudar, S.S., M.M. Varma, *Photoresist functionalisation method for high-density protein microarrays using photolithography.* Micro & Nano Letters, 2012. **7**(6): p. 549-553.
3. Nicholas E. Kurland, T.D., Subhas C. Kundu, Vamsi K. Yadavalli, *Precise Patterning of Silk Microstructures Using Photolithography.* Advanced Materials, 2013. **25**(43): p. 6207-6212.
4. Liu Jiang, H.Q., Gang Chen, , , Chunyan Li, Guangjun Yan, Yanling Luo, Peng Liu, Yashao Chen, Liu Jiang, Huaming Qian, Gang Chen, Chunyan Li, Guangjun Yan, Yanling Luo, Peng Liu, Yashao Chen, *Fabrication of micropatterns on polypropylene films via plasma pretreatment combined with UV-initiated graft polymerization.* Journal of Biomaterials Applications, 2017. **31**(10): p. 1346-1357.
5. Chunyan Li, A.G., Xiaofei Yuan, Zhixiong Hu, Ellie Pulleine, Jon Cooper, Wantai Yang, and Huabing Yin, *Creating "Living" Polymer Surfaces to Pattern Biomolecules and Cells on Common Plastics.* Biomacromolecules, 2013. **14**(5): p. 1278-1286.
6. Wenguang Yang, H.Y., Fanan Wei, Gongxin Li, Yuechao Wang, Lianqing Liu, *Selective pattern of cancer cell accumulation and growth using UV modulating printing of hydrogels.* Biomedical Microdevices, 2015. **17**(6).
7. Pierre-Olivier Strale, A.A., Ghislain Bugnicourt, Yohan Lecomte, Makhlad Chahid, Vincent Studer, *Multiprotein Printing by Light-Induced Molecular Adsorption.* Advanced Materials, 2015. **28**(10): p. 2024-2029.
8. Ansgar Waldbaur, B.W., Katja Schmitz, Bastian E Rapp, *Maskless Projection Lithography for the Fast and Flexible Generation of Grayscale Protein Patterns.* Small: nano micro., 2012. **8**(10): p. 1570-1578.
9. Yushin Jung, H.L., Tae-Joon Park, Sungsik Kim and Sunghoon Kwon, *Programmable gradational micropatterning of functional materials using maskless lithography controlling absorption.* Scientific Reports, 2015. **5**.
10. Whitesides, Y.X.a.G.M., *Soft Lithography.* Angewandte Chemie International Edition, 1998. **37**(5): p. 550-575.
11. Whitesides, A.K.a.G.M., *Features of gold having micrometer to centimeter dimensions can be formed through a combination of stamping with an elastomeric stamp and an alkanethiol "ink" followed by chemical etching.* Applied Physics Letters, 1993. **63**(14): p. 2002-2004.
12. Perl, A., D.N. Reinhoudt, and J. Huskens, *Microcontact Printing: Limitations and Achievements.* Advanced Materials, 2009. **21**(22): p. 2257-2268.
13. Laurent Libioulle, A.B., Heinz Schmid, Bruno Michel, and Emmanuel Delamarche, *Contact-inking stamps for microcontact printing of Alkanethiols on gold.* Langmuir, 1998. **15**(2): p. 300-304.
14. Amit Kumar, H.A.B., Nicholas L. Abbott, and George M. Whitesides, *The use of self-assembled monolayers and a selective etch to generate patterned gold features.* Journal of the American Chemical Society, 1992. **114**(23): p. 9188-9189.

15. Amit Kumar, H.A.B., and George M. Whitesides, *Patterning Self-Assembled Monolayers; Applications in Materials Science.* Langmuir, 1994. **10**(5): p. 1498-1511.

16. Dongliang Tian, Y.S.a.L.J., *Patterning of controllable surface wettability for printing techniques.* Chemical Society Reviews, 2013. **42**(12): p. 5184-5209.

17. Amare Benor, A.H., Veit Wagner, Dietmar Knipp, *Microcontact printing and selective surface dewetting for large area electronic applications.* Thin Solid Films, 2007. **515**(19): p. 7679-7682.

18. Zhibin Wang, P.Z., Brett Kirkland, Yingru Liu and Jingjiao Guan, *Microcontact printing of polyelectrolytes on PEG using an unmodified PDMS stamp for micropatterning nanoparticles, DNA, proteins and cells.* Soft Matter, 2012. **8**(29): p. 7630-7637.

19. C Thibault, V.L.B., S Casimirius, E Trevisiol, J Francois and C Vieu, *Direct microcontact printing of oligonucleotides for biochip applications.* Journal of Nanobiotechnology, 2005. **3**(7): p. 12.

20. Chang-Jiang Pan, Y.-D.N., Yun-Xiao Dong, *Microcontact Printed Protein Micropatterns on Titanium Surface Characterized by Confocal Laser Scanning Microscopy.* Advanced Materials Research, 2012. **487**: p. 730-734.

21. Hsiu-Wen Chien, W.-H.K., Meng-Jiy Wang, Shiao-Wen Tsai, and Wei-Bor Tsai, *Tunable Micropatterned Substrates Based on Poly(dopamine) Deposition via Microcontact Printing.* Langmuir, 2012. **28**(13): p. 5775-5782.

22. Chen, S.A.R.a.C.S., *Microcontact printing: A tool to pattern.* Soft Matter, 2007. **3**(2): p. 168-177.

23. Luisa Filipponi, P.L., Ondrej Kaspar, Viola Tokarova, Dan V. Nicolau, *Protein patterning by microcontact printing using pyramidal PDMS stamps.* Biomedical Microdevices, 2016. **18**(1): p. 1-7.

24. Nobuyuku Tanaka, H.O., Kazuhiro Fukumori, Jun Miyake, Masayuki Yamato, Teruo Okano, *Micro-patterned cell-sheets fabricated with stamping-forcecontrolled micro-contact printing.* Biomaterials, 2014. **35**(37): p. 9802-9810.

25. Jinhai Li, L.X., Soyoun Kim and Alexander A. Shestopalov, *Urethane-acrylate polymers in high-resolution contact printing.* Journal of Materials Chemistry C, 2016. **4**(19): p. 4155-4165.

26. McGuigan, E.D.A.a.A.P., *Micropatterning strategies to engineer controlled cell and tissue architecture in Vitro.* BioTechniques, 2018. **58**(1): p. 13-23.

27. Chang-Jiang Pan, H.Q., Yu-Dong Nie, Hong-Yan Ding, *Control of osteoblast cells adhesion and spreading by microcontact printing of extracellular matrix protein patterns.* Colloids and Surfaces B: Biointerfaces, 2013. **104**(April 1st): p. 18-26.

28. A. G. Castano, V.H., A. Lagunas, C. Cortina, N. Montserrat, J. Samitier and E. Martinez, *Protein patterning on hydrogels by direct microcontact printing: application to cardiac differentiation.* RSC Advances, 2014. **4**(55): p. 29120-29123.

29. C. L. Feng, A.E., I. Bredebusch, J. Schnekenburger, W. Domschke, G. J. Vancso, H. Schonherr, *Reactive Microcontact Printing on Block Copolymer Films: Exploiting Chemistry in Microcontacts for Sub‐micrometer Patterning of Biomolecules.* Advanced Materials, 2007. **19**(2): p. 286-290.

30. Nur Adilah Abd Rahman, M.H.B., M. Mahadi Abdul Jamil, *An overview: Investigation of electroporation technique on cell properties cultured on micropatterned surface.* Journal Teknologi, 2015. **77**(6): p. 61-65.

31. Chun-Tao Zhu, S.-H.M., Ying Zhang, Xue-Jing Wang, Peng Lv, Xiao-Jun Han, *Fabrication of Thickness-Controllable Micropatterned Polyelectrolyte-Film/Nanoparticle Surfaces by Using the Plasma Oxidation Method.* Chemistry An Asian Journal, 2016. **11**(7): p. 1059-1064.

32. Noo Li Jeon, S.K.W.D., Daniel T. Chiu, Insung S. CHoi, Abraham D. Stroock, and Geroge M. Whitesides, *Generation of solution and surface gradients using microfluidic systems.* Langmuir, 2000. **16**(22): p. 8311-8316.

33. Michael Mayer, J.Y., Irina Gitlin, David H. Gracias, George M. Whitesides, *Micropatterned agarose gels for stamping arrays of proteins and gradients of proteins.* Proteomics, 2004. **4**(8): p. 2366-2376.

34. Anne C von Philipsborn, S.L., Andre Bernard, Jurgen Loeschinger, Christian David, Dirk Lehnert, Martin Bastmeyer and Friedrich Bonhoeffer, *Microcontact printing of axon guidance molecules for generation of graded patterns.* Nature Protocols, 2006. **1**(3): p. 1322-1328.

35. Emmanuel Delamarche, A.B., Heinz Schmid, Bruno Michel, Hans Biebuyck, *Patterned delivery of immunoglobulins to surfaces using microfluidic networks.* Sceience, 1997. **276**(5313): p. 779-781.

36. Emmanuel Delamarche, A.B., Heinz Schmid, Alexander Bietsch, Bruno Michel, and Hans Biebuyck, *Microfluidic Networks for Chemical Patterning of Substrates: Design and Application to Bioassays.* Journal of the American Chemical Society, 1998. **120**(3): p. 500-508.

37. Anne C. von Philipsborn, S.L., Zhongxiang Jiang, Friedrich Bonhoeffer, and Martin Bastmeyer, *Substrate-Bound Protein Gradients for Cell Culture Fabricated by Microfluidic Networks and Microcontact Printing.* Science's STKE, 2007. **2007**(414): p. 16.

38. Shuichi Takayama, J.C.M., Emanuele Ostuni, Michael N. Liang, Paul J. A. Kenis, Rustem F. Ismagilov, and George M. Whitesides, *Patterning cells and their environments using multiple laminar fluid flows in capillary networks.* PNAS, 1999. **96**(10): p. 5545-5548.

39. George M. Whitesides, E.O., Shuichi Takayama, Xingyu Jiang, and Donald E. Ingber, *Soft lithography in biology and biochemistry.* Annual Review of Biomedical Engineering, 2001. **3**: p. 335-373.

40. Whitesides, S.K.S.a.G.M., *Microfluidic devices fabricated in poly(dimethylsiloxane) for biological studies.* Electrophoresis, 2003. **24**(21): p. 3563-3576.

41. Xingyu Jiang, Q.X., Stephan K. W. Dertinger, Abraham D. Stroock, Tzung-may Fu, and George M. Whitesides, *A General Method for Patterning Gradients of Biomolecules on Surfaces Using Microfluidic Networks.* Analytical Chemistry, 2005. **77**(8): p. 2338-2347.

42. Fuller, N.E.S.a.S.B., *A fast flexible ink-jet printing method for patterning dissociated neurons in culture.* Journal of Neuroscience Methods, 2004. **136**(2): p. 151-163.

43. J.D. Newman, A.P.F.T., G. Marrazza, *Ink-jet printing for the fabrication of amperometric glucose biosensors.* Analytica Chimica Acta, 1992. **262**(1): p. 13-17.

44. Leonardo R. Allain, M.A., David L. Stokes, Tuan Vo-Dinh, *Microarray sampling-platform fabrication using bubble-jet technology for a biochip system.* Fresenius' Journal of Analytical Chemistry, 2014. **371**(2): p. 146-150.

45. Roda A , G.M., Russo C , Pasini P , Baraldini M, *Protein microdeposition using a conventional ink-jet printer Biotechniques.* BioTechniques, 2000. **28**(3): p. 492-496.

46. Jayesh Bharathan, a.Y.Y., *Polymer electroluminescent devices processed by inkjet printing: I. Polymer lightemitting logo.* Applied Physics Letters, 1998. **72**(21): p. 2660-2662.

47. H. Sirringhaus, T.K., R. H. Friend, T. Shimoda, M. Inbasekaran, W. Wu, E. P. Woo, *High-Resolution Inkjet Printing of ALL-Polymer Transistor Circuits.* Science, 2000. **290**(5499): p. 2123-2126.

48. Veronica Marin, E.H., Martijn M. Wienk, Emine Tekin, Dmitry Kozodaev, Ulrich S. Schubert, *Ink-Jet Printing of Electron Donor/Acceptor Blends: Towards Bulk Heterojunction Solar Cells.* Macromolecular Rapid Communications, 2005. **26**(4): p. 319-324.

49. W. Voit, W.Z., L. Belova, K. V. Rao, *Application of inkjet technology for the deposition of magnetic nanoparticles to form micron-scale structures.* Journal of Applied Physics, 2003. **150**(5): p. 252-256.

50. K. Crowley, E.O.M., A. Morrin, M. R. Smyth, A. J. Killard, *An aqueous ammonia sensor based on an inkjet-printed polyaniline nanoparticle-modified electrode.* Analyst, 2008. **133**(3): p. 391-399.

51. Alexander Bietsch, J.Z., Martin Hegner, Hans Peter Lang and Christoph Gerber, *Rapid functionalization of cantilever array sensors by inkjet printing.* Nanotechnology, 2004. **15**(8): p. 873-880.

52. Madhusudan Singh, H.M.H., Parul Dhagat, Ghassan E. Jabbour, *Inkjet Printing—Process and Its Applications.* Advanced Materials, 2009. **22**(6): p. 673-685.

53. Miller, E.D., Phillippi, Julie A., Fisher, Gregory W., Campbell, Phil G., Walker, Lynn M., Weiss, Lee E, *Inkjet Printing of Growth Factor Concentration Gradients and Combinatorial Arrays Immobilized on Biologically-Relevant Substrates.* Combinatorial Chemistry & High Throughput Screening, 2009. **12**(6): p. 604-618.

54. Kaiyong Cai, H.D., Chong Chen, Li Yang, Klaus D. Jandt, Linhong Deng, *Inkjet printing of laminin gradient to investigate endothelial cellular alignment.* Colloids and Surfaces B: Biointerfaces, 2009. **72**(2): p. 230-235.

55. R. V. Martínez, N.S.L., J. Martinez, Y. Huttel, and R. Garcia, *Patterning polymeric structures with 2 nm resolution at 3 nm half pitch in ambient conditions.* Nano Letters, 2007. **7**(7): p. 1846-1850.

56. S. Sheng, D.M.C.a.Z.S., *AFM tips: how sharp are they?* Journal of Microscopy, 1999. **196**(Pt 1): p. 1-5.

57. Richard D. Piner, J.Z., Feng Xu, Seunghun Hong, Chad A. Mirkin, *"Dip-Pen" Nanolithography.* Sceience, 1999. **283**(5402): p. 661-663.

58. Manfred Jaschke, a.H.-J.B., *Deposition of Organic Material by the Tip of a Scanning Force Microscope.* Langmuir, 1995. **11**(4): p. 1061-1064.

59. G. Binnig, H.R., Ch. Gerber, and E. Weibel, *Surface studies by scanning tunneling microscopy.* Physical Review Letters, 1982. **49**(1): p. 57-61.

60. Christopher B. Gorman*, R.L.C., Yufan He, Fang Tian, and Ryan Fuierer, *Chemically Well-Defined Lithography Using Self-Assembled Monolayers and Scanning Tunneling Microscopy in Nonpolar Organothiol solutions.* Langmuir, 2000. **16**(15): p. 6312-6316.

61. J. A. Dagata, J.S., H. H. Harary, C. J. Evans, M. T. Postek, and J. Bennett, *Modification of hydrogen‐passivated silicon by a scanning tunneling microscope operating in air.* Applied Physics Letters, 1990. **56**(20): p. 2001-2003.

62. P. Avouris, R.M., T. Hertel, R. Sandstrom, *AFM-tip-induced and current-induced local oxidation of silicon and metals.* Applied Physics A, 1998. **66**(Supplement 1): p. S659-S667.

63. Gang-Yu Liu, S.X., and Yile Qian, *Nanofabrication of Self-Assembled Monolayers using scanning probe lithography.* Accounts of Chemical Research, 2000. **33**(7): p. 457-466.

64. Keith M Carroll, A.J.G., Debin Wang, Vamsi K Kodali, Jan Scrimgeour, William P King, Seth R Marder, Elisa Riedo, Jennifer E Curtis, *Fabricating Nanoscale Chemical Gradients with ThermoChemical NanoLithography.* Langmuir, 2013. **29**(27): p. 8675-8682.

65. Robert Szoszkiewicz, T.O., Simon C. Jones, Tai-De Li, William P. King, Seth R. Marder, and Elisa Riedo, *High-Speed, Sub-15 nm Feature Size Thermochemical Nanolithography.* Nano Letters, 2007. **7**(4): p. 1064-1069.

66. David S. Ginger, H.Z., Chad A. Mirkin, *The evolution of dip-pen nanolithography.* Angewandte Chemie International Edition, 2003. **43**(1): p. 30-45.

67. Seunghun Hong, C.A.M., *A nanoplotter with both parallel and serial writing capabilities.* Sceience, 2000. **288**(5472): p. 1808-1811.

68. Hojeong Jeon, R.S., Jeremy E. Barton, David J. Hwang, Lara J. Gamble, David G. Castner, Costas P. Grigoropoulos, and Kevin E. Healy, *Chemical Patterning of Ultrathin Polymer Films by Direct-Write Multiphoton Lithography.* Journal of the American Chemical Society, 2011. **133**(16): p. 6138-6141.

69. John H. Slater, J.S.M., Shann S. Yu, and Jennifer L. West, *Fabrication of Multifaceted Micropatterned Surfaces with Laser Scanning Lithography.* Advanced Functional Materials, 2011. **21**(15): p. 2876-2888.

70. Maurer, M.J.H.a.J.A., *Photoinduced Monolayer Patterning for the Creation of Complex Protein Patterns.* Langmuir, 2012. **28**(47): p. 16237-16242.

71. Jonathan M Bélisle, J.P.C., Paul W Wiseman, Timothy E Kennedy, Santiago Costantino, *Patterning protein concentration using laser-assisted adsorption by photobleaching, LAPAP.* Lab on a Chip, 2008. **8**(12): p. 2164-2167.

72. Moritz Wiesbauer, R.W., Borislav Vasic, Kurt Schilcher, Jaroslaw Jacak, Thomas A Klar, *Nano-Anchors with Single Protein Capacity Produced with STED Lithography.* Nano Letters, 2013. **13**(11): p. 5672-5678.

73. Wesley Sims, A.K., Carlton Farley, Anup Sharma, *Laser Micro-Printing of Dye-Molecules on Polymeric Surfaces.* Open Journal of Applied Sciences, 2016. **6**: p. 416-421.

74. Tengvall, B.L.a.P., *Molecular Gradients of w-substituted Alkanethiols on Gold: Preparation and Characterization.* Langmuir, 1995. **11**(10): p. 3821-3827.

75.   Jeongwook Lee, I.C., Woon-Seok Yeo, *Preparation of Gradient Surfaces by Using a Simple Chemical Reaction and Investigation of Cell Adhesion on a Two-Component Gradient.* Chemistry: a European journal., 2013. **19**(18): p. 5609-5616.

76.   Guan, Z.-Y.W., Chih-Yu; Wu, Jyun-Ting; Tai, Ching-Heng; Yu, Jiashing; Chen, Hsien-Yeh, *Multifunctional and Continuous Gradients of Biointerfaces Based on Dual Reverse Click Reactions.* ACS applied materials & interfaces, 2016. **8**(22): p. 13812-13818.

77.   Han, X., L. Wang, and X. Wang, *Fabrication of Chemical Gradient Using Space Limited Plasma Oxidation and its Application for Droplet Motion.* Advanced Functional Materials, 2012. **22**(21): p. 4533-4538.

78.   Morris, C.J. and P. Morris, *Molecular-sieve chromatography and electrophoresis in polyacrylamide gels.* The Biochemical journal, 1971. **124**(3): p. 517-528.

79.   Bode, H.-J., *A viscosity model of polyacrylamide gel electrophoresis.* Zeitschrift für Naturforschung C, 1979. **34**(7-8): p. 512-528.

80.   Pissis, P., A. Kyritsis, and V.V. Shilov, *Molecular mobility and protonic conductivity in polymers: hydrogels and ionomers.* Solid State Ionics, 1999. **125**(1): p. 203-212.

81.   Yoshioka, S., et al., *Molecular Mobility of Protein in Lyophilized Formulations Linked to the Molecular Mobility of Polymer Excipients, as Determined by High Resolution 13C Solid-State NMR.* Pharmaceutical Research, 1999. **16**(10): p. 1621-1625.

82.   Alves, N.M., J.F. Mano, and J.L. Gómez Ribelles, *Molecular mobility in polymers studied with thermally stimulated recovery. II. Study of the glass transition of a semicrystalline PET and comparison with DSC and DMA results.* Polymer, 2002. **43**(13): p. 3627-3633.

83.   Van Tomme, S.R., et al., *Mobility of model proteins in hydrogels composed of oppositely charged dextran microspheres studied by protein release and fluorescence recovery after photobleaching.* Journal of Controlled Release, 2005. **110**(1): p. 67-78.

84.   Smithies, O., *Zone electrophoresis in starch gels: group variations in the serum proteins of normal human adults.* Biochemical Journal, 1955. **61**(4): p. 629.

85.   Stellwagen, N.C., *Apparent pore size of polyacrylamide gels: Comparison of gels cast and run in Tris‐acetate‐EDTA and Tris‐borate‐EDTA buffers.* Electrophoresis, 1998. **19**(10): p. 1542-1547.

86.   Blattler, D., et al., *Quantitative electrophoresis in polyacrylamide gels of 2–40%.* Journal of Chromatography A, 1972. **64**(1): p. 147-155.

87.   Kremer, M., et al., *Pore-size distributions of cationic polyacrylamide hydrogels varying in initial monomer concentration and cross-linker/monomer ratio.* Macromolecules, 1994. **27**(11): p. 2965-2973.

88.   Morris, C. and P. Morris, *Molecular-sieve chromatography and electrophoresis in polyacrylamide gels.* Biochemical Journal, 1971. **124**(3): p. 517-528.

89.   West, R., *The mobility of polyions in gel electrophoresis.* Biopolymers: Original Research on Biomolecules, 1987. **26**(5): p. 609-611.

90.   Benguigui, L., *Comparison between the elasticity of polyacrylamide and polyacrylic gels.* Journal de Physique II, 1995. **5**(3): p. 437-443.

91.   Polymeropoulos, E. and J. Brickman, *Molecular dynamics of ion transport through transmembrane model channels.* Annual review of biophysics and biophysical chemistry, 1985. **14**(1): p. 315-330.

92.   Tong, J. and J.L. Anderson, *Partitioning and diffusion of proteins and linear polymers in polyacrylamide gels.* Biophysical journal, 1996. **70**(3): p. 1505-1513.

93.   Popov, S. and M. Poo, *Diffusional transport of macromolecules in developing nerve processes.* Journal of Neuroscience, 1992. **12**(1): p. 77-85.

94.   Bannur, S.V., et al., *Protein determination by ponceau S using digital color image analysis of protein spots on nitrocellulose membranes.* Anal Biochem, 1999. **267**(2): p. 382-9.

VITA

Ning Ge was born in Yancheng, Jiangsu, China. He received his B.S. degree in mechanical engineering from the School of Mechanical Engineering at Dalian University of Technology in Dalian, Liaoning, China. He received his M.S. degree in mechanical engineering from College of Engineering at Cleveland State University in Cleveland, Ohio, USA. He then continued his doctoral study in mechanical engineering at the Department of Mechanical Engineering, College of Engineering, University of Kentucky in Lexington, Kentucky, USA. He is currently a Ph.D. candidate whose research interest involves microfabrication, microfluidics and micro surface patterning.

<u>Publications and achievements</u>

- Ning Ge, R. Xu, C. Trinkle, *Electrophoresis in heterogeneous hydrogels and applications in surface patterning*, accepted in April 2020.

- W. Martin, Ning Ge, B. Srijanto, E. Furnish, C. Collier, C. Trinkle, C. Richards, *Real time sensing of single receptor-ligand interactions with nanoaperture integrated microfluidic devices*, ACS Omega. 2017 Jul 31;2(7);3858-3867.

- F.J. DiBartolomeo, Ning Ge, C. Trinkle, *High-throughput Creation of Micropatterned PDMS Surfaces Using Microscale Dual Roller Casting*, Journal of Micromechanics and Microengineering, 2012, Vol. 22, Issue 11.

- Ning Ge, Xin Xiong, Fuyuan Wang, *Design of Automatic Detection Device of the Resistance Force of Tracks on Brackets of Car Seats*, Instrument Technique and Sensor (CN), 2008, vol. 3, pgs 66-69.

- Ning Ge, Xin Xiong, Hongming Lv, *Development Design of Control System of Assembly Manipulator*, Industrial Control Computer (CN), 2007, vol. 20, pgs 22-23.

- Kim Le, Ning Ge, *Incorporation of Plant Architectures within Microfluidic Devices*, Poster Presentation at University of Kentucky, REU program on bioactive interfaces and devices, 2014

- Ning Ge, *Large Surface Area Micropatterned PDMS using Microscale Dual Roller Casting*, presentation at NanoSymposium, Kentucky, 2013

Patents

- *Water-saving Toilet with Drainage*, Utility models (patent No. ZL 03 2 22325.0), 1/1.

- *A Piston-pressed Infusion Pump*, Inventions (patent application No. 200710131111.6), 1/2.

- *A Pre-overflowing Infusion Pump*, Inventions (patent application No. 200710134827.1), 2/2.